Nitrogen Removal Models for Stormwater Bioretention Systems

A Dissertation

Presented to

the Faculty of the School of Engineering and Applied Science

University of Virginia

---

in Partial Fulfillment

of the requirements for the degree

Doctor of Philosophy

by

Jiayi Li

August 2023

Approval Sheet

This Dissertation

is submitted in partial fulfillment of the requirements

for the degree of

Doctor of Philosophy

Author: Jiayi Li

This Dissertation has been read and approved by

the examining committee:

Advisor:	Teresa B. Culver
Committee Chair:	Julianne Quinn
Committee Member:	Jonathan L. Goodall
Committee Member:	Lisa Colosi Peterson
Committee Member:	James N. Galloway

Accepted for the School of Engineering and Applied Science:

Jennifer L. West

August 2023

Acknowledgement

This dissertation would not have been possible without the support from my advisor Dr. Teresa B. Culver. Thank you for providing me the opportunity to pursue this amazing PhD program; for consistently trusting, encouraging, and guiding my research ideas; for mentoring my teaching assistant work; and for being an exceptional role model of life-long learning.

Thank you to my committee members, Dr. Julianne Quinn, Dr. Jonathan L. Goodall, Dr. Lisa Colosi Peterson, and Dr. James N. Galloway, for your valuable advice and suggestions to conduct more effective and impactful research work. I appreciate your acknowledgement of the potential significance of this study. Special thanks to my collaborators, Dr. Padmini P. Persaud, Dr. Jon Hathaway, Dr. Charles R. Burgis, Dr. Wuhuan Zhang, and Dr. James Smith, for sharing your data, answering my countless questions, and patiently providing help during our collaboration. A big thank you to my lab mates, Maria, and Seth, for proofreading the drafts and offering valuable inputs. This dissertation was funded as part of the National Science Foundation's Grant and supported by the University of Virginia. Your generous support is greatly appreciated.

Special thanks to my husband, Han Wang, for comforting my anxiety and bringing love and happiness to life. I would also like to express my deepest gratitude to my parents, Ming Li, and Wenbing Yu, for instilling in me a sense of independence, allowing their only child to study abroad, and being my lifelong confidants. Thank you to Yinzhu Jin, for teaching coding tricks and being the best roommate possible. Appreciation to my friends Runze Zhang, Yifan Mao, Shizhen Yin, Yongming Qin who have enriched my life in Cville with their colorful personalities and connections. You are all invaluable to me beyond words.

Abstract

With climate change scenarios and rapid urbanization projected for the coming decades, urban environments are facing more frequent extreme precipitation events and higher pollutant loads. While static bioretention systems have the potential to retain stormwater runoff volume and remove pollutant loads, their effectiveness in preventing floods is challenged by increasingly frequent extreme events. Although bioretention systems are effective in removing sediment, heavy metals, and phosphorous, nitrogen removal rates vary significantly with location, age, maintenance, and design of bioretention systems, and net nitrogen export has also been observed.

To enhance nitrogen removal in bioretention systems, submerged zones can be designed to provide long periods of high saturation in soil layer that facilitate denitrification. However, a deep submerged layer and higher saturation rate in the soil layer can hinder the system's ability to handle stormwater during subsequent events, leading to flooding. Balancing the conflicting requirements of hydraulic retention time from both volume reduction and nitrogen removal goals can be achieved by implementing real-time control (RTC), or valve control rules. To select the best valve control rules based on specific stormwater management goals, weather conditions, and bioretention designs, it is helpful to have modeling results that predict nitrogen loads or concentrations in bioretention underdrain effluents under different operational and environmental conditions in the field.

In this dissertation, a literature and a case study were first conducted to find a readily available modeling tool that accurately simulate nitrogen removal rates or transformations in bioretention systems under the impacts of environmental and operational conditions that varies over time. Statistical models lack accuracy for specific bioretention systems and are not able to predict discharged nitrogen loads during events. Current stormwater and agricultural models complement each other with their strengths on simulating hydraulic processes in bioretention systems and nitrogen transformations under impacts of environmental factors, respectively. A previous attempt has proved that adding a process-based nitrogen model to the Storm Water Management Model (SWMM) improved prediction accuracy on nitrogen removal for wet pounds, but similar models

have not been reported for bioretention systems. Therefore, we conclude that a process-based nitrogen model (NRM) needs to be developed for bioretention systems, and the most efficient way is by modifying the nitrogen module in agricultural models as extensions to the hydraulic modules in SWMM.

Six NRMs (SP-0, SP-1, SP-m, 3P-0, 3P-1. 3P-m) were developed with two model structures and three reaction kinetics. These NRMs were calibrated and validated using one set of laboratory data. The validation results show that 0-order kinetics is not suitable for NRMs. The SP-1, SP-m, 3P-1, and 3P-m models improved the prediction accuracy of percent removal of total load and event mean concentrations of total inorganic nitrogen in underdrain effluent by up to 20%. 3P-1, 3P-m outperformed SP-1 and SP-m in describing the impacts of environmental and operational conditions accurately.

The 3P-1 and 3P-m models were then updated and applied to simulate a field bioretention system. When simulating total dissolved nitrogen, the 3P-m model improved predictions of percent removal of total load by 5.5% to 10.6% and reduced scaled root mean square error by 16.2% to 53.0% when compared to SWMM. Statistical analysis confirmed that the 3P-m model accurately captures the impacts of environmental and operational conditions, and its simulated denitrification aligns with field isotope tests, providing strong evidence that the 3P-m model correctly describes the biochemical processes of nitrogen cycling in field-scale bioretention systems. Time-series generated by the models revealed that the 3P-1 model's calibration results are less reliable, but the 3P-m model can provide valuable insights to assist in the design of real-time control rules.

Despite some acknowledged limitations, the 3P-m model has demonstrated potential to significantly improve prediction accuracy on removal of nitrogen species, and to provide insights on nitrogen transformations under multiple environmental and operational conditions. Further updates and applications of the 3P-m model are encouraged, and its application in bioretention and valve control design is recommended as a potential research opportunity.

Table of Contents

List of Tables

List of Figures

Glossary of Acronyms

3P-0, 3P-1, 3P-m: models with higher complexity level, simulating three nitrogen pools, using 0 order kinetics, 1st order kinetics, and Michaelis-Menten equations.

AccMRR: accumulated mass removal rate

ADP: antecedent dry periods

BMP: best management practices

CNR: carbon to nitrogen ratio

CSTR: completely stirred tank reactor.

DOC: dissolved organic carbon

DON: dissolved organic nitrogen

EMC: event mean concentration.

EVT: evapotranspiration

FD: free drainage (control rule and type of column)

HLR: hydraulic loading rate

IWS: internal water storage (control rule and type of column)

NH_4-N: ammonium nitrogen

NNSE: normalized Nash-Sutcliff Efficiency coefficient

NO_3-N: nitrate nitrogen

NRMs: Nitrogen Removal Models

NSE: Nash-Sutcliff Efficiency coefficient

NxOy: nitrogen oxides gas emitted from nitrification and denitrification.

OrgN: organic Nitrogen

PGP: percent of good prediction

PWRMSE: peak-weighted root-mean square error

RMSE: root mean square error.

RTC: real time control

SM: soil moisture (control rule and type of column)

SOC: soil organic carbon

SP-0, SP-1, SP-m: model with lower complexity level, simulating only one total nitrogen pool, using 0 order kinetics, 1st order kinetics, and Michaelis-Menten equations.

SRMSE: scaled root-mean square error

St. Dev.: standard deviation

SWMM: the Storm Water Management Model

TDN: total dissolved nitrogen

TN: total nitrogen

TIN: total inorganic nitrogen

VC: volume control (control rule and type of column)

1 Research Background and Motivations

Rapid urbanization has led to an increase in impervious surfaces and changes in the water cycle, resulting in increased urban runoff, urban floods, and depletion of groundwater [1]. Pollutants from human activities accumulate on impervious surfaces and are carried downstream when stormwater runoff is directly discharged, making it a recognized source of non-point source pollution. Nitrogen is a critical pollutant in stormwater runoff due to its strong correlation with eutrophication and the large scale and difficulty of controlling non-point source nitrogen [2]–[4]. Shen et al. [5] reported total nitrogen (TN) load of 0.12-0.76 mg/m^2 on roads and rooftops in urban areas, and event mean concentrations (EMCs) of nitrate nitrogen in range of 0.3-47.9 mg/L. According to Dodds et al. [6], the potential value of losses from eutrophication in recreational water usage, waterfront real estate, recovery of endangered and threatened species, and drinking water can reach $ 2.2 billion or more annually in the US.

In addition, removal of nitrogen from the earth's water and soil cycles is difficult. Inorganic nitrogen can only be permanently removed from the water cycle through denitrification, which requires anaerobic or anoxic conditions and a supply electron donors. Inorganic nitrogen can be contributed from both stormwater inflow and decomposition of organic matters. The multiple biochemical processes involved in nitrogen cycle interrelate with each other and are all strongly impacted by environmental factors including temperature, soil saturation conditions, vegetation coverage and plant species, flow rates, and else [7]–[9]. With further urbanization and projected extreme weather conditions, hydraulic and water quality problems related to stormwater runoff are expected to worsen [10].

Stormwater best management practices (BMPs) are designed to address these challenges through two functions: stormwater quantity control and quality control. The goals of quantity control include reducing stormwater runoff volume, enhancing infiltration to deep groundwater, reducing peak flow rate by temporary storage and slow release of stormwater, and prolonging concentration times. Field-scale monitoring data have shown that BMPs are effective and reliable in terms of stormwater volume reduction [11], [12].

However, the effectiveness of BMPs on stormwater quantity control is challenged by global warming and climate change scenarios. Studies consistently show that the volume reductions of stormwater BMPs decrease significantly with increased peak rainfall intensity, decreased antecedent dry periods, and increased total depth of precipitation [13]. Modeling work by Abdelmoaty and Papalexiou [14] indicates that the frequency of 100-year events may double before 2067 and triple by the end of the century worldwide. A downscaled dataset from Gensini et al. [15] also suggests significant increases in annual average precipitation in the Pacific Northwest regions. With higher annual maximum daily precipitation projected across the globe by the IPCC [16], it is likely that effectiveness of BMPs on stormwater volume reduction will decrease.

The other function of stormwater BMPs is to manage quality of stormwater discharged into downstream water bodies. Numerous research has suggested that the primary mechanism for BMP to reduce pollution load is through stormwater volume reduction. Sediments, heavy metals, and phosphorus can be removed through settling and adsorption in a short hydraulic retention time and are thus efficiently removed in BMPs [17]. In contrast, mass removal of total nitrogen in field scale BMPs vary widely. Among eight roadside bioretention systems monitored by Shrestha et al. [18], mass removal of total suspended solid ranged in 89-99%, while that of nitrate nitrogen and total nitrogen ranged in -46%-55% and -14% to 45%, respectively. Nitrate net export was also observed in bioretention columns in the lab experiment from Henderson et al. [19], Hatt et al. [20], etc. The fact that multiple nitrogen species are dissolvable make it difficult to reach high nitrogen removal rates through settlement. Also, nitrogen has a complicated cycle that involves biochemical processes that influence each other and are impacted by environmental factors such as soil saturation rate, temperature, and organic matter supply.

Researchers and engineers are particularly interested in bioretention systems due to their potential for simultaneous volume and nitrogen reduction. Internal water storage (IWS) layer provides high saturation conditions for longer period to enhance denitrification process which permanently removes nitrogen by converting it to inactive nitrogen gas. However, the static design of IWS can reduce bioretention systems' ability to retain water for the next event and harm water quantity goals. Valve control strategies,

frequently referred to as real-time control (RTC) strategies in the literature, is a potential solution to this problem. By installing a valve to adjust the outflow rate based on given valve control strategies, it should be possible to maintain high saturation condition long enough during the dry periods to enhance denitrification, and discharge water prior to the subsequent events to avoid flooding, thereby reaching an optimal result for specific stormwater control objectives. However, discussions on developing such valve control strategies are limited, and previous research concentrates on balancing stormwater volume reduction and sediment removal [21]–[23]. One pilot study conducted by Shen et al. [24] recorded total nitrogen mass removal under two valve control strategies, but nitrogen removal was not the major purpose of this study. Given that nitrogen removal in bioretention systems are highly influenced by environmental and operational conditions such as temperature [25], vegetation type [9], soil amendments [26], among else, it is crucial to accurately quantify the impacts of these factors under current or future climate conditions when determining the optimal design for each field-scale bioretention system.

According to BMP Design Manual of Practice published by Virginia Department of Transportation [27], it is roughly estimated that 90% and 64% total nitrogen mass load removal is achieved by bioretention systems with or without IWS. In the widely applied Storm Water Management Model (SWMM) [28], nitrogen removal rates are simply estimated with percent reduction method. These coarse and static estimations cannot assist in optimizing the design of bioretention systems, nor anticipating their performance under changing or unexpected environmental conditions, and thus help us decide the best design of IWS depth or valve control rules. One of the obstacles limiting the research for developing and implementing bioretention system and valve control rules is our lack of accurate modeling tool that predicts nitrogen removal rates with small time steps and account for environmental factors or operational conditions.

Based on the previously discussed knowledge gap, this study aims to find the best modeling tool to assist the design of bioretention systems and valve control strategies. This dissertation is structured as follows: In chapter 2, current understanding on nitrogen cycling in bioretention systems, together with latest modeling tools are reviewed. A case study is developed to demonstrate the state of nitrogen modeling for bioretention. It is

concluded that the current models are not adequate for nitrogen simulations in stormwater bioretention systems. Thus, a new modeling tool, the nitrogen removal model (NRM), is developed in chapter 3. Two different model structures and three different descriptions of biochemical reaction rates are applied to develop a total of six different versions of NRM. In chapter 4, the six versions of NRM are calibrated and validated with a laboratory dataset to test their performances in prediction accuracy, stability of calibration results, and description of environmental or operational conditions. In chapter 5, two selected versions of NRM are further updated and generalized. They are tested with a dataset from a field bioretention system to validate their effectiveness under more complicated real-world scenarios. Finally, key conclusions from this dissertation, limitations of current NRM, and future research opportunities are discussed in chapter 6.

In conclusion, this dissertation made the attempt to develop a modeling tool to simulate nitrogen transformations and removal under the influences of important environmental and operational conditions. The selected NRM has the potential to provide accurate predictions on nitrogen removal for bioretention systems with different design of IWS layers, or under various valve control strategies, which is crucial for implementation of real time control strategies for smart stormwater management systems in the future urban environment.

References

[1] M. Osman et al., 'A Review of Nitrogen Removal for Urban Stormwater Runoff in Bioretention System', Sustainability, vol. 11, no. 19, 2019, doi: 10.3390/su11195415.

[2] K. A. Collins et al., 'Opportunities and challenges for managing nitrogen in urban stormwater: A review and synthesis', Ecol Eng, vol. 36, no. 11, pp. 1507–1519, 2010, doi: https://doi.org/10.1016/j.ecoleng.2010.03.015.

[3] J. Heisler et al., 'Eutrophication and harmful algal blooms: A scientific consensus', Harmful Algae, vol. 8, no. 1, pp. 3–13, 2008, doi: https://doi.org/10.1016/j.hal.2008.08.006.

[4] V. H. Smith, G. D. Tilman, and J. C. Nekola, 'Eutrophication: impacts of excess nutrient inputs on freshwater, marine, and terrestrial ecosystems', Environmental Pollution, vol. 100, no. 1, pp. 179–196, 1999, doi: https://doi.org/10.1016/S0269-7491(99)00091-3.

[5] Z. Shen, J. Liu, G. Aini, and Y. Gong, 'A comparative study of the grain-size distribution of surface dust and stormwater runoff quality on typical urban roads and roofs in Beijing, China', Environmental Science and Pollution Research, vol. 23, no. 3, pp. 2693–2704, 2016, doi: 10.1007/s11356-015-5512-5.

[6] W. K. Dodds et al., 'Eutrophication of U.S. Freshwaters: Analysis of Potential Economic Damages', Environ Sci Technol, vol. 43, no. 1, pp. 12–19, Jan. 2009, doi: 10.1021/es801217q.

[7] K. A. Collins et al., 'Opportunities and challenges for managing nitrogen in urban stormwater: A review and synthesis', Ecol Eng, vol. 36, no. 11, pp. 1507–1519, 2010, doi: https://doi.org/10.1016/j.ecoleng.2010.03.015.

[8] J. Liu, D. J. Sample, C. Bell, and Y. Guan, 'Review and Research Needs of Bioretention Used for the Treatment of Urban Stormwater', Water (Basel), vol. 6, no. 4, pp. 1069–1099, 2014, doi: 10.3390/w6041069.

[9] A. Skorobogatov, J. He, A. Chu, and B. Valeo Caterina and van Duin, 'The impact of media, plants and their interactions on bioretention performance: A review', SCIENCE OF THE TOTAL ENVIRONMENT, vol. 715, May 2020, doi: 10.1016/j.scitotenv.2020.136918.

[10] C. Saraswat, P. Kumar, and B. K. Mishra, 'Assessment of stormwater runoff management practices and governance under climate change and urbanization: An analysis of Bangkok, Hanoi and Tokyo', Environ Sci Policy, vol. 64, pp. 101–117, 2016, doi: https://doi.org/10.1016/j.envsci.2016.06.018.

[11] A. P. Davis, 'Field Performance of Bioretention: Hydrology Impacts', J Hydrol Eng, vol. 13, no. 2, pp. 90–95, Feb. 2008.

[12] K. Vijayaraghavan et al., ‘Bioretention systems for stormwater management: Recent advances and future prospects’, J Environ Manage, vol. 292, p. 112766, 2021, doi: https://doi.org/10.1016/j.jenvman.2021.112766.

[13] W. Sohn, J.-H. Kim, M.-H. Li, and R. Brown, ‘The influence of climate on the effectiveness of low impact development: A systematic review’, J Environ Manage, vol. 236, pp. 365–379, 2019, doi: https://doi.org/10.1016/j.jenvman.2018.11.041.

[14] H. M. Abdelmoaty and S. M. Papalexiou, ‘Changes of Extreme Precipitation in CMIP6 Projections: Should We Use Stationary or Nonstationary Models?’, J Clim, vol. 36, no. 9, pp. 2999–3014, 2023, doi: 10.1175/JCLI-D-22-0467.1.

[15] V. A. Gensini, A. M. Haberlie, and W. S. Ashley, ‘Convection-permitting simulations of historical and possible future climate over the contiguous United States’, Clim Dyn, vol. 60, no. 1, pp. 109–126, 2023, doi: 10.1007/s00382-022-06306-0.

[16] Core Writing Team, H. Lee, and J. Romero, ‘IPCC, 2023: Summary for Policymakers. In: Climate Change 2023: Synthesis Report. A Report of the Intergovernmental Panel on Climate Change. Contribution of Working Groups I, II and III to the Sixth Assessment Report of the Intergovernmental Panel on Climate Change’, Geneva, Switzerland, 2023.

[17] Y. Wang, H. Yin, Z. Liu, and X. Wang, ‘A Systematic Review of the Scientific Literature on Pollutant Removal from Stormwater Runoff from Vacant Urban Lands’, Sustainability, vol. 14, no. 19, 2022, doi: 10.3390/su141912906.

[18] P. Shrestha, S. E. Hurley, and B. C. Wemple, ‘Effects of different soil media, vegetation, and hydrologic treatments on nutrient and sediment removal in roadside bioretention systems’, Ecol Eng, vol. 112, pp. 116–131, 2018, doi: https://doi.org/10.1016/j.ecoleng.2017.12.004.

[19] C. Henderson, M. Greenway, and I. Phillips, ‘Removal of dissolved nitrogen, phosphorus and carbon from stormwater by biofiltration mesocosms’, WATER SCIENCE AND TECHNOLOGY, vol. 55, no. 4, pp. 183–191, 2007, doi: 10.2166/wst.2007.108.

[20] E. Hatt, D. Fletcher, and A. Deletic, ‘Hydraulic and pollutant removal performance of stormwater filters under variable wetting and drying regimes’, WATER SCIENCE AND TECHNOLOGY, vol. 56, no. 12, pp. 11–19, 2007, doi: 10.2166/wst.2007.751.

[21] E. Gaborit, D. Muschalla, B. Vallet, P. A. Vanrolleghem, and F. Anctil, ‘Improving the performance of stormwater detention basins by real-time control using rainfall forecasts’, Urban Water J, vol. 10, no. 4, pp. 230–246, Aug. 2013, doi: 10.1080/1573062X.2012.726229.

[22] E. Gaborit, F. Anctil, G. Pelletier, and P. A. Vanrolleghem, ‘Exploring forecast-based management strategies for stormwater detention ponds’, Urban Water J, vol. 13, no. 8, pp. 841–851, Nov. 2016, doi: 10.1080/1573062X.2015.1057172.

[23] S. Shishegar, S. Duchesne, and G. Pelletier, 'An integrated optimization and rule-based approach for predictive real time control of urban stormwater management systems', J Hydrol (Amst), vol. 577, p. 124000, 2019, doi: https://doi.org/10.1016/j.jhydrol.2019.124000.

[24] P. Shen, A. Deletic, K. Bratieres, and D. T. McCarthy, 'Real time control of biofilters delivers stormwater suitable for harvesting and reuse', Water Res, vol. 169, p. 115257, 2020, doi: https://doi.org/10.1016/j.watres.2019.115257.

[25] J. Xiong et al., 'Purification effect of bioretention with improved filler on runoff pollution under low temperature conditions', J Environ Manage, vol. 295, p. 113065, 2021, doi: https://doi.org/10.1016/j.jenvman.2021.113065.

[26] Z. S. Weng et al., 'Corncob-pyrite bioretention system for enhanced dissolved nutrient treatment: Carbon source release and mixotrophic denitrification', Chemosphere, vol. 306, 2022, doi: 10.1016/j.chemosphere.2022.135534.

[27] 'Part II B BMP Design Manual of Practice', Virginia Department of Transportation. https://www.virginiadot.org/business/resources/LocDes/Part_II_B_BMP_MOP_Combined_6-24-19.pdf (accessed Jun. 20, 2023).

[28] L. A. Rossman, 'Storm Water Management Model User's Manual Version 5.1', Cincinnati, Sep. 2015. Accessed: Jan. 26, 2022. [Online]. Available: https://www.epa.gov/sites/default/files/2019-02/documents/epaswmm5_1_manual_master_8-2-15.pdf

2 Review of Current Knowledge and Available Models[1]

2.1 Current Research on Nitrogen Removal in Bioretention Systems

Urban stormwater typically contains various nitrogen species, including particulate organic nitrogen, dissolved organic nitrogen (DON), ammonium-nitrogen (NH_4-N), and nitrate-nitrogen (NO_3-N). Nitrogen can change between forms through multiple biochemical processes. The occurrence and efficiency of these processes are influenced by a range of environmental factors and operational conditions. Understanding these factors is essential for effective management of urban stormwater and modeling nitrogen removal in bioretention systems.

- **Decomposition, Nitrification, Denitrification**

Decomposition, nitrification, and denitrification are the processes in nitrogen cycling in bioretention systems that are the most discussed in previous literature. In these processes, organic nitrogen is first converted to NH_4-N during decomposition, and then quickly converted to NO_3-N through nitrification in aerobic conditions. In soil media layers, particularly in conventional bioretention systems without IWS layers, NH_4-N can be effectively removed due to prevailing aerobic conditions. Although NO_2-N is an intermediate or byproduct of nitrification, it is typically not detected in bioretention underdrain discharge as it is quickly oxidized into NO_3-N. Davis et al. [1] reported 89% and 89% load removal for both NH_4-N and NO_2-N, respectively, from a field-scale bioretention system in Maryland. Denitrification is another important nitrogen transformation process where denitrifying bacteria convert NO_3-N into nitrogen gas under anaerobic or anoxic conditions. While denitrification is the preferred nitrogen sink, inorganic nitrogen can also be converted into N_2O which is a known air pollutant that contributes to global warming. Reaction rates of decomposition, nitrification, and denitrification have been described with zero-order, first-order, and the Michaelis-Menten

[1] This chapter is published in part in: J. Li and T. B. Culver, "Review of process-based nitrogen model for agricultural fields with implications for nitrogen simulations in stormwater BMPs," *Environmental Modelling & Software*, vol. 151, p. 105363, 2022, doi: https://doi.org/10.1016/j.envsoft.2022.105363

equations [2]–[8], and it remains unclear which kinetics best fits nitrogen cycling simulations in bioretention systems.

- **The impacts of vegetation**

Skorobogatov et al. [9] has provided a comprehensive review on the impacts of plants on nitrogen removal in bioretention system. While most previous research has reported improved nutrient removal with vegetation, some studies have found no statistically significant correlation between plant presence and improved nitrogen removal [10]–[12]. There are several mechanisms at play. Firstly, plants influence hydrologic processes by creating macropores and preferential flow paths through root growth and decay. Plant roots can also help maintain higher saturation rates over time and counteract clogging [13]. Although enhanced infiltration into deeper groundwater can improve nitrogen mass removal through volume reduction, the existence of preferential flow poses the risk of decreased water treatment due to shorter contact time with soil media [14]. Secondly, plants take up inorganic nitrogen and convert it into organic matter to support their growth. The rate of plant uptake varies with factors such as plant species, growth rate, root zone depth, and total biomass [15]–[17]. Regular plant harvests are necessary to avoid nitrogen release back into the bioretention soil when leaves fall or plants decay. Thirdly, plant roots can serve as a vital source of organic matter and oxygen for microbes in the soil media layer [18], [19]. This impact is particularly significant for urban stormwater bioretention systems where organic matter content is typically low. These processes are complex and interrelated, and their extent and mechanisms remain topics of ongoing research.

- **Other biochemical processes**

In recent years, several other mechanisms of nitrogen transformations have been proposed. Daims et al. [20] identified a bacterial species capable of completing the comammox process, where ammonia and nitrite are completely oxidized to nitrate in one step. They also suggest that this process may be common in natural and engineered microbial communities. Anammox has also been identified [21] as a process where specific bacteria convert NH_4-N into nitrogen gas without requiring oxygen or external carbon sources. Dissimilatory nitrate reduction to ammonium (DNRA) is the process of

microbes converting NO_3-N to NH_4-N. Silver et al. [22] found that reaction rate of this process was three times higher than that of denitrification in tropical forest soils. However, this process does not remove nitrogen from soil. Although genetic studies have provided evidence for the existence of these processes in natural soil and wastewater treatment plants, further research is still needed to evaluate their importance and contribution to the nitrogen cycle in stormwater BMPs [23]. Additionally, fitting reaction kinetics of these processes will be essential to obtain a better understanding of their mechanisms.

- **The impacts of antecedent dry periods**

The dry and rewetting cycle and antecedent dry periods (ADP) have been recognized as an impactful factor for nitrogen removal in bioretention systems. By observing the time series of effluent concentration during events, Subramaniam et al. [24] pointed out that the nitrification-denitrification process primarily occurs during the ADP rather than during events. Effluent concentration of bioretention system is essentially a result of mixing inflow stormwater and old clean water retained from the last event. Yao et al. [25] investigated the impact of ADP on microbial communities, finding that denitrifying bacteria decreased with increasing ADP, while the abundance of nitrifying bacteria first decreased and then increased. Results from Chen et al. [26] and Wu et al. [27] agree that the optimal ADP for total nitrogen removal is 5 days. Chen et al. observed plant decay over an extended high saturation rate period, which led to the release of NH_4-N and decreased total nitrogen removal rates. Wu et al. found that in addition to shorter ADP, a consistent dry-rewetting period can also increase the abundance of denitrifies.

- **The impacts of temperature and freeze-thaw cycle**

Temperature has a significant impact on biochemical reaction rates. According to Zhou et al. [28], there is a considerable decrease in NO_3-N removal from soil columns when the temperature drops from 25 ℃ (with removal rates ranging from 80.14% to 96.72%) to 1 ℃ (with removal rates ranging from 28.15% to 65.22%). Xiong et al. [29] also conducted laboratory experiment that showed NO_3-N removal rates decreasing from 70%-90% in autumn to -23% to 35% in winter, with total nitrogen removal rates also decreasing from 75%-90% in autumn to 20%-50% in winter. NH_4-N removal rates were

less affected by temperature. To the best of the author's knowledge, no mathematical equations have been published describing the impacts of temperature on nitrification and denitrification rates based on data acquired from bioretention systems.

- **The impacts of organic matter supply**

Amended media has recently garnered much research interest as a high-quality organic carbon source to support microbial growth, particularly of heterotrophic denitrifying bacteria. Yao et al. [25] observed a significant positive correlation between soil organic matter and both nitrifying and denitrifying bacteria. To enhance denitrification, woodchips [4], $FeCl_3$-modified hydrochar [30], and newspaper [31] have been added to the soil media as carbon sources. While effective in enhancing denitrification, the addition of external carbon sources raises concerns regarding increased dissolved organic carbon concentrations in underdrain effluent from bioretention systems [32].

- **Summary of Section 2.1**

As discussed in this section, nitrogen cycling in the soil media layers of bioretention systems is a complex system that involves multiple interrelated biochemical processes and is greatly impacted by various environmental factors and operational conditions. Previous research has provided some basis for building simulations of nitrogen transformations in bioretention systems, with reaction kinetics of decomposition, nitrification, and denitrification being fitted with 0-order kinetics, 1st order kinetics, or M-M function. However, extensive research is still needed to understand the mechanisms, contributions to nitrogen removal, as well as the kinetic descriptions of other nitrogen transformation processes, including anammox, comammox, DNRA, and plant uptake. Current understanding of the impacts of environmental factors, including antecedent dry periods, temperature, and organic content, also remains qualitative.

2.2 Review of Current Nitrogen Modeling Tools for Stormwater BMPs

This section reviews the current progresses made in modeling nitrogen removal and transformations in bioretention systems to evaluate if there are adequate tools available for accurate simulations that can support the design of IWS layers, operational

conditions, and valve control rules. Statistical models, commonly used stormwater modeling software, and the latest process-based nitrogen models are reviewed.

- **Statistical models**

Only a few researchers have attempted to predict nitrogen removal in bioretention systems with data-driven models.

Wang et al. [33] used univariate analysis to qualitatively assess the impacts of operational conditions and design parameters. The results indicated that larger depth of soil layer, the presence of an IWS layer, higher organic matter content, and mixed vegetation all have a significant positive correlation with total nitrogen (TN) removal. Multivariate linear regression models were developed, with the best performing model exhibiting an R^2 value of 0.75 for data collected from experiments using synthetic runoff and 0.86 for natural runoff.

Gilliom et al. [34] calibrated four different linear models using the International Stormwater BMP Database: a percent removal model, an ordinary least squares regression model, a Theil-Sen robust line model, and a linear decay model with an irreducible concentration parameter. The authors concluded that none of the four models showed good accuracy for predicting effluent concentrations of inorganic nitrogen species. The ordinary least squares regression model performing the best with generally good estimation on the average effluent Event Mean Concentration (EMC) of nitrate and nitrite (with a 4.4% bias) and acceptable TN effluent EMC estimation (with a -13.6% bias), but it fails to simulate the variation of EMCs among events, with Nash-Sutcliff Efficiency coefficient (NSE) values of 0.01 and -0.01 for nitrate and nitrite, respectively.

Zhang et al. [35] have developed various statistical models to predict TN effluent concentrations as a function of design characteristics and operational conditions. All tested statistical models have fair to good performances with NSE values ranging between 0.37-0.63. These models suggest that effective vegetation, submerged zone depth, and infiltration rate are the three most impactful factors for TN removal. However, the calibrated parameters for infiltration rate can have both positive or negative signs, indicating results from calibrated statistical models may not have physical meanings to

assist bioretention design, and that one set of calibrated parameters cannot accurately describe each specific bioretention system.

Statistical models suffer from other inherent weaknesses. Firstly, statistical models use effluent EMC as their primary target, providing no information about the impacts of rainfall characteristics, first flush phenomenon, or valve control rules that may alter soil moisture conditions during an event. This limitation inhibits statistical models from generating time series that aid in our comprehension of nitrogen transformation processes and the development of valve control rules. Secondly, the description of important factors is limited by the characteristics of linear regression methods. For instance, dummy variables are often used to describe factors such as vegetation type, which impacts TN effluent concentrations. But the use of dummy variables does not provide adequate information on the specific plant species, growth rate, seasonal changes, temperature, and other factors that influence TN removal through plant uptake.

- **Current stormwater models**

Some current stormwater models simulate some nitrogen transformation processes, but the descriptions of nitrogen cycle generally remain limited, indirect, and coarse [36], [37]. The HEC-HMS (Hydrologic Modeling System) [38] and MOUSE (Urban Drainage and Sewer) [39] models do not include nutrient simulations. The P8 Urban Catchment Model (Program for Predicting Polluting Particle Passage Through Pits, Puddles, and Ponds) [40], only includes sediments, not solutes. The WinSLAMM model (Source Loading and management Model) [41] simulates both dissolved and particulate nutrient loads, but sediment settling is the only described pathway for nutrient removal. BMPs are not directly represented but estimated with hydraulic nodes or detention ponds in BASINS (Better Assessment Science Integrating Point and Non-point Sources) [42]. Nitrogen simulations are limited to nitrogen concentrations in surface runoff and within the sewer systems. Other models, including SWMM (Storm Water Management Model) [43], SUSTAIN (System for Urban Stormwater Treatment and Analysis Integration) [44], and MUSIC (Model for Urban Stormwater Improvement Conceptualization) [45], directly represent BMPs, and use percent reduction or first-order kinetics to describe loss of dissolved nitrogen. Transformations among nitrogen species are not considered. None

of these stormwater models considers the impacts of soil saturation rate, temperature, and organic matter supply.

- **Novel nitrogen models**

Several research studies have reported on the first attempts at predicting nitrogen transformations or removal in bioretention systems. Fowdar et al. [46] combined the hydraulic module from MUSIC with a regression module calibrated with stormwater BMPs to predict TN effluent EMCs. The NSE value for underdrain drainage flowrates ranged from -1.49 to 0.71, while the NSE values of TN EMC in underdrain outflow were -0.41, 0.34, and 0.01 for the simulated bioretention system, vegetated swale, and constructed wetland, respectively. Moreover, the simulated total mass of TN discharged through underdrain effluent had an error of 30% when compared to the measured value, which is unsatisfactory. In comparison, Baek et al. [47] added a 0-order kinetics equation to the SWMM LID hydrology module to describe TN decay. Despite this simple modification, the results showed that the modified SWMM model could better describe the time series of effluent TN load. The root-mean square error scaled to standard deviation of observed data for TN EMC significantly decreased from (1.18, 0.57, 0.66) to (0.73, 0.26, 0.64) for two bioretention systems and one infiltration trench. However, the study did not report more direct evaluations of prediction accuracy, such as absolute error, root mean square error (RMSE), or NSE of predicted EMC. Furthermore, it is unclear if the pollutant removal equations in the SWMM LID module were utilized in this research as the control group. The lack of complete data reporting hinders our understanding of the real performances of this SWMM modification.

Wang et al. [48] developed a nitrogen removal model for bioretention systems. In this model, the growth and decay rate of microbes that carries out decomposition, nitrification, and denitrification are calculated with the Monod equation. Reaction rates are impacted by soil saturation conditions, the concentration of biomass, and the concentration of species of nitrogen used as reactants. The simulated soil column is divided into completely stirred tank reactor (CSTR) units of 1 cm depth. Despite the use of complex derivative equations and very good calibration results, validation results showed low prediction accuracy for removal rates of NO_3-N (R^2 = 0.99, NSE = 0.01,

Percent Bias = -76%), organic nitrogen (R^2= 0.37, NSE = -7.69, percent bias = -115%), and TN (R^2 = 0.037, NSE = -0.89, percent bias = -8%). The authors believe that the indirect description of organic nitrogen (OrgN) is the reason for the poor performance on OrgN and TN predictions. Other possible reasons for the poor validation performance might include a) the Monod equation may not be a suitable mechanism to describe the growth rate of certain microbes, b) the description of other important environmental factors, such as temperature, is missing, and c) the way denitrification is simulated in unsaturated and saturated zones could result in underestimated denitrification rates. Because though denitrification can occur in both anaerobic and anoxic environments, it is only simulated in the saturated layer in this model.

The RHESSys model developed by Bell et al. [49] describes the hydrologic and algae growth processes and is especially suitable for wetland and detention ponds. The model was calibrated and validated with one field-scale wet pond in Charlotte, NC. Results prove that the model was able to regenerate the distribution of NO_3-N and NH_4-N EMCs in underdrain effluent. While the impact of temperature is not directly simulated, the authors conducted sensitivity analysis and confirmed that the model's sensitivity to parameters (such as base algae growth rates and half saturation concentrations) varies with temperature.

To summarize, previous attempts have demonstrated the potential for significant improvement in prediction accuracy using process-based nitrogen models. However, a readily available nitrogen model that directly describes the effects of soil saturation rate and temperature and provides satisfactory performance in predicting stormwater bioretention systems has not yet been developed or reported.

- **Agricultural models**

As nitrogen is a crucial fertilizer for crop growth, simulation of nitrogen transportation and transformation in the agricultural systems is significantly more advanced than in the urban systems, and many processes-based agricultural models have been developed and successfully applied [50]. In this section, six agricultural models are selected based on the availability of mathematical descriptions of their nitrogen modules, and their general information are summarized in Table 2. 1. The Drainmod-N II (hereafter

referred to as DRAINMOD) model refines Drainmod-N's simulation of ammonium. The extended Soil and Water Assessment Tool (SWAT-N) was developed by adjusting the nitrogen module in the original Soil and Water Assessment Tool (SWAT) to that of the DeNitrification-DeComposition (DNDC) model. As EPIC, DNDC and SWAT-N are reviewed here, it is deemed unnecessary to include the original Drainmod-N and SWAT models.

Table 2. 1 General information on selected models and their nitrogen modules

Model	Reference	Year	Previous Versions	Dimension	Time Step	Spatial Scale
EPIC (Erosion-Productivity Impact Calculator)	J. R. Williams, et al. [51]	1984		2D	daily	Site scale
DNDC (De Nitrification-De Composition)	C. S. Li, et al. [52]	1992		1D	hourly, daily	Site scale
Drainmod-N II	M.A. Youssef, et al. [53]	2005	Drainmod - N [54]	1D	daily	Site scale
WNMM (Water and Nitrogen Management Model)	Y. Li, et al. [55]	2007		1D	daily	Site and regional
SWAT-N (Soil and Water Assessment Tool)	T. Pohlert, et al. [56]	2007	SWAT [57]	2D	daily	Site and regional
IWSS* (Integrated Water System Simulation)	Y. Y. Zhang, et al. [58]	2016		1D	daily	Site and regional

* The Integrated Water System Simulation model is not named as 'IWSS' by its developer but is referred to by this acronym for conciseness in this review.

The temporal and spatial resolutions differ between models. DNDC can take an hourly time step during wet periods, while other agricultural nitrogen modules use a daily time step. Agricultural models often simulate periods longer than a season or a year, and accurate predictions of hourly nitrogen losses from agricultural fields are not necessary. In contrast, hydraulic processes in stormwater models have time steps as small as per second, and the precipitation and flooding events normally complete within hours. In terms of spatial resolution, all reviewed agricultural models can operate site-scale simulation, in which the vegetation, management practices, weather conditions, and soil

characteristics are homogeneous. Only WNMM and SWAT-N are capable of regional simulation, where sub-catchments with different soil characteristics, crops, weather conditions, and land management are simulated at the same time.

Table 2. 2 summarizes the reported sources and sinks of nitrogen in the 6 reviewed agricultural models. Various water flows (precipitation, runoff, run-on, subsurface underdrain flow, and leaching into deeper groundwater) may transport dissolved nitrogen species and in some models, nitrogen associated with sediment transport can be simulated. As EPIC, DNDC, and DRAINMOD only perform site-scale simulations, the simulated soil can't be divided into sub-catchments, and surface run-on can't be calculated. DNDC does not consider surface runoff. Surface runoff and run-on are not calculated by WNMM despite its ability to do regional simulation, because the model was developed for the North China Plain where the topography is flat and surface runoff and run-on are not significant waterflows.

Table 2. 2 The Nitrogen sources and sinks simulated in the reviewed agricultural models.

	EPIC	DNDC	IWSS	DRAINMOD	WNMM	SWAT-N
N sources						
Fertilization	√	√	√	√	√	√
Plant residue	√	√	√	√	√	√
Fixation	√			√	√	√
Wet deposition	√	√		√	√	√
Dry deposition				√	√	
Surface run-on			√			√
N losses						
Surface runoff	√		√	√		√
Drainage				√		
Leaching		√	√		√	√
Sediment transport	√					
Subsurface lateral flow	√					√
Plant uptake	√	√	√	√	√	√
N_xO_y emission†		√	√		√	√
NH_3 volatilization		√	√	√	√	√

†N_xO_y refers to nitrogen oxides, including N_2O, NO and N_2.

In the reviewed models, organic and inorganic fertilizers enter the soil in the form of large organic molecules, urea, and/or ammonium. Plant residues supplement the soil with fresh organic matter through tillage, where these supplements are evenly mixed in the topsoil to a given depth. Nitrogen fixation, which refers to the process in which nitrogen gas (N_2) is reduced to ammonia (NH_3) and enters the soil [59], is only included to maintain nitrogen mass balance, and its detailed biochemical processes are neglected. Wet deposition represents inorganic nitrogen input directly to the simulated soil during rainfall while dry deposition occurs between precipitation events. Inorganic nitrogen input through wet and dry deposition is usually simulated in the form of nitrate. Deposition rates are estimated with average rainwater concentrations and annual total dry deposition. The two nitrogen sources simulated by all agricultural models are plant residue and fertilization. Unlike agricultural fields, fertilizers are rarely applied to stormwater BMPs, and plant residues may be removed through maintenance.

For all agricultural models, nitrogen plant uptake is simulated in detail as it directly affects crop yields. Ammonia volatilization is also calculated in all agricultural models except for EPIC, as it accounts for up to 60% of applied inorganic fertilizers [60]. EPIC assumes that ammonium in the soil is instantly oxidized to nitrate, and thus ammonia volatilization is not simulated. Inorganic nitrogen dissolved in the surface runoff and organic nitrogen carried by sediments are often neglected. DNDC, IWSS, and WNMM report N_2O, NO, and N_2 emissions during both nitrification and denitrification processes, while SWAT-N only calculates these gas emissions during nitrification.

Figure 2. 1 summarizes the nitrogen transportation and transformation processes in the reviewed agricultural models except for EPIC. In each agricultural model, nitrogen concentrations in its simulated water flows are reported.

The surface and bottom of the simulated soil are marked with heavy line. Boxes indicate nitrogen pools. Arrows indicate the nitrogen-related processes simulated by all (solid arrows) or some (dashed arrows) agricultural models (see Table 2. 2). In Figure 2. 1(a), percolation refers to the water flow between soil layers.

As stated, the structure of the EPIC nitrogen module is more unique as it omits ammonia. Agricultural models except for EPIC calculate nitrogen transformations among

three pools: organic nitrogen (OrgN), NH_4-N, and NO_3-N. Biochemical processes that are important for nitrogen transformations in stormwater bioretention systems, including decomposition, immobilization, nitrification, denitrification, and plant uptake, are all simulated in detail in reviewed agricultural models except for EPIC.

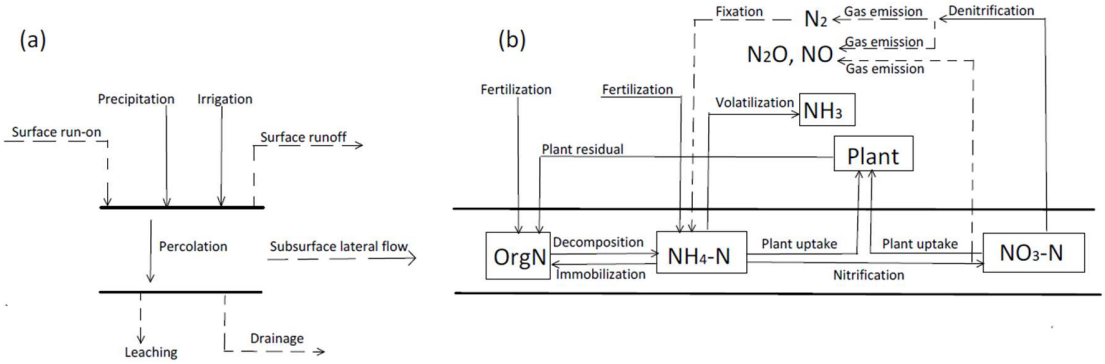

Figure 2. 1 Diagram of (a) nitrogen transportation with water flows and (b) nitrogen transformations in agricultural models except for EPIC.

To conclude, agricultural models are very similar in terms of the simulated sources, sinks, and cycling of nitrogen. There are significant differences in soil hydraulic characteristics, management objectives, nitrogen sources and sinks, soil nitrogen content, and effluent TN concentrations between agricultural field and stormwater BMPs [60], [61], while the key biochemical processes in the nitrogen cycle can be similar in the two systems [62]. Although these reviewed agricultural models are not perfectly suitable for simulating hydraulic processes in bioretention systems, their descriptions of nitrogen transformations may be leveraged to guide the development of a nitrogen model for stormwater BMPs.

2.3 Simulation Case Study

To gain a better understanding of how well current models can simulate nitrogen removal in bioretention systems, the Storm Water Management Model (SWMM) and DRAINMOD [53] were selected to simulate a bioretention system as a case study. SWMM was developed by the US EPA and is widely used as a stormwater modeling tool, particularly in the United States. DRAINMOD, on the other hand, is a widely applied agricultural model and is able to not only provide detailed descriptions of nitrogen cycling in the soil layer, but also simulate drainage flows through underdrains. Since the

TN EMC and mass load discharged through underdrain effluent are the most important parameters for simulating urban bioretention systems, DRAINMOD's ability to simulate this hydraulic process makes it a suitable choice for this particular application. In this section, the calibrated nitrogen removal rates are compared to illustrate differences in simulation accuracy between the two types of models. Other operational challenges in simulating bioretention systems with agricultural models and SWMM are also summarized.

A dataset from field experiment is selected for this case study. Over the years of 2016 and 2017, two experimental scale bioretention systems (122 cm (length) × 45.7 cm (width)) treated both natural and artificial rainwater in East Tampa, Florida. A published reference article [10] provides detailed information on the bioretention design, soil and media characteristics, weather conditions, and contaminant concentrations in the synthetic stormwater. This dataset is selected for the following reasons: a) it compares bioretention systems with and without an IWS layer; b) it compares bioretention systems with and without plants; c) it studies real bioretention systems influenced by the temperature changing over time; and d) it reports mass removal rates of NO_3-N, NH_4-N, and TN in each of 20 events over a comparatively long period of time. By simulating this dataset, it is possible to observe the ability of the chosen models to simulate soil saturation conditions in bioretention systems, as well as the impacts of soil saturation rates, temperature, and plants on nitrogen removal. Additionally, it is possible to compare the models' ability to simulate various nitrogen species. There is still a lack of information that can lead to inaccurate simulation results, including the hydraulic characteristics of the bioretention systems, the initial TN and soil organic matter content in the bioretention systems, the accurate date of artificial stormwater inflow, and the nitrogen concentrations in surface run-on from the contributing drainage catchment, and surface run off from the bioretention systems. Despite these limitations, this case study aims to compare the general performance of the two modeling tools rather than to accurately predict nitrogen removal rates for these specific bioretention systems. The dataset is hence deemed appropriate.

2.3.1 Simulated Field Bioretention System

The structures of the conventional and modified bioretention systems are shown in Figure 2. 2. In each artificial rain event, a known volume of artificial stormwater that contains 1.0 mg/L NO_3-N, 1.0 mg/L NH_4-N, and 1.0 mg/L OrgN is directly applied to the bioretention systems. The artificial stormwater is made of tap water and added chemicals and contains no sediment. All artificial stormwater infiltrates into the bioretention systems and flows out through the drainage pipe. The sides and bottom of the bioretention systems are otherwise sealed. Nitrogen concentrations in the drainage were measured to calculate percent mass removal.

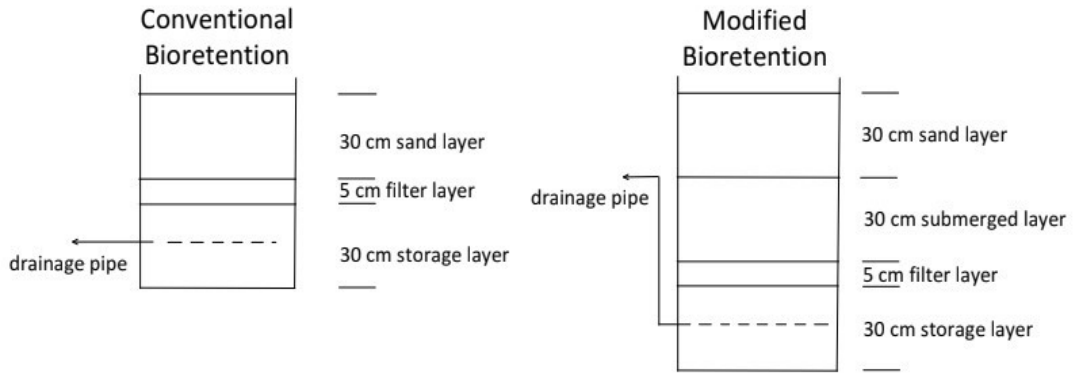

Figure 2. 2 Cross section schematics of the conventional and modified bioretention system

During natural rain events, the bioretention systems receive rainwater from the nearby impervious contributing catchment. Stormwater quantity and the quality of natural rain events are not recorded. For this case study, natural rain events are simulated based on local weather records of precipitation and air temperature [63], [64], and it is assumed that the bioretention systems occupied 5% of the contributing drainage area.

2.3.2 Simulating Hydraulic Processes in Bioretention Systems

To simulate these two bioretention systems in SWMM, stormwater generated from a contributing sub-catchment is directed to a LID sub-catchment that is 100% occupied by a bioretention cell. Time series of natural and artificial precipitation are applied to the two sub-catchments. As DRAINMOD does not support the simulation of sub-catchments with different soil profiles (as the contributing drainage area and bioretention area have different soils), separate DRAINMOD models are developed to describe the surface run-off from the contributing catchment and for the hydraulic simulations of the bioretention

systems. The reported surface runoff from the first DRAINMOD model is used as the input time series of run-on for the DRAINMOD bioretention models.

SWMM simulation. As the detailed soil characteristics were not reported in the field study, the conventional bioretention is simulated with parameter values suggested by the SWMM help file. The value of hydraulic conductivity of the sand layer was adjusted to the minimum value that avoids surface runoff from the bioretention system during artificial rain events, as no runoff was recorded for the artificial rain events. Although the elevation of the drainage pipe can be raised in SWMM LID module, it is not clear from the reported data whether the stormwater flows down into the internal storage layer before being drained. Whether stormwater mixes with 'old water' retained in the modified bioretention after the previous event would significantly influence the nitrogen concentrations in the system outflow [24]. Therefore, to approximate the modified bioretention in SWMM, the underdrain pipe effluent from LID sub-catchment was directed to a storage unit with the same volume as the maximum water content of the submerged layer.

DRAINMOD simulation. While DRAINMOD simulates artificial subsurface drainage from agricultural fields, the piping systems of bioretention systems violates the drainage assumptions used in the agricultural fields when an IWS layer is used. Thus, simulation of the underdrain effluents from the conventional and modified bioretention systems with DRAINMOD was achieved indirectly through calibration, based on available references [65], [66], of the soil water characteristic curve, Green-Ampt infiltration curve, and the water table-volume drained-upward flux curve. The bioretention systems are assumed to be homogeneous to simplify the calibration process. The soil characteristic curves were calibrated to achieve complete infiltration of all artificial stormwater. Hydraulic performances of the conventional bioretention were approximated by keeping the simulated depth of the water table at the depth of the drainage pipe. For the modified bioretention system, hydraulic conditions were approximated by keeping the simulated total soil column saturation at around 68% after rain events, which is the average saturation rate of the total column when the IWS layer is saturated, and the upper layer is at field capacity. The DRAINMOD simulated daily

surface infiltration and underdrain effluent volumes were used to calculate nitrogen mass removal. It is worth mentioning that the disadvantages of configuring DRAINMOD to simulate the submerged layer are twofold: a) the calibrated soil characteristic parameters are no longer representative to the actual soil media. Thus, there can be errors in DRAINMOD simulated soil moisture content even when precipitation and drainage volumes are calibrated; and b) even if the same soil were to be used in a system, when a different depth of IWS layer is used, the soil water characteristic curve, Green-Ampt infiltration curve, and the water table- volume drained- upward flux curve would need to be recalibrated. Thus, as a calibrated approximation of a bioretention system, DRAINMOD model cannot make predictions for systems with different designed depths for the IWS layers, and thus would be limited as a design tool.

2.3.3 Simulating Nitrogen Transformations

In the field experiment, artificial storm events were applied to the conventional and modified bioretention systems in two phases. Both conventional and modified bioretention systems have bare soil surfaces during phase I (January to July 2016). Local plants were present during phase II (March to August 2017).

- **SWMM simulation**

SWMM uses the parameter of percent removal to estimate contaminant removal in the LID module. When the conventional bioretention is simulated, the parameter of percent removal is calibrated for NO_3-N and NH_4-N, and OrgN in each of the two phases respectively. These calibrated values of percent reduction were directly applied when simulating the modified bioretention. For the modified bioretention, nitrogen removal in the storage unit is described with equation 2.1, where HRT is the hydraulic retention time calculated by SWMM, and k is calibrated for each of the two phases.

$$C_{out} = C_{in} \times \exp(-k \times HRT) \qquad \textbf{Equation 2. 1}$$

- **DRAINMOD simulation**

When doing phase I simulation, the growing season is set in DRAINMOD in a way that no crops are grown due to late planting. A total of 12 parameters describing the reaction rates of decomposition, nitrification, and denitrification are calibrated to simultaneously simulate removal rates of NO_3-N and NH_4-N. OrgN removal rates are not

calibrated because OrgN concentrations are not reported by DRAINMOD. When simulating phase II, the plant uptake process is included. The same set of parameter values calibrated for phase I simulation can be directly applied and reproduce NO_3-N and NH_4-N mass removal well, with the only adjustment of one empirical exponent describing the soil moisture factor for denitrification. In each phase, the conventional and modified bioretention systems share the same set of parameter values.

- **Comparing calibration results**

For each nitrogen species, the EMCs reported from SWMM, and the daily average nitrogen concentrations reported from DRAINMOD, were used to calculate the simulated nitrogen mass removal rate of each event (R_i). Parameters were calibrated to minimize the relative error (ER_{rel}) of the simulated average removal rates $\overline{R_{sim}}$ compared to the observed average removal rates $\overline{R_{obs}}$. In addition, lower root-mean square error (RMSE) and similar standard deviation with the field-tested data were also considered as better calibration results. These evaluation parameters are calculated with equations 2.2 – 2.4:

$$ER_{rel} = \frac{|\overline{R_{sim}} - \overline{R_{obs}}|}{\overline{R_{obs}}} \times 100\% \qquad \textbf{Equation 2. 2}$$

$$RMSE = \sqrt{\frac{\sum_{i=1}^{n}(R_{sim,i} - R_{obs,i})^2}{n}} \qquad \textbf{Equation 2. 3}$$

$$Standard\ Deviation = \sqrt{\frac{\sum_{i=1}^{n}(R_i - \bar{R})^2}{n}} \qquad \textbf{Equation 2. 4}$$

where subscripts *sim* and *obs* refer to simulated and observed results respectively, and *n* is the number of artificial storm events, which equals to 20.

2.3.4 Simulation Results

After calibration, the relative errors of underdrain effluent volumes of artificial rain events are less than 5% for both SWMM and DRAINMOD. As shown in Figure 2. 3, SWMM and DRAINMOD can accurately simulate the average mass removal rates of NO_3-N and NH_4-N with relative errors of less than 10%.

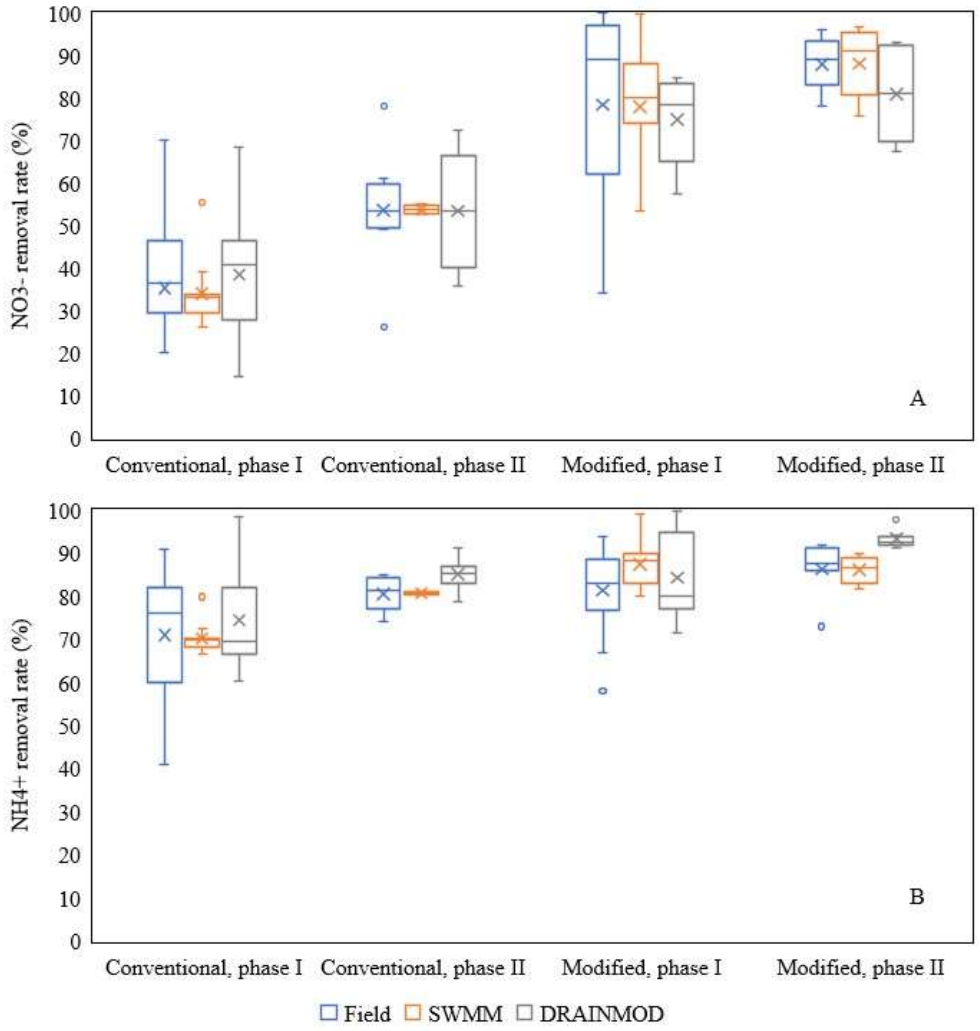

Figure 2. 3 Observed and simulated removal rates of (a) NO_3-N and (b) NH_4-N

It is more difficult for the models to accurately reproduce the variability in nitrogen removal among storm events. DRAINMOD reproduces the standard deviation better for conventional bioretention, while SWMM does better for the modified bioretention. For the conventional bioretention system, the standard deviation values from SWMM simulations are especially small. This reveals a risk of underestimating the variation of nitrogen removal rates when using SWMM as a deterministic model. For the modified bioretention system, simulated average mass removal rates from SWMM is influenced by hydraulic retention time that varies in a larger range, resulting in larger, more realistic variations. For DRAINMOD, the soil temperature factor is a major source of variation of simulated mass removal rates. In the field study, the values of standard deviation in both

conventional and modified bioretention systems were significantly smaller in Phase II, which suggests that plants may help stabilize nitrogen removal performances. The similar standard deviation of DRAINMOD-simulated removal rates between conventional and modified bioretention systems indicate that the plants' influences on nitrogen cycling in bioretention systems are not fully described by the DRAINMOD models.

2.3.5 Discussion and Conclusions

While this case study does not involve validation of the calibrated SWMM and DRAINMOD models, the limitations of these two models in predicting bioretention nitrogen removal are not hard to see. Neither SWMM nor DRAINMOD can be directly applied to simulate nitrogen transportation and transformations in bioretention systems, and their characteristics summarized in Table 2. 3 may also be applicable to simulating other stormwater BMPs.

In SWMM, nitrogen is tracked primarily through the transport of water. Simulated water flows include surface run-on, precipitation, leaching to deep groundwater, drainage through outlet pipes, and surface runoff. Time series of nitrogen concentrations in these water flows are reported. Within a BMP, multiple nitrogen species can be simulated as independent contaminants, but transformation between nitrogen species is not possible. For each nitrogen species, a simple percent removal can be applied to a BMP, where the nitrogen concentration exported through drainage and leaching is a constant percentage of the nitrogen concentration in well-mixed inflows [67]. The impacts of temperature, soil saturation rate, organic matter supply, plant uptake, and antecedent dry periods on nitrification and denitrification are not represented. Hydraulic analysis in SWMM is more advanced. However, it might be helpful if the soil columns can be stratified into soil layers in the vertical direction according to BMP designs or soil moisture conditions to obtain time series of water contents and water flows as the basis of further process-based nitrogen simulations with higher accuracy.

Table 2. 3 Strengths and weaknesses of simulating bioretention systems with SWMM and DRAINMOD

SWMM	DRAINMOD
Simulates surface run-on from the contributing catchment and the bioretention system in one model.	Simulates one sub-catchment at a time. An additional model is needed to calculate surface run-on.
The LID module describes the structure of conventional bioretention systems, but the internal water storage layer is not included.	Separates soil into horizontal layers as users needed, but the internal water storage layer cannot be directly simulated
Easier parameterization as SWMM offers suggested values or ranges for parameters.	Multiple curves are needed for each soil layer to describe hydraulic characteristics, and suggested parameter values are not provided.
Only reports average soil moisture content of the total bioretention system.	Reports detailed soil water content and water fluxes of each soil layer.
Reporting and simulating time steps are determined by users and can be as short as in seconds.	Only average concentrations are reported in a daily time step.
Detailed nitrogen transformations are not described. Not able to predict the influences of changing bioretention structures, vegetation, or weather conditions.	Nitrogen transformations are calculated and reported in detail.
Math equations that simulate contaminant removal are simpler and easy to calibrate.	The larger number of parameters can bring in difficulty and uncertainty for model calibration.

While providing more detailed simulation on biochemical reactions and transformation among nitrogen species, DRAINMOD prioritizes the simulation of the plant uptake rate of inorganic nitrogen. While plant uptake can be important in urban stormwater BMPs, it is not feasible or necessary to apply an agricultural level of detail of this process in bioretention systems. More importantly, DRAINMOD is not capable of directly simulating hydraulic performances of BMPs. The soil parameters need to be recalibrated for different thicknesses of IWS layer, and thus the performances of bioretention system cannot be predicted at the time of design.

Given that the stormwater models and agricultural models each have their advantages of simulating hydraulic processes and nitrogen transformations, it is natural to propose that the most efficient approach to improving the accuracy of predicting nitrogen

removal and transformations in bioretention systems is adapting the mathematical expressions of nitrogen-related biochemical processes in agricultural models and using them to develop nitrogen removal models as extensions to hydraulic analysis in current stormwater models.

2.4 Review of Nitrogen Modules in Current Agricultural Models

In this section, the math equations used in the nitrogen modules of the six previously reviewed agricultural models are further analyzed to assist the development of the nitrogen removal model (NRM) as extensions to current stormwater models. Math expressions used in each reviewed agricultural nitrogen modules are modified for easier comparison. Math expressions used in this section and their meanings are summarized in Table S 1 in the Supplementary Material.

2.4.1 Nitrogen Transformations

Equations for decomposition, nitrification, and denitrification are summarized in Table 2. 4. C_p and N_p refer to changes of carbon and nitrogen over time respectively, with the subscript indicating the relevant process (dec: decomposition, nit: nitrification, and den: denitrification). k_p is an optimal rate constant, which may be reduced by a comprehensive environmental factor f_{en} due to deficient environmental conditions. f_{en} can be calculated with specific environmental factors including soil saturation rate, temperature, soil pH, soil organic carbon content (OC), and carbon to nitrogen ratio (CNR) of organic matters. The original environmental factor of clay content in DNDC is not listed in Table 2. 4 but reformed to a factor of OC, as clay tends to slow down the decomposition process by absorbing organic matters [68]. The equations used to calculate the environmental factors are further discussed in later sections. In Table 2. 4, NH_4, NO_3, and TNO are concentrations of ammonium, nitrate, and total nitrogen oxides. In DNDC and IWSS, the denitrification rate is influenced by the growth rate and abundance of denitrifying bacteria. B_{den} refers to the total denitrifying biomass, and N_aO_b is the concentration of various species of nitrogen oxide ions that are utilized by denitrifying bacteria. μ, Y, and M describes the growth and decay rate of denitrifying bacteria and vary with nitrogen oxide species.

- **Decomposition**

As biological transformations of carbon and nitrogen during decomposition are simultaneous and intertwined, nitrogen transformations in these processes are often calculated based on the carbon cycle. As is shown in Table 2. 4, in all agricultural models except for EPIC, inorganic carbon released from decomposition, C_{dec}, is first simulated with first-order reaction dynamics. The amount of released inorganic nitrogen, N_{dec}, is then calculated with CNR. The value of optimum reaction rates and CNR are different among various soil organic matter sub-pools. Most agricultural models assume constant CNR values in each sub pool of soil organic matters, with the only exception of DRAINMOD, which recalculates CNR in sub-pools at each time step. N_{dec} is then added to the ammonia pool. In EPIC, inorganic nitrogen is directly released in the form of nitrate as there is not an ammonia pool, and the amount released is calculated based on organic nitrogen content.

- **Nitrification and Denitrification**

Nitrification and denitrification rates have been fitted with zero-order reaction kinetics, first-order reaction kinetics, or Michaelis-Menten functions in urban bioretention systems [69], [70]. In agricultural nitrogen modules, nitrification and denitrification rates are described by either the first-order equation or the Michaelis-Menten function. In the Michalis-Mention function, the described process behaves as a first-order reaction when the substrate is limited and gradually changes to a zero-order reaction with increasing substrate concentrations.

It is also shown in the last column of Table 2. 4 that environmental factors are integrated with optimal reaction rate k_p in various ways, and are described with empirical functions in various forms. Thus, their impacts on nitrogen transformation simulations can be complex, and their sensitivity can only be analyzed with actual simulation results.

Table 2. 4 Mathematical expressions for decomposition, nitrification, and denitrification

	Decomposition	Nitrification	Denitrification	Note
EPIC	$N_{dec} = ON \times k_{dec} \times f_{en}$		$N_{den} = \begin{cases} 0 & s < 0.9 \\ NO_3 \times [1 - \exp(k_{den} \times OC \times f_T)] & s \geq 0.9 \end{cases}$	for FOM, $f_{en} = f_s f_T f_{CNR}$ for humus, $f_{en} = f_s f_T f_{OC}$
DNDC **IWSS**	$C_{dec} = OC \times k_{dec} \times f_{en,dec}$ $N_{dec} = C_{dec}/CNR$	$N_{nit} = NH_4 \times f_s \times [1 - \exp(-k_{nit} \times f_T)]$	$N_{den} = B_{den} \times (\frac{\mu}{Y} + \frac{M \times N_a O_b}{TNO}) \times f_{en,den}$	$f_{en,dec} = f_T f_{CNR} f_{OC}$ $f_{en,den} = f_T f_{pH}$
DRAINMOD	$C_{dec} = OC \times k_{dec} \times f_{en}$ $N_{dec} = C_{dec}/CNR$	$N_{nit} = \frac{NH_4}{K_{m,nit} + NH_4} \times k_{nit} \times f_{en}$	$N_{den} = \frac{NO_3}{K_{m,den} + NO_3} \times k_{den} \times f_{en,den}$	$f_{en} = \min(f_s f_T, f_T f_{pH}, f_s f_{pH})$ $f_{en,den} = f_{en} f_{OC}$
WNMM	$C_{dec} = \alpha \times OC \times k_{dec} \times f_{en,dec}$ $N_{dec} = C_{dec}/CNR$	$N_{nit} = NH_4 \times [1 - \exp(-f_{en,nit})]$	$N_{den} = \begin{cases} 0 & s < 0.8 \\ NO_3 \times [1 - \exp(-1.4OC \times f_{en,den})] & s \geq 0.8 \end{cases}$	for FOM, $\alpha = 0.4$, $f_{en,dec} = f_{CNR}\sqrt{f_s f_T}$ for humus, $\alpha = 1$, $f_{en,dec} = \sqrt{f_s f_T}$ $f_{en,nit} = f_s f_T f_{pH}$ $f_{en,den} = f_s f_T$
SWAT-N	$C_{dec} = OC \times k_{dec} \times f_{en,dec}$ $N_{dec} = C_{dec}/CNR$	$N_{nit} = NH_4 \times f_s \times f_{pH} \times [1 - \exp(-k_{nit} \times f_T)]$	$N_{den} = NO_3 \times [1 - \exp(-k_{den} \times f_{en,den})]$	$f_{en,dec} = \frac{2 f_s f_T}{f_s + f_T}$ $f_{en,den} = f_s f_T$

It is worth mentioning that agricultural nitrogen modules take different strategies to describe the significant impact of soil moisture on denitrification rate. DNDC and IWSS switch between a dry weather submodule, where denitrification is not calculated, and a wet weather submodule, where denitrification is the only biochemical process simulated. The wet weather submodule is switched on as the rain events start and is switched off when saturation rate in the top 20 cm of soil drops below 40%, or after 10 days since the rain event. Under the wet weather submodule, the growth rate of denitrifying bacteria is calculated with the Michaelis-Menten function with two substrates (nitrogen oxide and organic matter), and the denitrification rate is influenced by concentration of denitrifying biomass.

In EPIC, denitrification only occurs when the saturation rate is over 90%, and the calculation of real-time reaction rate does not involve soil saturation rate. The WNMM model sets the threshold for denitrification to start to 80% saturation, and the denitrification rate increases exponentially with higher soil moisture content. In DRAINMOD, the threshold of denitrification is expressed with the soil moisture factor f_s, which has a value of 0.0 when soil moisture drops below a user-defined threshold. This would result in a value of 0.0 for the denitrification rate. In SWAT-N, the value of f_s and denitrification rate changes significantly over the range of soil moisture content but does not drop to 0.0.

- **Immobilization**

Immobilization is of great importance in the soil nitrogen cycle because it not only affects the mass balance of inorganic nitrogen pools in the current time step but also influences the decomposition rate in the next time step by changing the availability of decomposable soil organic matters. Similar to decomposition, nitrogen flux of immobilization is generally calculated based on carbon transformations. Although the exact forms of mathematical equations can vary significantly due to the different divisions of sub-pools of soil organic matters, the basic procedures can be generalized as: a) calculate immobilized carbon (C_{imm}) as a fraction of carbon released through decomposition C_{dec}; b) calculate immobilized nitrogen (N_{imm}) according to CNR of the

entering soil organic matter sub-pool and C_{imm}; c) represent the restrictions of inorganic nitrogen availability on immobilization.

The math equations used to calculate nitrogen immobilization are summarized in Table 2. 5. FR refers to flat residues in the agricultural field. NP refers to nitrogen content in crop plant, with subscripts indicating parts of plant (CR: in crop residues) and simulation date (day: currently simulated day of the year; day-1: the previous day). E_{micro} is an empirical efficiency coefficient of microbial assimilating C_{dec}, and α_{imm} is a mass fraction of immobilized carbon over C_{dec}. In EPIC, net nitrogen immobilization is directly proportional to N_{dec}. DNDC and IWSS divide soil organic matters into 3 sub-pools (residues, biomass, and hummus), and each of the sub-pools is divided into two components (the active and stable components). C_{imm} and N_{imm} that enter each component are calculated with total C_{dec} from all sub-pools, constant empirical fractions, and constant CNR values. C_{imm} and N_{imm} would drop to the level of available inorganic nitrogen content when inorganic nitrogen is insufficient. The entire biomass sub-pool is subject to decomposition. It is worth mentioning that the aerobic biomass evolved in decomposition and immobilization is different from the denitrifying biomass B_{den}, and their mass balances and growth rates are calculated separately in the dry and wet weather submodules, respectively.

WNMM has the same division of soil organic matters as DNDC, but decomposition only occurs in the active hummus component, and all immobilized carbon and nitrogen contribute to active biomass. Active (living) biomass decays to stable (dead) biomass, and then degrades back to active hummus through first-order kinetics. As shown in Table 2. 5, nitrogen demand for immobilization is set to a constant fraction (0.048) of decomposition-derived carbon. This calculated amount is then compared to the actual amount of inorganic nitrogen released through the decomposition process. As the content of soil organic maters in sub-pools with different CNR values change over time, N_{imm} can be positive or negative, representing net decrease or increase of the soil inorganic nitrogen pool.

Table 2. 5 Mathematical expressions for immobilization and plant uptake

Model	Immobilization	Plant uptake
EPIC	$N_{imm} = \frac{N_{dec}}{ON} \times FR \times (0.016 - NP_{CR})$	$N_{pde} = NP_{opt,day} \times PB_{day} - NP_{opt,day-1} \times PB_{day-1}$
DNDC	$N_{imm} = \begin{cases} C_{dec} \times E_{micro} \times \frac{1}{CNR} & in\ the\ dry\ weather\ sub\ module \\ k_{imm} \times B_{den} \times \frac{1}{CNR} & in\ the\ \ wet\ weather\ sub\ module \end{cases}$	
IWSS	$N_{imm} = \begin{cases} C_{dec} \times E_{micro} \times \frac{1}{CNR} & in\ the\ dry\ weather\ sub\ module \\ k_{imm} \times B_{den} \times \frac{1}{CNR} & in\ the\ \ wet\ weather\ sub\ module \end{cases}$	$N_{pde} = NP_{opt,day} \times PB_{day} - NP_{act,day-1} \times PB_{day-1}$
WNMM	$N_{imm} = 0.048 C_{dec} - N_{dec}$	$N_{pde} = NP_{opt,day} \times PB_{day} - NP_{act,day-1} \times PB_{day-1}$
SWAT-N	$N_{imm} = N_{mde} - N_{dec}$	$N_{pde} = NP_{opt,day} \times PB_{day} - NP_{act,day-1} \times PB_{day-1}$
DRAINMOD	$N_{imm} = \frac{C_{imm}}{CNR}$ $C_{imm} = \alpha_{imm} \times E_{micro} \times C_{dec}$ $CNR = CNR_{min} + (CNR_{max} - CNR_{min}) \times (1 - \frac{InN}{InN_{max}})$	$N_{pde} = \frac{YLD}{100} \times (NP_{grain} + NP_{shoot} \times \frac{1 - HI}{HI} + NP_{root} \times \frac{RSR}{HI})$

Instead of immobilization, SWAT-N calculates ammonification. Ammonification can be taken as the reverse of the immobilization process and is the result of soil organic matter decomposition from 3 organic litter pools (very labile, labile, and stabile), growth and decay of microbes from 2 microbes pools (labile and stabile), and decomposition of soil organic matters from 2 humic pools (labile and stabile). Nitrate is reduced to ammonium when ammonium is depleted. The equation listed in Table 2. 5 for SWAT-N is reformed and simplified, where N_{mde} is the nitrogen demand for microbe growth. Further details on equations describing microbe growth and decay can be found in Li.et al [52].

In DRAINMOD, total soil organic matter is divided into 8 sub-pools, including 4 litter pools describing plant residues and animal waste (surface metabolic litters, soil metabolic litters, surface structural litters, and soil structural litters), 3 soil biomass pools (active, slow, and passive), and 1 surface biomass pool. Carbon and nitrogen flow from litter pools to, and transform among, the biomass pools. As shown in Table 2. 5, the CNR values of organic matters synthesized into each sub-pool change with inorganic nitrogen availability. CNR_{max} and CNR_{min} are the maximum and minimum CNR values entering a certain soil organic matter sub pool. InN_{max} is the inorganic nitrogen content that is adequate for synthesized organic matter to enter the soil organic matter sub pool with CNR_{max}.

- **Plant uptake**

In all agricultural nitrogen modules, plant uptake is a major sink of inorganic nitrogen in the soil. In all reviewed agricultural models, nitrogen plant uptake is simulated with a demand versus supply method. Available math equations describing plant nitrogen demand N_{pde} are summarized in Table 2. 5. $NP_{opt,day}$, $NP_{opt,day-1}$, $NP_{act,day}$, and $NP_{act,day-1}$ refer to optimal and actual nitrogen concentration in plants at currently simulated day or the previous day. Subscripts also indicate the part of plant (grain, shoot, and root). PB is the plant mass (mass / area). *YLD, HI*, and *RSR* are crop yield (mass / area), plant harvest index (dimensionless), and the root-to-shoot ratio of plant at maturity (dimensionless), respectively.

In DNDC, plant uptake is only considered in the dry weather module, and is estimated based on average nitrogen uptake rate, crop species, and seeding date. The crop growth module in IWSS is adapted from EPIC. EPIC, WNMM, and SWAT-N use the same equation to calculate N_{pde}, which is the difference between optimal nitrogen content in plant biomass at the current simulated day, and the actual nitrogen content in plant biomass at the previous day. DRAINMOD adapts a slightly different approach, where nitrogen contents in various parts of plant are considered.

In general, inorganic nitrogen supply is decided by inorganic nitrogen content in soil layer, plant water uptake, and diffusion rates, and is further relevant to the growth of plant roots. The equations for inorganic nitrogen supply are further referred to earlier models and literature [57], [71], [72]. When the supply of inorganic nitrogen is not sufficient to support plant uptake demand, a nitrogen stress factor is calculated based on the ratio of actual plant nitrogen content to the optimal value. The nitrogen stress factor decreases nonlinearly as inorganic nitrogen availability decreases and will constrain plant growth rates. Fixation can occur if legumes are present. The upper limit of the fixation rate is set to 2.0 kg N hectare $^{-1}$ day^{-1} in EPIC. SWAT-N assumes that nitrate is preferred to ammonium by plants, and inorganic nitrogen is taken from the ammonium pool only when the nitrate pool is depleted. DNDC and DRAINMOD assume equal preference by plant between NO_3-N and NH_4-N.

- **Gas Emissions**

Nitrogen Oxide gases (N_xO_y) are byproducts of nitrification and denitrification [73]. DNDC and IWSS report N_2O and N_2 emissions. WNMM reports only N_2O emission. In SWAT-N, total emission of N_2O and NO is reported, but the partition between N_2O and NO is not calculated. N_xO_y emission is not reported in other models. As shown in Table 2. 6, N_xO_y emissions can be estimated with either empirical formulas or first-order reaction kinetics. $NH_{4,x}$ and $NH_{3,x}$ represent ammonium and ammonia content, with subscript x indicating whether they are in the solid (s) or liquid (l) phase. AD and D are the adsorption and diffusion

coefficients. As noted earlier, f are the environmental factor parameters, with subscripts indicating the specific environmental factors and the relevant biochemical reactions.

In WNMM, DNDC, and SWAT-N, ammonia volatilization is calculated in each horizontal layer, while in DRAINMOD, volatilization only happens in the soil surface layer. Ammonia volatilization is the result of multiple physio-chemical equilibriums, as shown in equations 2.5, 2.6, and 2.7.

$$NH_{4,l}^{+} \rightleftharpoons NH_{3,l} + H^{+} \qquad \textbf{Equation 2. 5}$$

$$NH_{3,l} \rightleftharpoons NH_{3,g} \qquad \textbf{Equation 2. 6}$$

$$NH_{4,l}^{+} \rightleftharpoons NH_{4,s}^{+} \qquad \textbf{Equation 2. 7}$$

Soil characteristics and environmental factors that impact these equilibriums include soil cation exchange capacity (CEC), tortuosity, soil temperature, soil pH, and wind speed. Despite the complexity of this three-phase equilibrium system, many of these listed parameters are neglected by the nitrogen modules as they are often constant over time.

As ammonia volatilization in an acidic environment is slow, its simulation is designed as optional in DRAINMOD. When soil pH is higher than a user-defined threshold (default at 7.5), the gas diffusion is driven by the concentration gradient of ammonia between pores and the atmosphere. When soil pH is below the threshold, ammonia content is assumed to be 0.0, and ammonium partitions between the solid and aqueous phase. WNMM was developed for fields with stable pH of around 8.5, and thus, the impact of soil pH on ammonia volatilization is not considered.

Table 2. 6 Mathematical expressions for gas emissions

Model	N_xO_y Emission	NH_3 Volatilization
DNDC **IWSS**	$N_2O_{nit} = 2.95 \times 10^{-6} \times NH_4 \times (0.54 + 0.51T)$ $N_2O_{den} = (0.0006 + 0.0013AD) + (0.013 - 0.005AD)(1 - s)$ $N_{2,den} = 0.017 + (0.025 - 0.0013AD)(1 - s)$	$N_{vol} = 2NH_{3,l}\sqrt{\frac{D}{3.14}}$ $\log(K_{NH_4}) - \log(K_{H_2O})$ $= \log(NH_{4,l}) - log(NH_{3,l} \times \frac{CLAY_{max}}{CLAY}) + pH$
WNMM	$N_2O_{nit} = \alpha_{nit}N_{nit}f_{T,gas}f_{s,nit}$ $N_2O_{den} = \begin{cases} 0.05N_{den} & s \geq 1 \\ \alpha_{den}N_{den}(1 - f_{s,den}) & s < 1 \end{cases}$	$N_{vol} = NH_{4,s}[1 - \exp(-f_{vol})]$ $f_{vol} = \begin{cases} f_{T,nit}f_{wind} & surface \\ f_{T,nit}f_{CEC}f_{depth} & subsurface \end{cases}$
SWAT-N	$N_xO_{y,nit} = 2.72^{f_{T,gas}}\beta_{N_xO_y}N_{nit}\theta$	$N_{vol} = 2NH_{3,l}\sqrt{\frac{D}{3.14}}$ $\log(K_{NH_4}) - \log(K_{H_2O}) = \log(NH_{4,l}) - log(NH_{3,l}) + pH$
DRAINMOD		$N_{vol} = \frac{NH_{3,g} - NH_{3,air}}{\gamma\theta R_f Z}$

- **Environmental Factors**

The equations used to describe the impacts of environmental factors in the agricultural nitrogen modules are mostly empirical and take a variety of forms. Detailed equations are listed in Table 2. 7, and the meaning of mathematical symbols are listed in Table S 1. The value of each environmental factor is estimated under the assumption that other environmental conditions are optimum for the related biochemical reaction. In the field, multiple environmental conditions may change simultaneously and have a collective effect that can't be precisely calculated by simply multiplying the estimated factors. This estimation approach, however, is still widely applied for simplicity.

Soil Temperature The soil temperature factor f_T has a value of 1.0 at the optimum soil temperature (or in the optimum soil temperature range) and decreases linearly or exponentially when above or below this optimal value. The optimum soil temperature varies with biochemical reactions. User-defined optimum soil temperature ranges are required by DRAINMOD and SWAT-N. The soil temperature profile is determined based on the annual average soil temperature, daily air temperature, and the average depth of the soil layer according to Williams et al. [51].

Saturation The impacts of soil saturation conditions on biochemical processes are more complex. Forms of equations applied include exponential equations, first-order, second order, and fourth-order linear equations. User-defined optimum ranges of saturation rate for decomposition and nitrification, together with a user-defined threshold for denitrification to start, are required by DRAINMOD. As previously discussed, DNDC and IWSS switch between the wet and dry submodules. Denitrification is not simulated in the dry submodules, and soil moisture is not a limiting factor in the wet submodules.

Soil pH In DRAINMOD, reaction rates decrease exponentially with the increasing deviation of soil pH from the user-defined optimum range. In SWAT-N, the soil pH factor is fitted with a second-order equation. Empirical linear equations are also adopted in DNDC and

WNMM. Soil pH changes with fertilizer application, plant uptake, and nitrification, and is modified by soil buffering capacity.

CNR The factor of carbon to nitrogen ratio of organic matters (CNR) is extensively used in decomposition and immobilization processes. As previously stated, most models set constant CNR values for their organic pools. In DRAINMOD, CNR values change over time because of decomposition, immobilization, and additional supply of soil organic matters. When calculating the CNR factor f_{CNR}, DNDC uses the ratio of inorganic carbon to inorganic nitrogen, instead of CNR in organics.

Organic Carbon Due to the complexity and variability of the chemical components of soil organic matters, this environmental factor is not directly calculated based on organic matter content. Instead, it is implicitly estimated with soil bulk density, clay content, and soil depth in EPIC, DNDC (IWSS), and DRAINMOD, respectively. The vertical distribution of organic carbon is not described in the WNMM model, but the developers acknowledge that this simplification may lead to errors.

Table 2. 7 Mathematical expressions for environmental factors

Temperature	
EPIC	$f_{T,dec}\,(f_{T,den}) = \begin{Bmatrix} 0.1 + \dfrac{0.9T}{T + \exp(9.93 - 0.312T)} & T > 0 \\ 0 & T \le 0 \end{Bmatrix}$
DNDC IWSS	$f^{\dagger}_{T,dec} = \begin{Bmatrix} \dfrac{T}{30} & 0 \le T < 30 \\ 1 & 30 \le T < 40 \\ -0.04T + 2.6 & T \ge 40 \end{Bmatrix}$ $f^{\dagger}_{T,nit} = \begin{Bmatrix} \dfrac{T}{35} & 0 \le T < 35 \\ -0.1T + 4.5 & 35 \le T < 45 \\ 0 & T \ge 45 \end{Bmatrix}$ $f_{T,den} = \begin{Bmatrix} 2^{\frac{T-22.5}{10}} & T < 60 \\ 0 & T \ge 60 \end{Bmatrix}$
DRAINMOD	$f_{T,dec}, (f_{T,nit}, f_{T,den}) = \exp\,[-0.5\beta T_{opt} + \beta T(1 - \dfrac{0.5T}{T_{opt}})]$
WNMM	$f_{T,dec}\,(f_{T,den}, f_{T,gas}) = 0.1 + \dfrac{0.9T}{T + \exp(9.93 - 0.312T)}$ $f_{T,nit} = 0.41 \times \dfrac{T - 5}{10} \qquad T > 5$
SWAT-N	$f_{T,dec}\,(f_{T,nit}) = \left(\dfrac{T_{max} - T}{T_{max} - T_{opt}}\right)^{T_A} \exp\left(T_A \dfrac{T - T_{opt}}{T_{max} - T_{opt}}\right)$ $f_{T,den} = \begin{Bmatrix} \exp[0.08(\mathrm{T} - 15)] & T > 10 \\ 0.67\exp[0.43(\mathrm{T} - 10)] & T \le 10 \end{Bmatrix}$
Soil Moisture	
EPIC	$f_{s,dec} = \dfrac{\theta + WP}{n}$
DNDC IWSS	$f^{\dagger}_{s,nit} = \begin{Bmatrix} \dfrac{10s}{9} & 0 \le s < 0.9 \\ -10s + 10 & 0.9 \le s \le 1 \end{Bmatrix}$
DRAINMOD	$f_{s,den} = \begin{Bmatrix} 0 & s < s_{dn} \\ (\dfrac{s - s_{dn}}{1 - s_{dn}})^{e_1} & s \ge s_{dn} \end{Bmatrix}$ $f_{s,dec}\,(f_{s,nit}) = \begin{Bmatrix} f_{sat} + (1 - f_{sat})\left(\dfrac{1 - s}{1 - s_h}\right)^{e_2} & s_h < s \le 1 \\ 1 & s_l \le s \le s_h \\ f_{wp} + (1 - f_{wp})\left(\dfrac{s - s_{wp}}{s_l - s_{wp}}\right)^{e_2} & s_{wp} < s \le s_l \\ 0 & s \le s_{wp} \end{Bmatrix}$

Table 2.7 (cont.) Mathematical equations for environmental factors

Soil Moisture	
WNMM	$f_{s,dec} = \min\left(1, \frac{\theta}{FC}\right)$ $f_{s,nit} = \begin{cases} 1 - \frac{\theta - \mathrm{WP}}{\mathrm{n} - \mathrm{FC}} & s > FC \\ 1 & SW25 \le s \le FC \\ \frac{\theta - WP}{SW25 - WP} & s < SW25 \end{cases}$ $f_{s,den} = \exp\left(-23.77 + 23.77s\right)$ $SW_{25} = WP + 0.25(FC - WP)$
SWAT-N	$f_{s.dec} = 1 - [1 + \exp\left(\frac{s - M_{sat}}{\gamma}\right)]^{-1}$ $f_{s,nit} = -12.904s^4 + 17.651s^3 - 5.5368s^2 + 0.9975s - 0.0243$ $f_{s,den} = \exp\left[0.304 + 2.94(n - \theta) - 47(n - \theta)^2\right]$
pH	
DNDC **IWSS**	$\begin{cases} f_{pH,den,NO3} = \frac{7.14(pH - 3.8)}{22.8} \\ f_{pH,den,NO2} = 1 \\ f_{pH,den,N2O} = \frac{7.22(pH - 4.4)}{18.8} \end{cases}$
DRAINMOD	$f_{pH,dec}\left(f_{pH,nit}, f_{pH,den}\right)$ $= \begin{cases} r_{max} + (1 - r_{max})\left(\frac{pH_{max} - pH}{pH_{max} - pH_h}\right)^{e_3} & pH_h < pH \le pH_{max} \\ 1 & pH_l \le pH \le pH_h \\ r_{min} + (1 - r_{min})\left(\frac{pH - pH_{min}}{pH_l - pH_{min}}\right)^{e_3} & pH_{min} \le pH \le pH_l \end{cases}$
WNMM	$f_{pH,nit} = \begin{cases} 5.367 - 0.599pH & pH > 7.4 \\ 1 & 7.0 \le pH \le 7.4 \\ 0.307pH - 1.269 & pH < 7.0 \end{cases}$
SWAT-N	$f_{pH,nit} = -0.0604pH^2 + 0.7347pH - 1.2314$
CNR	
WNMM	$f_{CNR,dec} = \min\left[1, \exp\left(-0.693\frac{0.4CNR_{FOM} - 25}{25}\right)\right]$
Organic Carbon	
EPIC	$f_{OC,dec} = \left(\frac{\rho}{\rho_{till}}\right)^2$
DNDC **IWSS**	$f_{OC,dec} = \log\left(\frac{0.14}{\mathrm{CLAY}}\right) + 1$
DRAINMOD	$f_{OC,den} = \exp\left(-\alpha z\right)$

Table 2.7 (cont.) Mathematical equations for environmental factors

	Other factors
wind speed, WNMM	$f_{wind} = 0.335 + 0.16 \ln(u_2)$
CEC, WNMM	$f_{CEC} = \max(0, 1 - 0.038\ \mathrm{CEC})$
Soil depth, WNMM	$f_{depth} = 1 - \frac{1000Z}{1000Z + \exp(4.706 - 30.5Z)}$

†: These formulas are calculated based on the line charts in the reference paper.

2.4.2 Nitrogen Transportation

In all agricultural models, nitrogen transportation is solved with the assumption that partition and dispersion equilibriums are achieved instantly at the beginning or end of each time step. Nitrogen transformations are calculated using substrate concentrations either after or before transportation. Though actually transformation and transportation happen simultaneously, the model developers deemed the error caused by this assumption acceptable for these agricultural models with daily time steps.

The concentrations of inorganic nitrogen transported by water flows can be calculated with the advection-dispersion-reaction equation, as shown in equation 2.8. This function is numerically solved for nitrate and ammonium in DRAINMOD.

$$\frac{\partial}{\partial t}\left(\theta_l C_l + \theta_g C_g + \rho_b C_s\right) = \frac{\partial}{\partial z}\left(\theta_l D_l \frac{\partial C_l}{\partial z} + \theta_g d_g \frac{\partial C_g}{\partial z}\right) - \frac{\partial (v_l C_l)}{\partial z} + S_o \quad \textbf{Equation 2. 8}$$

Alternatively, empirical formulas can be used. In WNMM, the calculation of ammonium transportation through leaching ($NH_{4\ loss}$, kg N ha^{-1} day^{-1}) is simplified to an empirical equation as shown in equation 2.9:

$$NH_{4\ loss} = WNH_4\left(1 - \exp\left(-\frac{Q}{FC}\right)\right) \quad \textbf{Equation 2. 9}$$

where WNH_4 is the total mass of ammonium in the soil layer (kg N ha^{-1}), FC is field capacity and Q is the water leaching rate (m day^{-1}). EPIC uses a similar empirical equation for nitrate transportation as shown in equation 2.10:

$$NO_{3\ loss} = WNO_3\left(1 - \exp\left(-\frac{Q}{UL}\right)\right) \quad \textbf{Equation 2. 10}$$

where WNO_3 is the total mass of nitrate in the soil layer (kg N ha^{-1}), and UL is the upper limit of water storage. On top of calculating inorganic nitrogen concentrations in

soil water, SWAT-N uses a constant fraction to divide each nitrogen pool into mobile and immobile fractions. Only mobile nitrogen can be carried by surface runoff, lateral subsurface flow, and leaching (into deep groundwater) to leave the simulated soil system.

As shown in Table 2. 2, only EPIC calculates organic nitrogen losses with sediment transport. It is calculated with an empirical equation regulated by sediment production and organic nitrogen concentration in the topmost soil layer.

2.5 Discussions and Conclusions

This chapter begins with a comprehensive review of the current understanding of nitrogen transformations in bioretention systems. Previous studies have reported on successful fitting of decomposition, nitrification, and denitrification processes in bioretention systems with zero-order kinetics, first-order kinetics, and Michaelis-Menten equations. However, further research is still needed to ascertain other nitrogen transformation pathways associated with microbial activity, the influence of plants, and the impacts of environmental and operational factors in bioretention systems.

Next, a review of available modeling tools for nitrogen in bioretention systems reveals that current stormwater models are effective at simulating hydraulic processes in bioretention systems but are not capable of accurately describing nitrogen transformations and removal under the influence of fluctuating temperature and soil moisture conditions. Statistical models have limitations that hinder their ability to simulate specific bioretention systems or generate time series data of effluent loads, effluent concentrations, and biochemical reaction rates that are necessary for selecting the best design of bioretention structures, operational conditions, or valve control rules. Incorporating statistical models into current stormwater models does not provide satisfactory prediction accuracy of nitrogen removal rates. However, process-based nitrogen models, developed either in combination with hydraulic modules of current stormwater models or independently with hydraulic analysis included, have the potential to yield higher accuracy in nitrogen simulation, but no such models have been developed for bioretention systems. Conversely, agricultural models calculate biochemical reaction rates in the nitrogen cycle in detail, while their hydraulic modules are less suitable for bioretention systems.

Through a case study, the strengths and weaknesses of using current stormwater and agricultural models to simulate nitrogen removal in urban stormwater bioretention systems were demonstrated and compared. This experience highlighted the conclusion that current stormwater and agricultural models are not readily applicable for accurately simulating nitrogen removal rates in urban stormwater bioretention systems, nor can they predict nitrogen removal under environmental and operational conditions that changes with time. However, leveraging the mathematical equations utilized in nitrogen modules of agricultural models and integrating them with the hydraulic module of stormwater models presents an efficient approach to improve nitrogen simulation accuracy for urban bioretention systems.

The mathematical equations and structure of nitrogen modules in six current agricultural models are reviewed to aid in developing the Nitrogen Removal Models (NRM) as extensions to stormwater models. While equations related to decomposition, nitrification, denitrification, and environmental factors can be utilized, distinctions between urban stormwater bioretention systems and agricultural fields must be considered. Modifications to nitrogen modules in agricultural models are necessary to enhance suitability for urban stormwater bioretention systems.

References

[1] L. Li and A. P. Davis, “Urban Stormwater Runoff Nitrogen Composition and Fate in Bioretention Systems,” Environ Sci Technol, vol. 48, no. 6, pp. 3403–3410, Mar. 2014, doi: 10.1021/es4055302.

[2] T. A. Bonde, T. H. Nielsen, M. Miller, and J. Sorensen, “Arginine ammonification assay as a rapid index of gross N mineralization in agricultural soils,” Biol Fertil Soils, vol. 34, no. 3, pp. 179–184, Sep. 2001, doi: 10.1007/s003740100395.

[3] C. M. Cho, D. L. Burton, and C. Chang, “Kinetic formulation of oxygen consumption and denitrification processes in soil,” Can J Soil Sci, vol. 77, no. 2, pp. 253–260, May 1997, doi:10.4141/S96-056.

[4] L. Liu, F. Wang, S. Xu, W. Sun, Y. Wang, and M. Ji, “Woodchips bioretention column for stormwater treatment: Nitrogen removal performance, carbon source and microbial community analysis,” Chemosphere, vol. 285, p. 131519, 2021, doi: https://doi.org/10.1016/j.chemosphere.2021.131519.

[5] X. Fang, R. Zheng, X. Guo, Q. Fu, F. Fan, and S. Liu, “Yak excreta-induced changes in soil microbial communities increased the denitrification rate of marsh soil under warming conditions,” Applied Soil Ecology, vol. 165, p. 103935, 2021, doi: https://doi.org/10.1016/j.apsoil.2021.103935.

[6] B. Singh, B. Singh, and T. Singh, “Potential and kinetics of nitrification in soils from semiarid regions of northwestern India,” Arid Soil Research and Rehabilitation, vol. 7, no. 1, pp. 39–50, Jan. 1993.

[7] X. Jiang, X. Shi, W. Liu, and A. L. Wright, “Kinetics of net nitrification associated with soil aggregates under conventional and no-tillage in a subtropical rice soil,” Plant Soil, vol. 347, no. 1–2, SI, pp. 305–312, Oct. 2011, doi: 10.1007/s11104-011-0849-0.

[8] L. J. Liu, F. Wang, S. H. Xu, W. Sun, Y. Wang, and M. Ji, “Woodchips bioretention column for stormwater treatment: Nitrogen removal performance, carbon source and microbial community analysis,” Chemosphere, vol. 285, 2021, doi: 10.1016/j.chemosphere.2021.131519.

[9] A. Skorobogatov, J. He, A. Chu, and B. Valeo Caterina and van Duin, “The impact of media, plants and their interactions on bioretention performance: A review,” SCIENCE OF THE TOTAL ENVIRONMENT, vol. 715, May 2020, doi: 10.1016/j.scitotenv.2020.136918.

[10] E. V Lopez-Ponnada, T. J. Lynn, S. J. Ergas, and J. R. Mihelcic, “Long-term field performance of a conventional and modified bioretention system for removing dissolved nitrogen species in stormwater runoff,” Water Res, vol. 170, p. 115336, 2020, doi: https://doi.org/10.1016/j.watres.2019.115336.

[11] P. Shrestha, S. Hurley, and E. Adair, “Soil Media CO2 and N2O Fluxes Dynamics from Sand-Based Roadside Bioretention Systems,” Water (Basel), vol. 10, no. 2, p. 185, 2018, doi: 10.3390/w10020185.

[12] J. Liu, D. J. Sample, J. S. Owen, J. Li, and G. Evanylo, “Assessment of Selected Bioretention Blends for Nutrient Retention Using Mesocosm Experiments,” J Environ Qual, vol. 43, no. 5, pp. 1754–1763, Sep. 2014, doi: https://doi.org/10.2134/jeq2014.01.0017.

[13] S. Le Coustumer, T. D. Fletcher, A. Deletic, S. Barraud, and P. Poelsma, “The influence of design parameters on clogging of stormwater biofilters: A large-scale column study,” Water Res, vol. 46, no. 20, pp. 6743–6752, 2012, doi: https://doi.org/10.1016/j.watres.2012.01.026.

[14] K. Beven and P. Germann, “Macropores and water flow in soils revisited,” Water Resour Res, vol. 49, no. 6, pp. 3071–3092, Jun. 2013, doi: https://doi.org/10.1002/wrcr.20156.

[15] J. Read, T. D. Fletcher, T. Wevill, and A. Deletic, “Plant Traits that Enhance Pollutant Removal from Stormwater in Biofiltration Systems,” Int J Phytoremediation, vol. 12, no. 1, pp. 34–53, Nov. 2009, doi: 10.1080/15226510902767114.

[16] J. Read, T. Wevill, T. Fletcher, and A. Deletic, “Variation among plant species in pollutant removal from stormwater in biofiltration systems,” Water Res, vol. 42, no. 4, pp. 893–902, 2008, doi: https://doi.org/10.1016/j.watres.2007.08.036.

[17] E. G. I. Payne, T. Pham, A. Deletic, B. E. Hatt, P. L. M. Cook, and T. D. Fletcher, “Which species? A decision-support tool to guide plant selection in stormwater biofilters,” Adv Water Resour, vol. 113, pp. 86–99, 2018, doi: https://doi.org/10.1016/j.advwatres.2017.12.022.

[18] S. Wang et al., “Nitrogen removal from urban stormwater runoff by stepped bioretention systems,” Ecol Eng, vol. 106, pp. 340–348, 2017, doi: https://doi.org/10.1016/j.ecoleng.2017.05.055.

[19] E. Kavehei, B. Shahrabi Farahani, G. A. Jenkins, C. Lemckert, and M. F. Adame, “Soil nitrogen accumulation, denitrification potential, and carbon source tracing in bioretention basins,” Water Res, vol. 188, p. 116511, 2021, doi: https://doi.org/10.1016/j.watres.2020.116511.

[20] H. Daims, S. Lücker, and M. Wagner, “A New Perspective on Microbes Formerly Known as Nitrite-Oxidizing Bacteria,” Trends Microbiol, vol. 24, no. 9, pp. 699–712, Sep. 2016, doi: 10.1016/j.tim.2016.05.004.

[21] R. Bai, D. Xi, J. Z. He, H. W. Hu, Y. T. Fang, and L. M. Zhang, “Activity, abundance and community structure of anammox bacteria along depth profiles in three different paddy soils,” Soil Biol Biochem, vol. 91, pp. 212–221, 2015, doi: 10.1016/j.soilbio.2015.08.040.

[22] W. L. Silver, D. J. Herman, and M. K. Firestone, “Dissimilatory nitrate reduction to ammonium in upland tropical forest soils,” Ecology, vol. 82, no. 9, pp. 2410–2416, Sep. 2001, doi: https://doi.org/10.1890/0012-9658(2001)082[2410:DNRTAI]2.0.CO;2.

[23] M. Shirdashtzadeh, L. H. C. Chua, and L. Brau, “Microbial Communities and Nitrogen Transformation in Constructed Wetlands Treating Stormwater Runoff,” FRONTIERS IN WATER, vol. 3, 2022, doi: 10.3389/frwa.2021.751830.

[24] D. Subramaniam, P. Mather, S. Russell, and J. Rajapakse, “Dynamics of Nitrate-Nitrogen Removal in Experimental Stormwater Biofilters under Intermittent Wetting and Drying,” Journal of Environmental Engineering, vol. 142, no. 3, p. 04015090, Mar. 2016, doi: 10.1061/(ASCE)EE.1943-7870.0001043.

[25] Y. Chen et al., “Nitrogen process in stormwater bioretention: effect of the antecedent dry days on the relative abundance of nitrogen functional genes,” Water Science and Technology, vol. 86, no. 5, pp. 1269–1283, 2022, doi: 10.2166/wst.2022.228.

[26] Y. Chen et al., “Bioretention system mediated by different dry–wet alterations on nitrogen removal: Performance, fate, and microbial community,” Science of The Total Environment, vol. 827, p. 154295, 2022, doi: https://doi.org/10.1016/j.scitotenv.2022.154295.

[27] Q. Wu et al., “Metabolism characteristics of nitrogen functional microorganisms in bioretention system under multiple dry-wet alternation,” Journal of Water Process Engineering, vol. 53, p. 103685, 2023, doi: https://doi.org/10.1016/j.jwpe.2023.103685.

[28] J. J. Zhou, J. Q. Xiong, J. J. Ni, X. F. Xie, and Y. Z. Liu, “Nitrogen transfer and transformation in bioretention cells under low temperature conditions,” SCIENCE OF THE TOTAL ENVIRONMENT, vol. 871, 2023, doi: 10.1016/j.scitotenv.2023.162087.

[29] J. Xiong et al., “Purification effect of bioretention with improved filler on runoff pollution under low temperature conditions,” J Environ Manage, vol. 295, p. 113065, 2021, doi: https://doi.org/10.1016/j.jenvman.2021.113065.

[30] F. Wang, H. K. Wang, C. Sun, and Z. Yan, “Conventional bioretention column with Fe-hydrochar for stormwater treatment: Nitrogen removal, nitrogen behaviour and microbial community analysis,” Bioresour Technol, vol. 334, 2021, doi: 10.1016/j.biortech.2021.125252.

[31] M. T. Randall and A. Bradford, “Bioretention gardens for improved nutrient removal,” WATER QUALITY RESEARCH JOURNAL OF CANADA, vol. 48, no. 4, pp. 372–386, 2013, doi: 10.2166/wqrjc.2013.016.

[32] Z. S. Weng et al., “Corncob-pyrite bioretention system for enhanced dissolved nutrient treatment: Carbon source release and mixotrophic denitrification,” Chemosphere, vol. 306, 2022, doi: 10.1016/j.chemosphere.2022.135534.

[33] R. Wang, X. Zhang, and M.-H. Li, “Predicting bioretention pollutant removal efficiency with design features: A data-driven approach,” J Environ Manage, vol. 242, pp. 403–414, 2019, doi: https://doi.org/10.1016/j.jenvman.2019.04.064.

[34] R. L. Gilliom, C. D. Bell, T. S. Hogue, and J. E. McCray, “Adequacy of Linear Models for Estimating Stormwater Best Management Practice Treatment Performance,” J Sustain Water Built Environ, vol. 6, no. 4, p. 04020016, Nov. 2020, doi: 10.1061/JSWBAY.0000921.

[35] K. Zhang et al., “The impact of stormwater biofilter design and operational variables on nutrient removal - a statistical modelling approach,” Water Res, vol. 188, p. 116486, 2021, doi: https://doi.org/10.1016/j.watres.2020.116486.

[36] A. H. Elliott and S. A. Trowsdale, “A review of models for low impact urban stormwater drainage,” Environmental Modelling & Software, vol. 22, no. 3, pp. 394–405, 2007, doi: https://doi.org/10.1016/j.envsoft.2005.12.005.

[37] V. M. Jayasooriya and A. W. M. Ng, “Tools for Modeling of Stormwater Management and Economics of Green Infrastructure Practices: a Review,” Water Air Soil Pollut, vol. 225, no. 8, p. 2055, 2014, doi: 10.1007/s11270-014-2055-1.

[38] Hydrologic Engineering Center, “HEC-HMS Technical Reference Manual,” 2021. Accessed: Dec. 23, 2021. [Online]. Available: https://www.hec.usace.army.mil/confluence/hmsdocs/hmstrm

[39] DHI Inc., “Hydrologic Modeling Inventory Model Description Form ,” Jun. 1999. Accessed: Dec. 23, 2021. [Online]. Available: https://ut8vn2uf0te1sqbrasrcrold-wpengine.netdna-ssl.com/wp-content/uploads/sites/103/2018/09/MOUSE.pdf

[40] W. W. Walker and J. D. Walker, “P8 Urban Catchment Model Version 3.5,” 2015. Accessed: Dec. 22, 2021. [Online]. Available: http://www.wwwalker.net/p8/v35/webhelp/p8HelpWebMain.html

[41] R. Pitt and J. Voorhees, “WinSLAMM and Low Impact Development,” in LID Conference, College Park, Maryland, 2004. Accessed: Dec. 23, 2021. [Online]. Available: http://unix.eng.ua.edu/~rpitt/Publications/Stormwater%20Management%20and%20Modeling/WinSLAMM%20and%20LID%20Pitt%20MD%202004.pdf

[42] U.S. EPA, “Better Assessment Science Integrating Point and Nonpoint Sources BASINS User’s Manual Version 4.5,” RTP, North Carolina, Jan. 2019.

[43] L. A. Rossman, “Storm Water Management Model User’s Manual Version 5.1,” Cincinnati, Sep. 2015. Accessed: Jan. 26, 2022. [Online]. Available: https://www.epa.gov/sites/default/files/2019-02/documents/epaswmm5_1_manual_master_8-2-15.pdf

[44] Tetra Tech, “SUSTAIN-programmer’s manual: simulation engine,” Edison, NJ, 2012.

[45] T. H. F. Wong, T. D. Fletcher, H. P. Duncan, J. R. Coleman, and G. A. Jenkins, “A Model for Urban Stormwater Improvement: Conceptualization,” in Global Solutions for Urban Drainage, Reston, VA: American Society of Civil Engineers, Sep. 2002, pp. 1–14. doi: 10.1061/40644(2002)115.

[46] H. S. Fowdar, T. H. Neo, S. L. Ong, J. Hu, and D. T. McCarthy, “Performance analysis of a stormwater green infrastructure model for flow and water quality predictions,” J Environ Manage, vol. 316, p. 115259, 2022, doi: https://doi.org/10.1016/j.jenvman.2022.115259.

[47] S.-S. Baek et al., “A novel water quality module of the SWMM model for assessing low impact development (LID) in urban watersheds,” J Hydrol (Amst), vol. 586, p. 124886, 2020, doi: https://doi.org/10.1016/j.jhydrol.2020.124886.

[48] J. Wang, L. H. C. Chua, and P. Shanahan, “Modeling and designing for nitrogen removal in bioretention basins,” Environmental Modelling & Software, vol. 146, p. 105212, 2021, doi: https://doi.org/10.1016/j.envsoft.2021.105212.

[49] C. D. Bell, C. L. Tague, and S. K. McMillan, “A model of hydrology and water quality for stormwater control measures,” Environmental Modelling & Software, vol. 95, pp. 29–47, 2017, doi: https://doi.org/10.1016/j.envsoft.2017.05.007.

[50] K. Nurulhuda, D. S. Gaydon, Q. Jing, M. P. Zakaria, P. C. Struik, and K. J. Keesman, “Nitrogen dynamics in flooded soil systems: an overview on concepts and performance of models,” J Sci Food Agric, vol. 98, no. 3, pp. 865–871, Feb. 2018, doi: https://doi.org/10.1002/jsfa.8683.

[51] J. R. Williams, C. A. Jones, and P. T. Dyke, “A Modeling Approach to Determining the Relationship Between Erosion and Soil Productivity,” Transactions of the ASAE, vol. 27, no. 1, pp. 129–144, 1984, doi: https://doi.org/10.13031/2013.32748.

[52] C. Li, S. Frolking, and T. A. Frolking, “A model of nitrous oxide evolution from soil driven by rainfall events: 1. Model structure and sensitivity,” Journal of Geophysical Research: Atmospheres, vol. 97, no. d9, pp. 9759–9776, Jun. 1992.

[53] M. A. Youssef, R. W. Skaggs, G. M. Chescheir, and J. W. Gilliam, “THE NITROGEN SIMULATION MODEL, DRAINMOD-N II,” Transactions of the ASAE, vol. 48, no. 2, pp. 611–626, 2005, doi: https://doi.org/10.13031/2013.18335.

[54] M. A. Brevé, R. W. Skaggs, J. E. Parsons, and J. W. Gilliam, “DRAINMOD-N, A NITROGEN MODEL FOR ARTIFICIALLY DRAINED SOIL,” Transactions of the ASAE, vol. 40, no. 4, pp. 1067–1075, 1997, doi: https://doi.org/10.13031/2013.21359.

[55] Y. Li et al., “A spatially referenced water and nitrogen management model (WNMM) for (irrigated) intensive cropping systems in the North China Plain,” Ecol Modell, vol. 203, no. 3, pp. 395–423, 2007, doi: https://doi.org/10.1016/j.ecolmodel.2006.12.011.

[56] T. Pohlert, J. A. Huisman, L. Breuer, and H.-G. Frede, “Integration of a detailed biogeochemical model into SWAT for improved nitrogen predictions—Model development, sensitivity, and GLUE analysis,” Ecol Modell, vol. 203, no. 3, pp. 215–228, 2007, doi: https://doi.org/10.1016/j.ecolmodel.2006.11.019.

[57] S. L. Neitsch, Arnold J. G., Kiniry J. R., and Williams J. R., Soil and Water Assessment Tool Theoretical Documentation Version 2009. Texas Water Resources Institute, 2011.

[58] Y. Y. Zhang, Q. X. Shao, A. Z. Ye, H. T. Xing, and J. Xia, "Integrated water system simulation by considering hydrological and biogeochemical processes: model development, with parameter sensitivity and autocalibration," Hydrol. Earth Syst. Sci., vol. 20, no. 1, pp. 529–553, Feb. 2016, doi: 10.5194/hess-20-529-2016.

[59] G. Hanrahan and G. Chan, "NITROGEN," in Encyclopedia of Analytical Science, Elsevier, 2005, pp. 191–196. doi: 10.1016/B0-12-369397-7/00401-5.

[60] B. Sun et al., "Bacillus subtilis biofertilizer mitigating agricultural ammonia emission and shifting soil nitrogen cycling microbiomes," Environ Int, vol. 144, p. 105989, 2020, doi: https://doi.org/10.1016/j.envint.2020.105989.

[61] R. A. Tirpak, A. N. Afrooz, R. J. Winston, R. Valenca, K. Schiff, and S. K. Mohanty, "Conventional and amended bioretention soil media for targeted pollutant treatment: A critical review to guide the state of the practice," Water Res, vol. 189, p. 116648, Feb. 2021, doi: 10.1016/j.watres.2020.116648.

[62] A. C. Gold, S. P. Thompson, and M. F. Piehler, "Nitrogen cycling processes within stormwater control measures: A review and call for research," Water Res, vol. 149, pp. 578–587, 2019, doi: https://doi.org/10.1016/j.watres.2018.10.036.

[63] "NOAA. Daily summaries of temperature local details." https://www.ncdc.noaa.gov/cdo-web/datasets/GHCND/locations/CITY:US120041/detail (accessed Dec. 21, 2021).

[64] "USGS National Water Information System." Accessed: Dec. 21, 2021. [Online]. Available: https://nwis.waterdata.usgs.gov/nwis/uv?site_no=275917082222500

[65] D. K. Todd and L. W. Mays, Groundwater Hydrology, 3rd ed. 2004.

[66] K. Twitty and J. Rice, "Chapter 10 Water Table Cotrol," in National Engineering Handbook Part 624, United States Department of Agriculture, 2001.

[67] L. A. Rossman and W. C. Huber, "Storm Water Management Model Reference Manual Volume III – Water Quality," Washington DC, Dec. 2016. Accessed: Jan. 26, 2022. [Online]. Available: https://nepis.epa.gov/Exe/ZyPDF.cgi/P100P2NY.PDF?Dockey=P100P2NY.PDF

[68] H. Zhao, Y. Yang, X. Shu, Y. Wang, and Q. Ran, "Adsorption of organic molecules on mineral surfaces studied by first-principle calculations: A review," Adv Colloid Interface Sci, vol. 256, pp. 230–241, Jun. 2018, doi: 10.1016/j.cis.2018.04.003.

[69] S. Igielski, "Understanding urban stormwater denitrification in bioretention internal water storage zones," Water environment research, vol. 91, no. 1, pp. 32–44, Jan. 2019.

[70] B. J. Halaburka, G. H. LeFevre, and R. G. Luthy, “Evaluation of Mechanistic Models for Nitrate Removal in Woodchip Bioreactors,” Environ Sci Technol, vol. 51, no. 9, pp. 5156–5164, May 2017, doi: 10.1021/acs.est.7b01025.

[71] H. Johnsson, L. Bergstrom, P.-E. Jansson, and K. Paustian, “Simulated nitrogen dynamics and losses in a layered agricultural soil,” Agric Ecosyst Environ, vol. 18, no. 4, pp. 333–356, 1987, doi: https://doi.org/10.1016/0167-8809(87)90099-5.

[72] C. A. Jones, “A survey of the variability in tissue nitrogen and phosphorus concentrations in maize and grain sorghum,” Field Crops Res, vol. 6, pp. 133–147, 1983, doi: https://doi.org/10.1016/0378-4290(83)90053-9.

[73] V. Rassamee, “Effect of oxic and anoxic conditions on nitrous oxide emissions from nitrification and denitrification processes,” Biotechnol Bioeng, vol. 108, no. 9, pp. 2036–2045, Sep. 2011.

3 Development of Nitrogen Removal Model (NRM) as Extensions to Current Storm Water Management Model (SWMM)[2]

3.1 Introduction

As concluded in the previous chapter's review and case study, the development of Nitrogen Removal Models (NRMs) for urban stormwater bioretention systems is necessary. The most efficient approach is through modifying nitrogen modules from agricultural models and merging them with hydraulic modules in existing stormwater models. Given its wide application and the detailed description on the physical structure and hydraulic processes of the bioretention system in its LID module, the Storm Water Management Model (SWMM) is selected as the basis for NRMs development.

For several reasons, developing NRMs for bioretention systems poses a significant challenge. Firstly, the biochemical processes underlying nitrogen transformations in bioretention systems are still under investigation. While decomposition, nitrification, and denitrification are the most intensively discussed nitrogen-related biochemical processes, studies on their reaction kinetics in stormwater bioretention systems are limited. Previous literature has described reaction rates with various equations such as zero-order, first-order, and the Michaelis-Menten equations [1]–[6]. However, it remains unclear which dynamic best suits nitrogen cycling simulations in bioretention systems. Furthermore, various other nitrogen transformation mechanisms such as plant uptake, dissimilatory nitrate reduction to ammonium (DNRA), annamox, and comammox are yet to be fully characterized. Ongoing debates surround their contribution to nitrogen cycling [7]–[9]. The lack of understanding on important nitrogen transformation mechanisms hinders the development of process-based models.

The second challenge in developing NRMs is striking a balance between the level of detail simulated and the number of parameters being calibrated. While inclusion of more

[2] This chapter is published in part in: J. Li, T. B. Culver, P. P. Persaud, and J. M. Hathaway, "Developing Nitrogen Removal Models for Stormwater Bioretention Systems," Water Research, p. 120381, 2023, doi: https://doi.org/10.1016/j.watres.2023.120381

processes and a higher number of calibrated parameters can lead to higher prediction accuracy of nitrogen removal, the improved performance can also be a result of overparameterization [10]. Additionally, it is essential to develop NRMs that are resilient to uncertainties in initial conditions. This is particularly important for urban stormwater bioretention systems, where complete records of initial nitrogen species and organic matter contents are often unavailable.

To tackle these challenges, NRMs must simplify the nitrogen cycle in bioretention systems while integrating relevant environmental factors such as soil moisture and temperature and test the best fitting reaction kinetics. This study developed six different NRMs by simplifying the nitrogen cycle into two complexity levels and testing three reaction kinetics for each level. To improve the models' resilience to uncertainty caused by estimated initial conditions, warm-up periods are added at the beginning of the simulated period. In section 3.2 of this chapter, we provide an overview of the general structure and assumptions of all the NRMs, followed by a detailed description of the two different types of NRMs with model structures at different complexity levels in sections 3.3 and 3.4, respectively.

3.2 Overview of the Nitrogen Removal Model (NRM)

- **Time and spatial resolution.**

Simulating nitrogen transformations in stormwater BMPs requires small time steps since rain events often complete within hours. Shorter time steps will also assist the adoption of automatic valve control of stormwater BMPs [11], [12]. The time step of NRMs can be decided by users and is dependent on the time step of hydraulic simulations carried out in SWMM. In terms of the spatial resolution, site-scale simulation is sufficient for nitrogen transformations in each bioretention system given their small scale. When mixed plant species are grown [13], [14], a single conceptual plant species is used to approximate the average plant nitrogen uptake rate. Depending on the design of specific bioretention system and available soil moisture data, the soil media layer and storage layer can be divided into horizontal layers defined by users. Each soil layer is simulated as a continuous stirred-tank reactor where the reactants are immediately completely mixed after waterflow enters or leaves the soil layer.

- **Nitrogen transformation and transportation processes.**

Figure 3. 1 shows the nitrogen transformation and transportation processes relevant to urban stormwater bioretention systems, where optional processes are marked with dashed lines. Surface run-on, surface overflow, and deposition only occur in the top-most soil layer. Leaching to groundwater and underdrain effluent are only simulated for the bottom layer. Important nitrogen species that should be simulated in stormwater bioretention include organic nitrogen (OrgN), nitrate nitrogen (NO_3-N), and ammonium nitrogen (NH_4-N). In NRMs, they are transported with water flows between soil layers. Biochemical processes that take place in each soil layer are influenced by environmental conditions through different values of environmental factors.

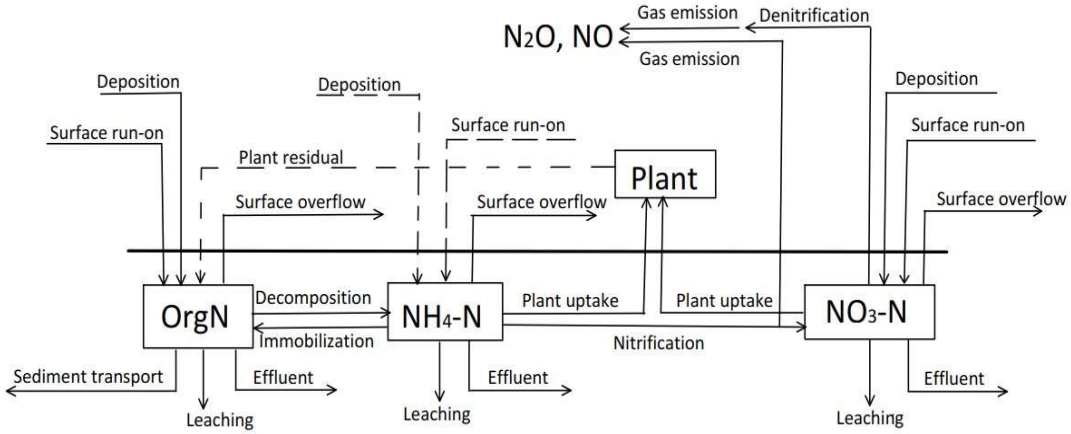

Figure 3. 1 Nitrogen transformation and transportation in urban stormwater bioretention systems

Surface run-on is the main nitrogen sources in stormwater bioretention systems. Plant residuals may release a significant amount of organic nitrogen if they are not periodically harvested. At some locations, animal waste may be another seasonal source of organic nitrogen. Organic matter from falling leaves and animal waste are estimated together with the process of external organic matter supply. Different from agricultural fields, fertilizers are rarely applied in urban bioretention systems and thus is not considered in NRMs.

The sinks of nitrogen in bioretention systems include transport of dissolved organic nitrogen (DON) and inorganic nitrogen via water flows (leaching into deeper groundwater, underdrain effluent, and surface runoff), plant uptake, and gas emissions

through the nitrification-denitrification process. In urban areas, the quality and quantity of surface runoff, drainage, and leaching can have a significant impact on the surface water, sewer pipelines, and groundwater of downstream catchments. Therefore, these data are important indicators to measure the performances of stormwater bioretention systems and need accurate simulation. DON concentrations in the effluent from stormwater BMPs may be similar in magnitude to nitrate concentrations [15], [16], which means that DON losses with water flows should not be overlooked. In Figure 3.1, ammonia volatilization is not included, since it is unlikely to happen given the low TN level in stormwater BMPs media and the acidic to neutral soil pH environments [17]. Emission of N_2O is roughly estimated and reported by NRMs as it is a known greenhouse gas. In contrast, the release of N_2 is not tracked as it does not have negative environmental impacts.

Although other biochemical processes including DNRA, anammox, and comammox have been discussed in the literature, quantitative data and math descriptions on these processes are currently limited [18]. It is thus suggested that the overall nitrogen transformation to be expressed only with processes included in Figure 3. 1, and the impacts of other processes to be expressed with empirical environmental factors.

- **The six versions of NRM.**

To find the best balance between nitrogen prediction accuracy and complexity level of model structures, and test out the best fitting reaction kinetics, a total of six versions of NRMs are developed as listed in Table 3. 1. Detailed description of simulated nitrogen pools and reaction kinetics are provided in section 3.3 and 3.4.

Table 3. 1 Summary of the six versions of Nitrogen Removal Models

Notation	Complexity	Kinetics
SP-0	Single pool of TN	Zero-order
SP-1	Single pool of TN	First-order
SP-m	Single pool of TN	Michaelis-Menten
3P-0	Three pools of nitrogen	Zero-order
3P-1	Three pools of nitrogen	First-order
3P-m	Three pools of nitrogen	Michaelis-Menten

3.3 The Single Pool (SP) Models

The SP models have a low complexity level focusing on a single pool of total nitrogen (TN). Each single pool model is combined with zero order kinetics, first order kinetics, or Michaelis-Menten equations to simulate nitrogen loss through denitrification and plant uptake to form the SP-0, SP-1, and SP-m models, respectively. As shown in Figure 3. 2 (a), nitrogen in all forms in the bioretention systems are included in the single TN pool. The sources of TN are stormwater inflow and external organic matter supply. TN exits bioretention systems through denitrification, plant uptake,bottom exfiltration, and underdrain effluent. The organic nitrogen supply and underdrain effluent are marked with dashed line because they only apply to the topmost and bottom layers respectively.

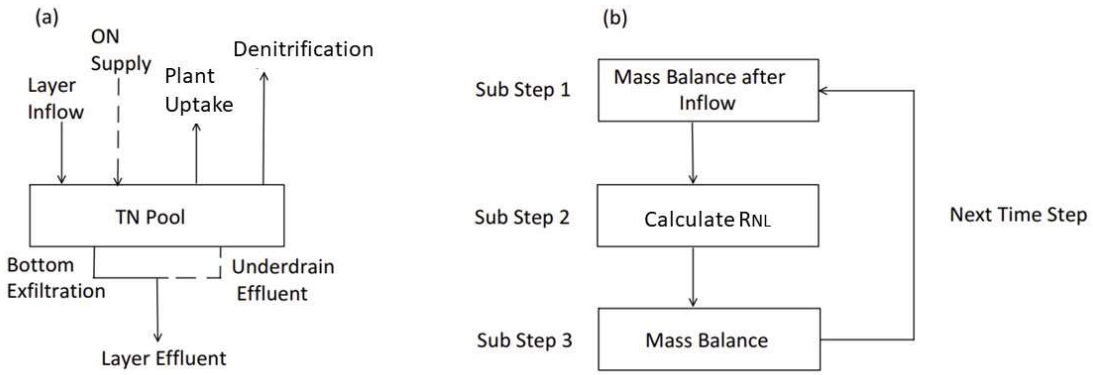

Figure 3. 2 Model structure of the Single Pool (SP) models. (a) simplified nitrogen cycling of one soil layer (b) the sub steps in each time step

The sub-steps of calculations in each time step are shown in Figure 3. 2 (b). In sub-step 1, SP models will calculate TN content in the soil layer after TN enters the layer with equation 3.1, where *WTN0* and *WTN* are the masses of TN in the soil layer before and after layer inflow, in units of mg TN/kg dry soil. V_{inflow} is the total volume of the layer inflow during this time step (in Liters). CTN_{in} is the TN concentration in layer inflow (mg/L), and M_{soil} is the mass of dry soil (kg).

$$\boldsymbol{WTN = WTN_0 + V_{inflow} \times CTN_{in} / M_{soil}} \qquad \textbf{Equation 3. 1}$$

In sub-step 2, total nitrogen loss through denitrification and plant uptake (R_{NL}) is calculated with equations 3.2, 3.3, and 3.4 in SP-0, SP-1, and SP-m, respectively.

$$\boldsymbol{R_{NL} = min\begin{Bmatrix} k_0 \times timestep \times f_{sat} \times f_{tem} \\ WTN \times p_{lia} \end{Bmatrix}} \qquad \textbf{Equation 3. 2}$$

$$R_{NL} = WTN \times p_{lia} \times f_{sat} \times (1 - \exp(-k_1 \times timestep \times f_{tem})) \quad \text{Equation 3. 3}$$

$$R_{NL} = WTN \times p_{lia} \times k_2 \times f_{sat} \times f_{tem} \times timestep \,/\, (WTN \times p_{lia} + k_m) \quad \text{Equation 3. 4}$$

where p_{lia} is the percentage of total nitrogen that is liable to biochemical reactions and remains the same throughout the simulation. R_{NL} is in units of mg TN/kg dry soil and is calculated for each time step. k_m is the Michaelis constant, and k_0, k_1, and k_2 are maximum gas emission rates under ideal environmental conditions. For SP-0, R_{NL} is not influenced by the mass of reactant unless it takes up all liable TN. For SP-1 and SP-m, liable TN is the reactant for all biochemical processes. The factors of saturation rate and temperature (f_{sat} and f_{tem}) are calculated with equations 3.5 and 3.6, as in WNMM and SWAT-N [19]–[21].

$$f_{sat} = a + b \times sat + c \times sat^2 + d \times sat^3 \quad \text{Equation 3. 5}$$

$$f_{tem} = 0.1 + \frac{0.9T}{T + \exp(9.93 - 0.312T)} \quad \text{Equation 3. 6}$$

The ratio of N_2O emission and denitrification has been reported to range from 0.3% to 200% according to land use, soil depth, temperature, and microbe community [22]–[25]. For this work, it is estimated that N_2O emissions takes up 1% of R_{NL} in the SP models.

Sub-step 3 calculates TN mass balance at the end of each time step with equation 3.7, in which V_{eff} and CTN_{eff} are the volume and TN concentration of layer effluent in each time step.

$$WTN_t = WTN - R_{g,p} - \frac{CTN_{eff} \times V_{eff}}{M_{soil}} + \frac{ONSP \times timestep}{M_{soil}} \quad \text{Equation 3. 7}$$

ONSP is the rate of external organic nitrogen supply in the unit of mg N/min and is only applied to the topmost layer. The value of *ONSP* depends on the selected species and management practices of the bioretention system's plants. CTN_{eff} of one layer is used as the inflow TN concentration of the next lower soil layer. WTN_t is the resulting TN content at the end of this time step and is also the initial TN content of the next time step.

3.4 The 3 Pools (3P) Models

As shown in Figure 3. 3 (a), nitrogen is simulated with three separate pools in the 3P models: the organic nitrogen pool (ON), the ammonium-nitrogen (NH_4-N) pool, and the nitrate-nitrogen (NO_3-N) pool. Organic nitrogen supply with external organic matter is

only simulated in the surface soil layer. Nitrogen transforms among different pools through decomposition, nitrification, and denitrification, and is lost through denitrification, layer effluent, and plant uptake.

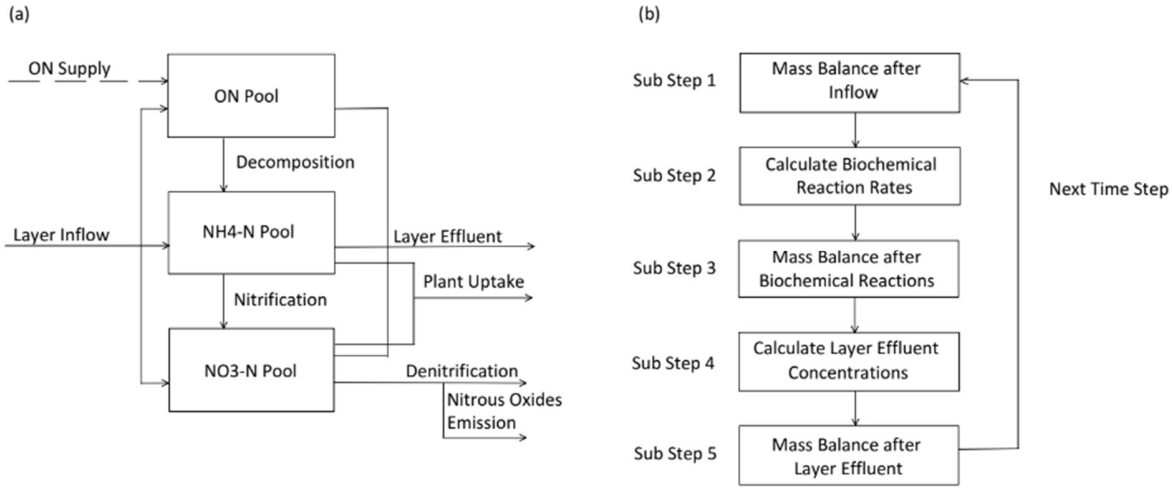

Figure 3. 3 Model structure of the 3 Pools (3P) models. (a) simplified nitrogen cycling of one soil layer (b) the sub steps in each time step

As shown in Figure 3. 3 (b), the nitrogen-related processes are simulated in five sub-steps. In the first sub-step, supplies to the three nitrogen pools are assumed to be immediately completely mixed within that layer of the bioretention system. In equations 3.8 to 3.10, *WON, WNH4*, and *WNO3* are the mass per layer of organic nitrogen, NH_4-N, and NO_3-N, respectively, and the subscripts '0' and 'a' refer to values before and after immediate complete mixing of layer inflow and old water in the simulated soil layer.

$$\boldsymbol{WON_a = WON_0 + V_{inflow} \times CON_{in} / M_{soil}} \quad \textbf{Equation 3. 8}$$

$$\boldsymbol{WNH_{4a} = WNH_{40} + V_{inflow} \times CNH_{4in} / M_{soil}} \quad \textbf{Equation 3. 9}$$

$$\boldsymbol{WNO_{3a} = WNO_{30} + V_{inflow} \times CNO_{3in} / M_{soil}} \quad \textbf{Equation 3. 10}$$

In the second sub-step, zero-order kinetics (equation 3.11), first-order kinetics (equation 3.12), or the Michaelis-Menten function (equation 3.13) are used to calculate biochemical reaction rates in 3P-0, 3P-1, and 3P-m models, respectively.

$$\boldsymbol{R_{bio} = k_{bio} \times timestep \times f_{sat} \times f_{tem}} \quad \textbf{Equation 3. 11}$$

$$\boldsymbol{R_{bio} = WN_{bio} \times f_{sat} \times (1 - \exp(-k_{bio} \times timestep \times f_{tem}))} \quad \textbf{Equation 3. 12}$$

$$\boldsymbol{R_{bio} = WN_{bio} \times k_{bio} \times f_{sat} \times f_{tem} \times timestep / (WN_{bio} + k_m)} \quad \textbf{Equation 3. 13}$$

In these equations, R_{bio} is the amount of nitrogen that goes through a specific biochemical process in each time step, calculated in unit of mg N/kg soil. k_{bio} and WN_{bio} are reaction rate and mass of reactant for specific biochemical reaction. For decomposition, WN_{dec} is the mass of organic nitrogen that is prone to decomposition. It is calculated using the ON content and a pre-set faction of p_{lia}, which represents the constant fraction of organic matter that is liable to decompose. f_{tem} is calculated with equation 3.6. f_{sat} in the 3P models is simplified to equation 3.14 to avoid overparameterization, as k_{bio} of each biochemical process is calibrated separately. In 3P models, denitrification starts when soil saturation rate reaches a user-defined threshold of saturation rate, but all other biochemical reactions are not affected by saturation rate. The emitted N_2O gas is estimated as 1% of $R_{denitrification}$ [26].

$$f_{sat} = \begin{cases} 0 & if\ sat < threshold \\ 1 & if\ sat \geq threshold \end{cases} \qquad \textbf{Equation 3. 14}$$

For sub-step 3, mass balances of the three nitrogen pools after all biochemical processes are calculated with equations 3.15 to 3.17, where subscript *b* refers to nitrogen mass after biochemical processes. Organic nitrogen supply represented by *ONSP* is only calculated for the topmost soil layer. At time steps when the sum of NH_4-N consumed by nitrification and plant uptake is greater than WNH_{4a}, plant uptake rate of the time step is reduced to 0, and the amount of NH_4-N consumed by nitrification is then reduced to the smaller value between calculated $R_{nitrification}$ and WNH_{4a}. The same procedure is applied to NO_3-N.

$$WON_b = WON_a - R_{deco} + ONSP \times timestep/M_{soil} \qquad \textbf{Equation 3. 15}$$

$$WNH_{4b} = WNH_{4a} + R_{deco} - R_{nitr} - R_{plant} \qquad \textbf{Equation 3. 16}$$

$$WNO_{3b} = WNO_{3a} + R_{nitr} - R_{deni} - R_{plant} \qquad \textbf{Equation 3. 17}$$

In sub-step 4, concentrations of ON (CON_{eff}), NH_4-N (CNH_{4eff}), and NO_3-N (CNO_{3eff}) in layer effluent are calculated. It is assumed that all NH_4-N and NO_3-N are in pore water, and a constant percentage (p_{DON}) of ON is dissolved. In the last sub-step, the amount of nitrogen lost through layer effluent is subtracted from the nitrogen pools, and the resulted masses per layer are used as the initial values of the next time step.

3.5 NRM Model Calibration

The Dynamically Dimensioned Search algorithm [28], which has been proven to outperform other global search algorithms for complex models with high convergence speed, was used to calibrate NRM in this study. The SP models and 3P models were all calibrated to minimize the sum of root mean square error of EMC ($SSEC_k$) calculated with equation 3.18 or sum of root mean square error of load ($SSEL_k$) calculated with equation 3.19, with subscript k indicating the calibrated model.

$$\boldsymbol{SSEC_k = \sum_s^{forms\ of\ nitrogen}(RMSE\ of\ EMC_{k,s}/(\max(EMC_{k,s}) - \min\ (EMC_{k,s}))}$$

Equation 3. 18

$$\boldsymbol{SSEL_k = \sum_s^{forms\ of\ nitrogen}(RMSE\ of\ Load_{k,s}/(\max(Load_{k,s}) - \min\ (Load_{k,s}))}$$

Equation 3. 19

$$\boldsymbol{RMSE\ of\ EMC_{k,s} = \sqrt{\sum_{i=1}^{n_{event}}(EMC_{k,s,obs} - EMC_{k,s,sim})^2 / n_{event}}} \quad \textbf{Equation 3. 20}$$

$$\boldsymbol{RMSE\ of\ Load_{k,s} = \sqrt{\sum_{i=1}^{n_{event}}(Load_{k,s,obs} - Load_{k,s,sim})^2 / n_{event}}} \quad \textbf{Equation 3. 21}$$

The SP models simulate all nitrogen species with one TN pool in soil layers, and only calculate TN load in the underdrain effluent. Thus, there is only one form of nitrogen considered for equations 3.18 and 3.19. Conversely, the 3P models simulate organic nitrogen, NO_3-N, and NH_4-N in different nitrogen pools, and report effluent concentration or discharged loads of the three forms of nitrogen separately. Thus, three forms of nitrogen are considered in equations 3.18 and 3.19. The root-mean square errors between the NRM simulated and lab-tested EMCs or loads of the three nitrogen species are first calculated with equations 3.20 and 3.21 and then scaled to their respective observed results' variances. This approach ensures that all nitrogen species' simulated results are appropriately calibrated, even when their observed concentrations or loads differ in magnitudes. It should be noted that if certain nitrogen species' concentration falls below the detection limit in lab experiments, any simulated concentrations lower than the detection limit are considered accurate, and the difference between observed value and simulated value goes to 0.

Table 3. 2 presents the calibrated parameters of the SP and 3P models. The total number of calibrated parameters for each SP and 3P model is limited to 4-8 to avoid

overparameterization. In 3P models, 4-8 parameters that describe reaction kinetics are calibrated and the description of saturation rate factor is simplified. In contrast, 4parameters are calibrated to describe the saturation rate factor in SP models, nitrogen loss is only simulated with 1 optimal reaction rate in SP-0 and SP-1, or 2 reaction rate parameters in SP-m.

Table 3. 2 Calibrated parameters in the six versions of NRM.

Module	Calibrated Parameters	Meaning	units
SP-0	k_0	0-order reaction rate of nitrogen loss	mg N / kg soil / min
	p_{dis}	percentage of dissolved TN	%
	a, b, c, d	constant coefficients used to calculate the saturation factor f_{sat}	unitless
SP-1	k_1	1st-order reaction rate of nitrogen loss	/ min
	p_{dis}	percentage of dissolved TN	%
	a, b, c, d	constant coefficients used to calculate the saturation factor f_{sat}	unitless
SP-m	k_2	maximum reaction rate of nitrogen loss	mg N / kg soil / min
	k_m	Michaelis constant of gas emission	mg N / kg soil
	p_{dis}	percentage of dissolved TN	%
	a, b, c, d	constant coefficients used to calculate the saturation factor f_{sat}	unitless
3P-0	k_{deco}	0-order reaction rate of decomposition	mg N / kg soil / min
	k_{nitr}	0-order reaction rate of nitrification	
	k_{deni}	0-order reaction rate of denitrification	
	k_{plant}	0-order reaction rate of plant uptake	
3P-1	k_{deco}	1st-order reaction rate of decomposition	/ min
	k_{nitr}	1st-order reaction rate of nitrification	
	k_{deni}	1st-order reaction rate of denitrification	
	k_{plant}	1st-order reaction rate of plant uptake	
3P-m	k_{deco}	maximum reaction rate of decomposition	mg N / kg soil / min
	k_{nitr}	maximum reaction rate of nitrification	
	k_{deni}	maximum reaction rate of denitrification	
	k_{plant}	maximum reaction rate of plant uptake	
	k_{mdeco}	Michaelis constant of decomposition	mg N / kg soil
	k_{mnitr}	Michaelis constant of nitrification	
	k_{mdeni}	Michaelis constant of denitrification	
	k_{mplant}	Michaelis constant of plant uptake	

3.6 Summary

This chapter developed six NRM models and presented the approach to calibration. Demonstration of the performance of these models will occur in subsequent chapters. In chapter 4, the models are applied to a set of laboratory experiments, while in chapter 5 selected models are applied to a field bioretention system.

References

[1] T. A. Bonde, T. H. Nielsen, M. Miller, and J. Sorensen, “Arginine ammonification assay as a rapid index of gross N mineralization in agricultural soils,” *Biol Fertil Soils*, vol. 34, no. 3, pp. 179–184, Sep. 2001, doi: 10.1007/s003740100395.

[2] C. M. Cho, D. L. Burton, and C. Chang, “Kinetic formulation of oxygen consumption and denitrification processes in soil,” *Can J Soil Sci*, vol. 77, no. 2, pp. 253–260, May 1997, doi: 10.4141/S96-056.

[3] L. Liu, F. Wang, S. Xu, W. Sun, Y. Wang, and M. Ji, “Woodchips bioretention column for stormwater treatment: Nitrogen removal performance, carbon source and microbial community analysis,” *Chemosphere*, vol. 285, p. 131519, 2021, doi: https://doi.org/10.1016/j.chemosphere.2021.131519.

[4] X. Fang, R. Zheng, X. Guo, Q. Fu, F. Fan, and S. Liu, “Yak excreta-induced changes in soil microbial communities increased the denitrification rate of marsh soil under warming conditions,” *Applied Soil Ecology*, vol. 165, p. 103935, 2021, doi: https://doi.org/10.1016/j.apsoil.2021.103935.

[5] B. Singh, B. Singh, and T. Singh, “Potential and kinetics of nitrification in soils from semiarid regions of northwestern India,” *Arid Soil Research and Rehabilitation*, vol. 7, no. 1, pp. 39–50, Jan. 1993.

[6] X. Jiang, X. Shi, W. Liu, and A. L. Wright, “Kinetics of net nitrification associated with soil aggregates under conventional and no-tillage in a subtropical rice soil,” *Plant Soil*, vol. 347, no. 1–2, SI, pp. 305–312, Oct. 2011, doi: 10.1007/s11104-011-0849-0.

[7] C. Li, C. Peng, P.-C. Chiang, Y. Cai, X. Wang, and Z. Yang, “Mechanisms and applications of green infrastructure practices for stormwater control: A review,” *J Hydrol (Amst)*, vol. 568, pp. 626–637, 2019, doi: https://doi.org/10.1016/j.jhydrol.2018.10.074.

[8] A. C. Gold, S. P. Thompson, and M. F. Piehler, “Nitrogen cycling processes within stormwater control measures: A review and call for research,” *Water Res*, vol. 149, pp. 578–587, 2019, doi: https://doi.org/10.1016/j.watres.2018.10.036.

[9] A. Skorobogatov, J. He, A. Chu, and B. Valeo Caterina and van Duin, “The impact of media, plants and their interactions on bioretention performance: A review,” *SCIENCE OF THE TOTAL ENVIRONMENT*, vol. 715, May 2020, doi: 10.1016/j.scitotenv.2020.136918.

[10] K. Beven*, “How far can we go in distributed hydrological modelling?,” *Hydrol Earth Syst Sci*, vol. 5, no. 1, pp. 1–12, 2001, doi: 10.5194/hess-5-1-2001.

[11] P. P. Persaud, A. A. Akin, B. Kerkez, D. T. McCarthy, and J. M. Hathaway, “Real time control schemes for improving water quality from bioretention cells,” *Blue-Green Systems*, vol. 1, no. 1, pp. 55–71, 2019.

[12] P. Zhang, Y. Cai, and J. Wang, “A simulation-based real-time control system for reducing urban runoff pollution through a stormwater storage tank,” *J Clean Prod*, vol. 183, pp. 641–652, 2018, doi: https://doi.org/10.1016/j.jclepro.2018.02.130.

[13] “Virginia DEQ stormwater design specification No. 3 Grass Channels,” Mar. 2011. Accessed: Dec. 21, 2021. [Online]. Available: https://swbmpvwrrc.wp.prod.es.cloud.vt.edu/wp-content/uploads/2017/11/BMP-Spec-No-3_GRASS-CHANNELS_v1-9_03012011.pdf

[14] “Virginia DEQ Stormwater Design Specification vol. No.9 Bioretention,” Mar. 2011. Accessed: Dec. 21, 2021. [Online]. Available: https://www.swbmp.vwrrc.vt.edu/wp-content/uploads/2017/11/BMP-Spec-No-9_BIORETENTION_v1-9_03012011.pdf

[15] M. Mohtadi, “Adsorption of Compounds that Mimic Urban Stormwater Dissolved Organic Nitrogen,” *Water environment research*, vol. 89, no. 2, pp. 105–116, Feb. 2017.

[16] L. Li and A. P. Davis, “Urban Stormwater Runoff Nitrogen Composition and Fate in Bioretention Systems,” *Environ Sci Technol*, vol. 48, no. 6, pp. 3403–3410, Mar. 2014, doi: 10.1021/es4055302.

[17] E. Kavehei, B. Shahrabi Farahani, G. A. Jenkins, C. Lemckert, and M. F. Adame, “Soil nitrogen accumulation, denitrification potential, and carbon source tracing in bioretention basins,” *Water Res*, vol. 188, p. 116511, 2021, doi: https://doi.org/10.1016/j.watres.2020.116511.

[18] A. C. Gold, S. P. Thompson, and M. F. Piehler, “Nitrogen cycling processes within stormwater control measures: A review and call for research,” *Water Res*, vol. 149, pp. 578–587, 2019, doi: https://doi.org/10.1016/j.watres.2018.10.036.

[19] Y. Li *et al.*, “A spatially referenced water and nitrogen management model (WNMM) for (irrigated) intensive cropping systems in the North China Plain,” *Ecol Modell*, vol. 203, no. 3, pp. 395–423, 2007, doi: https://doi.org/10.1016/j.ecolmodel.2006.12.011.

[20] T. Pohlert, J. A. Huisman, L. Breuer, and H.-G. Frede, “Integration of a detailed biogeochemical model into SWAT for improved nitrogen predictions—Model development, sensitivity, and GLUE analysis,” *Ecol Modell*, vol. 203, no. 3, pp. 215–228, 2007, doi: https://doi.org/10.1016/j.ecolmodel.2006.11.019.

[21] J. Li and T. B. Culver, “Review of process-based nitrogen model for agricultural fields with implications for nitrogen simulations in stormwater BMPs,” *Environmental Modelling & Software*, vol. 151, p. 105363, 2022, doi: https://doi.org/10.1016/j.envsoft.2022.105363.

[22] M. Tenuta and B. Sparling, “A laboratory study of soil conditions affecting emissions of nitrous oxide from packed cores subjected to freezing and thawing,” *Can J Soil Sci*, vol. 91, no. 2, pp. 223–233, May 2011, doi: 10.4141/cjss09051.

[23] P. H. Masscheleyn, R. D. DeLaune, and W. H. Patrick Jr, “Methane and nitrous oxide emissions from laboratory measurements of rice soil suspension: effect of soil oxidation-reduction status,” *Chemosphere*, vol. 26, no. 1–4, pp. 251–260, 1993, doi: 10.1016/0045-6535(93)90426-6.

[24] J. G. Koops, M. L. van Beusichem, and O. Oenema, “Nitrogen loss from grassland on peat soils through nitrous oxide production,” *Plant Soil*, vol. 188, no. 1, pp. 119–130, 1997, doi: 10.1023/A:1004252012290.

[25] G. Braker, P. Dorsch, and L. R. Bakken, “Genetic characterization of denitrifier communities with contrasting intrinsic functional traits,” *FEMS Microbiol Ecol*, vol. 79, no. 2, pp. 542–554, 2012, doi: 10.1111/j.1574-6941.2011.01237.x.

[26] E. Kavehei, N. Iram, M. Rezaei Rashti, G. A. Jenkins, C. Lemckert, and M. F. Adame, “Greenhouse gas emissions from stormwater bioretention basins,” *Ecol Eng*, vol. 159, p. 106120, 2021, doi: https://doi.org/10.1016/j.ecoleng.2020.106120.

[27] B. A. Tolson and C. A. Shoemake, “Dynamically dimensioned search algorithm for computationally efficient watershed model calibration DYNAMICALLY DIMENSIONED SEARCH ALGORITHM,” *Water Resour Res*, vol. 43, no. 1, Jan. 2007.

4 NRM Calibration and Validation with Laboratory Data[3]

In this chapter, the six versions of NRM are calibrated and validated with a dataset from a laboratory bioretention experiment [1]. Their performances are evaluated in terms of prediction accuracy of percent removal of total loads (PRL_{total}) and event mean concentrations (EMCs). Statistical analysis is also performed to determine their ability to reproduce the dataset from laboratory experiment. Time series generated by the 3P-1 and 3P-m models are further analyzed to better understand the functions of these better performing processes-based models.

4.1 Dataset and Pretreatment

4.1.1 Dataset from Lab Experiment

The dataset used in this chapter is from a laboratory study of bioretention outlet valve control strategies [1]. Four types of column outlet control rules were developed and applied to large, vegetated soil columns. The 30-cm diameter columns were 117 cm tall, plus 10 cm of ponding depth, and there were 5 duplicate columns per outlet control type. The designs of the four types of columns are shown in Figure 4. 1. Each column has a bottom exfiltration outlet that mimics waterflow from the unlined bottom of bioretention systems to deeper groundwater, and an underdrain outlet that is controlled by the given rules. The four underdrain control rules are as follows: a) the Free Draining (FD) rule: The drainage outlets are left open throughout the experiment period; b) the Internal Water Storage (IWS) rule: drainage outlet is raised to a height of 45 cm from bottom of column to mimic bioretention systems with internal water storage layers; c) the Soil Moisture (SM) rule: the underdrain outlets are actively controlled with a real time control (RTC) algorithm to try to maintain field capacity in the column throughout the experimental period; and d) the Volume Control (VC) rule: the underdrain outlets are actively controlled with a RTC algorithm to try to maintain a 30 cm submerged zone throughout

[3] This chapter is published in part in: J. Li, T. B. Culver, P. P. Persaud, and J. M. Hathaway, "Developing Nitrogen Removal Models for Stormwater Bioretention Systems," Water Research, p. 120381, 2023, doi: https://doi.org/10.1016/j.watres.2023.120381

the experimental period. Active control practices are based on real-time monitoring data of soil moisture and rainfall predictions.

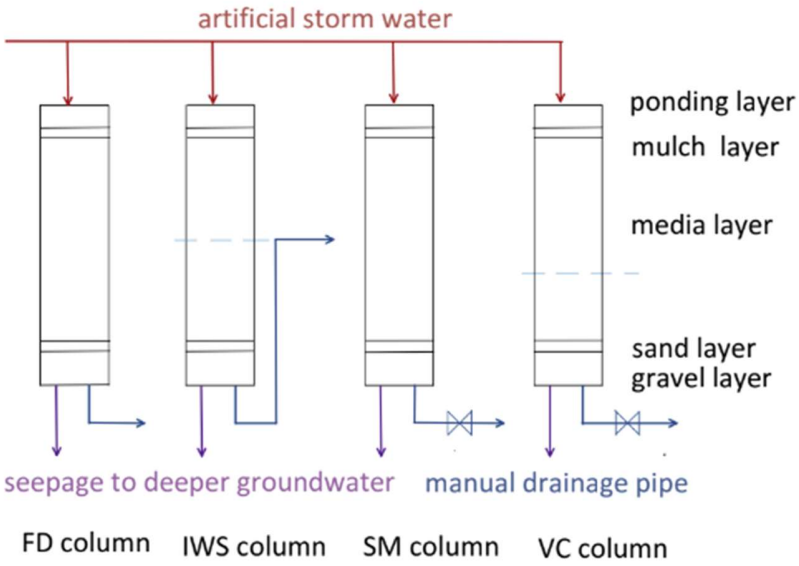

Figure 4. 1 Diagram of the four types of columns

Two soil moisture sensors were applied to each column at the depth of 30 cm and 60 cm. Starting from August 2019, synthetic stormwater was applied to the columns mimicking 12 recorded natural precipitation events in Knoxville, Tennessee, assuming a typical 20:1 sizing ratio of contributing drainage area to bioretention. The applied events ranged from 2.3 to 25.4 mm, with a median depth of 9.4 mm. The EMCs of NO_3-N and NH_4-N in synthetic stormwater and column underdrain outlets of each event were recorded. The average inflow NO_3-N and NH_4-N concentrations was 1.65 and 0.63 mg/L, and no organic matter was added. Sensor-tested time series of soil moisture content are also available.

The advantage of this dataset is that it records differences of nitrogen removal performances from the same initial soil under various hydrologic conditions, while mimicking bioretention performance under different engineering designs of drainage outlets and RTC algorithms. Further details of lab design and test methods are discussed in the published paper [1].

4.1.2 Pretreatment of Soil Moisture Time Series Raw Data

Before used for calibration, the original data from the soil moisture sensors with 1 min time steps are smoothed to time series with 5 min steps to minimize influences of sensor noises. For all columns, discontinuous missing data are replaced with the average of the previous and the next record. Missing data is also found for a continuous period of less than 30 min during a 7-day dry period during. Given that the soil moisture condition is very stable during this long dry period, these missing data are replaced with the average value of the previous and next 30 min.

Noise in soil moisture time series can lead to negative values of calculated flow rates, which interferes with the NRMs calibration. To ensure the development of effective water flow time series, two data smoothing steps are applied. Firstly, a 30-minute centered running average is calculated over the 42-day experimental period. Secondly, an additional code is used to eliminate noise during dry periods when soil moisture is expected to be more stable. This code searches for the range of soil moisture values within a specified time period and calculates the average value if the range is smaller than the noise threshold. If the range of soil moisture within the time period is larger than the noise threshold, the code searches for the range within a smaller period. The cursor moves to the next time step whenever an average value is calculated. The exact noise thresholds used are 0.02 for 24-hour time periods and 0.01 for 12 hours, 6 hours, 3 hours and 30 min periods based on observations of the raw data. If the range of soil moisture in a 30-minute time period is larger than 0.01, the current timing and soil moisture value will be taken, and the cursor will move to the next time step.

As an example of the results, Figure 4. 2 shows the time series of soil moisture content in one of the FD columns at a depth of 30 cm before and after the two-step smoothing process. During the dry period, the raw data frequently fluctuates with a difference of 0.01 or 0.02 without any observed inflow or discharge of water. Such fluctuations are considered as noise and are removed through the two-step smoothing process. After this process, most of the noise was successfully eliminated, leading to more reliable data for the next steps. However, based on observations of time series

graphs, one FD column and one IWS column were excluded from further simulation because of unreliable soil moisture records.

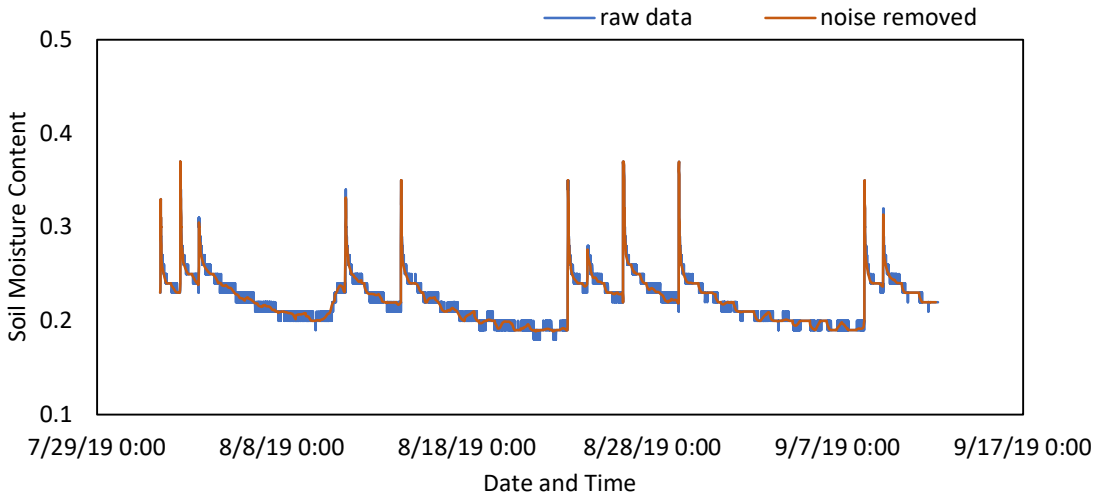

Figure 4. 2 Time series of soil moisture content in one of the FD columns at 30 cm depth, raw data and final time series after noise is removed.

Given the design of columns and control rules, average soil moisture content of the entire soil column is calculated in different ways for different types of columns. The IWS columns were conceptualized as two 45 cm thick vertical soil layers, while the FD, SM, and VC columns were separated into three 30 cm thick vertical layers. Sensor recorded soil moisture data are used for the top and bottom layers of all columns. The soil moisture contents of the middle layers of the FD and SM columns were estimated by the averages of two sensor-recorded time series. Since the Volume Control rule should create a more distinct difference in moisture contents between the lower level and the upper levels, the upper sensor time series (at 30 cm) was also applied to the middle layer of the VC columns. For each column, the average soil moisture content is estimated with the average of all soil layers in the column, and soil porosity is estimated as the maximum recorded soil moisture content.

Figure 4. 3 displays the time series of soil saturation rate averaged over each column type. All four column types reach a saturation rate higher than 0.7 in 11 out of the 12 events. IWS columns have a higher saturation rate during dry periods, followed by VC columns, while SM columns have the lowest saturation rates throughout the entire experiment period. These observations correspond well with the characteristics of the

four control rules. The IWS rule maintains a saturated layer of 45 cm, whereas VC columns maintain a saturated layer of 30 cm. Conversely, FD columns are drier than the IWS and VC columns as no saturated layer is maintained. SM columns have the lowest saturation rate because the Soil Moisture rule aims to keep soil moisture content at field capacity level even during events.

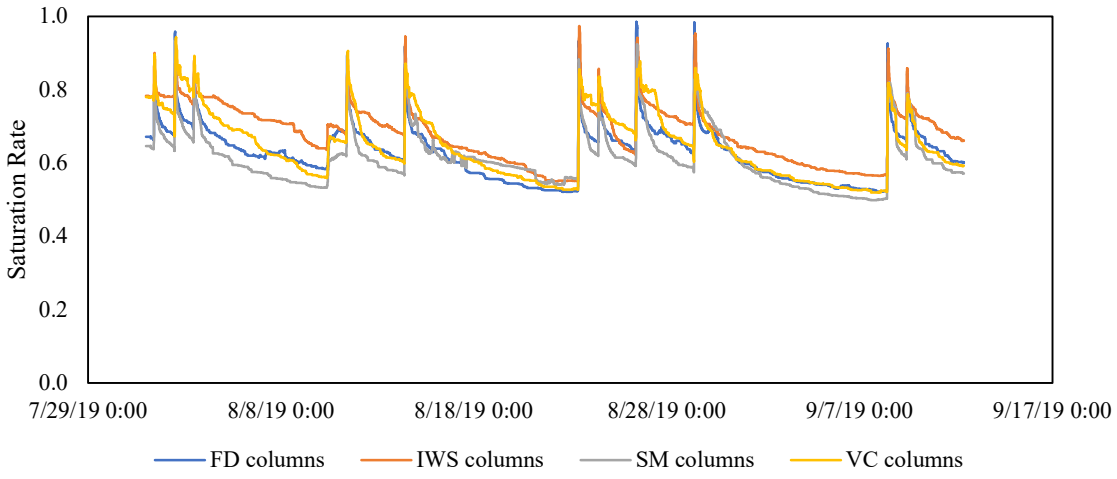

Figure 4. 3 Soil saturation rate of the entire soil column, averaged over 4 (for FD and IWS) and 5 (SM and VC) columns of each type of control rule applied.

4.1.3 Simulating Hydraulic Processes with SWMM

As stated in chapter 3, the six versions of NRM are developed as extensions to current stormwater models, and SWMM is selected as the basis for NRM due to its wide application and detailed description of hydraulic processes in LID. For this dataset, a SWMM LID model is calibrated to generate the time series of stormwater infiltration into the soil column. Given that important soil parameters, such as porosity, saturate hydraulic conductivity, field capacity etc. are similar among all columns, and that the valve operations of SM and VC columns, as well as high water level in the IWS column cannot be simulated in SWMM, the SWMM LID hydraulic model is only calibrated with soil saturation rate time series of the 5 FD columns. The calibrated set of parameters is then used to generate time series of stormwater infiltration rate into soil layers for all other columns.

In the SWMM model, one sub catchment is 100% occupied by one bio-retention cell. Thickness of the surface layer, soil media layer, and storage layer are set according to

column design parameters. Total precipitation of each event is given by lab record, and total precipitation is evenly distributed within 15, 30 or 45 min starting at 9:00 AM on days with predicted rain events. Parameters of the soil layer are calibrated according to the Nash-Sutcliffe efficiency coefficient (NSE) and the peak-weighted root mean square error (PWRMSE) calculated with equations 4.1 and 4.2.

$$\mathbf{NSE} = \mathbf{1} - \frac{\sum_{t=0}^{t_{end}} (sat_{obs}^{t} - sat_{SWMM}^{t})^2}{\sum_{t=0}^{t_{end}} (sat_{obs}^{t} - \overline{sat_{obs}})^2} \qquad \textbf{Equation 4. 1}$$

$$\boldsymbol{PWRMSE} = \sqrt{\sum_{t=0}^{t_{end}} ((sat_{obs}^{t} - sat_{SWMM}^{t})^2 \times \frac{sat_{obs}^{t} - \overline{sat_{obs}}}{2 \times \overline{sat_{obs}}})} \qquad \textbf{Equation 4. 2}$$

In equations 4.1 and 4.2, sat_{obs}^{t} and sat_{SWMM}^{t} are average saturation rate of the FD column and the saturation rate of bioretention system simulated by SWMM at time step *t*. As shown in Table 4. 1, the calibrated parameter values fall within the recommended ranges provided in the SWMM help file, and the resulting NSE and PWRMSE values confirm good accuracy. The NSE and PWRMSE of soil saturation rate simulated by SWMM for all columns ranged in 0.16-0.90 (average 0.74) and 0.009-0.088 (average 0.024), respectively.

Table 4. 1 Calibration results of the SWMM LID model

Porosity	Ks (mm/hour)	Field Capacity	Wilting Point	Conductivity Slope	Suction Head (mm)	NSE	PWRMSE
0.38	11	0.225	0.024	40	2	0.8648	0.0098

Time series of stormwater infiltration rates into the soil column and evapotranspiration are calculated with the calibrated SWMM LID model for all columns, and time series of underdrain effluent flows and internal flows between soil layers are generated using mass balance calculations. The time series of SWMM simulated infiltration rates, average soil saturation rate, and soil moisture content in each soil layer are used as input data for these calculations. Figure 4. 4 shows the percent error of simulated total volume of stormwater infiltration (to soil column), underdrain effluent, and evapotranspiration (EVT) according to column type. The percent errors fall within the ranges of (-0.02% to 0.24%) and (-1.03% to 0.95%) for total stormwater infiltration volume and total underdrain effluent volume, respectively. For EVT, the error range is (0.88% to 3.42%) with one outlier of column VC2. Despite the high percent error

(110%), we consider the calibration result acceptable since the total EVT from lab tests is notably smaller for this column (4.36 L) compared to other columns (average 25.43 L excluding VC2). Additionally, the SWMM simulated total EVT is within the range of total EVT tested for other columns. Further details are provided in Table S 2 in the supplementary material.

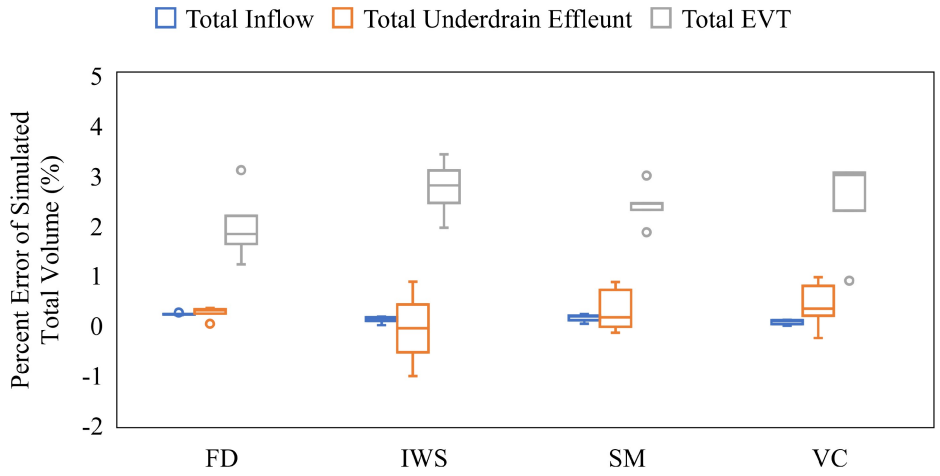

Figure 4. 4 Percent error of simulated total volume of stormwater inflow, underdrain effluent, and evapotranspiration of the entire experiment period

4.2 Calibration of the NRMs

4.2.1 Data for Calibration

The available data for calibration comprises EMCs of total inorganic nitrogen (TIN), which is the sum of NO_3-N and NH_4-N, in the underdrain effluent for 12 events from 18 columns. Since no organic matter is added to the artificial stormwater inflow, the organic nitrogen concentration in the underdrain effluent was not tested in the lab experiment and was assumed to be negligible. As stated in chapter 3, NRM is calibrated with the Dynamically Dimensioned Search (DDS) algorithm to minimize the root mean square error calculated with equations 3.18 and 3.20.

$$\boldsymbol{SSEC_k = \sum_s^{forms\ of\ nitrogen}(RMSE\ of\ EMC_{k,s}/(\max(EMC_{k,s}) - \min\ (EMC_{k,s}))}$$

Equation 3. 22

$$\boldsymbol{RMSE\ of\ EMC_{k,s} = \sqrt{\sum_{i=1}^{n_{event}}(EMC_{k,s,obs} - EMC_{k,s,sim})^2 / n_{event}}}$$

Equation 3. 23

For the single pool (SP) models, TN concentration is assumed to be equal TIN concentrations. For three pool (3P) models, NO_3-N and NH_4-N were included in the calculations as the two forms of nitrogen, and OrgN was not calibrated. To test the performance of each NRM in predicting nitrogen effluent concentrations and removal rates under various moisture conditions, each of the six versions of NRM was calibrated with only datapoints from FD columns (48 datapoints), and the other types of columns were used for validation (168 datapoints). 300 iteration times was selected for this calibration based on the observation that after 300 iterations, the calculated $SSEC_k$ becomes stable. The calibration was repeated five times, and the five calibration sets were compared to explore the stability of calibration results.

To quantify the improvement brought by NRM, the SWMM LID water quality module (referred to as the SWQ model thereafter) was calibrated as a comparison model. In the SWMM LID module, pollutant concentration in underdrain effluent is determined by its inflow concentration and a constant user-inputted removal rate (%). Thus, the single nutrient calibration parameter (the removal rate) in the SWQ model was calibrated manually with 1% step for NO_3-N and NH_4-N to minimize sum of error calculated with equations 4.3 and 4.4.

$$\sum \Delta EMC_{SWQ,NH4} = \sum_{calibrated\ events}(EMCNH_{4,SWQ} - EMCNH_{4,lab}) \quad \textbf{Equation 4. 3}$$

$$\sum \Delta EMC_{SWQ,NO3} = \sum_{calibrated\ events}(EMCNO_{3,SWQ} - EMCNO_{3,lab}) \quad \textbf{Equation 4. 4}$$

4.2.2 Initial Conditions and Start-up Period

The initial conditions and constant values used for parameters in the SP and 3P models are listed in Table 4. 2. The soil columns are made with 3% soil organic matter (SOM). Due to a lack of lab-tested data, the content of soil organic carbon (SOC) and total nitrogen (TN) are inferred from previous literature, as cited in the table. The content of soil organic nitrogen (SON) is calculated with SOC content and a Carbon to Nitrogen Ratio (CNR) of 20:1 [2], [3]. Initial TIN content is the difference between initial TN and SON. Then, initial TIN partitions between NO_3-N and NH_4-N with a ratio of 9:1, which is estimated with the ratio of lab-tested EMCs of NO_3-N and NH_4-N. It is also assumed that a constant portion of SON is dissolved in water (p_{DON}), while the rest is absorbed to the surface of soil particles. Throughout the duration of simulation, the portion of SOM

that is labile to microbial decomposition is set to 2.7%. External organic nitrogen supply is only applied to the top layer of each column.

Table 4. 2 Values of initial mass and constant parameters

	Meaning	Unit	Initial Value	Reference
SOM	Soil Organic Matters	g/kg soil	30	Lab test
SOC	Soil Organic Carbon	mg C/kg soil	17400	USDA Natural Resources Conservative Service [4]
TN	Total Nitrogen	mg N/kg soil	900	P. Shrestha, S. E. Hurley, and E. C. Adair [5]
SON	Soil Organic Nitrogen	mg N/kg soil	870	Calculated with SOC and CNR of 20:1
TIN	Total Inorganic Nitrogen	mg N/kg soil	30	Calculated difference of TN and SON
NO_3-N	Nitrate Nitrogen	mg N/kg soil	27	Divided TIN with ratios of NO_3-N and NH_4-N concentrations in artificial stormwater.
NH_4-N	Ammonium Nitrogen	mg N/kg soil	3	
	Meaning	**Unit**	**Constant Value**	**Reference**
CNR	Carbon to Nitrogen Ratio in soil OM	unitless	20:1	Bioretention/ Biofiltration Design Criteria, Long Beach, California [3]
p_{DON}	Percent of TN dissolved	%	3	Wright, et. al [6]
p_{lia}	Percent of OM liable	%	2.7	Zuo, et.al [7]
ONSP	Rate of ON supply	mg N/min	0.0002	Galletti, et. al [8]

Given that many values listed in Table 4. 2 are estimated, and this set of initial conditions may bring in errors to simulations results, replication of the first three events was added at the beginning of the simulated time period as a warm-up period, during which nitrogen processes were simulated, but effluent EMCs were not used for calibration and validation. The appropriate length of the warm-up period is relevant to model structure and specific environmental conditions of the simulated system [9]. No reference on length of warm up period for water quality models like NRM has been found to the best of the author's knowledge. However, with three events as a warm-up period, the NRM models generally have good prediction accuracy on underdrain TIN concentrations starting from the first validated event (as illustrated in the section 4.4). A

sharp decrease of TN weight content in the soil column from 27 mg N/kg dry soil to around 0.05 mg N/kg dry soil during the warm-up period was observed repeatedly in six versions of NRM and all calibration sets. These results demonstrate that the three-event warm-up period is efficiently long for this study case, despite the overestimation of initial nitrogen content.

4.3 Validation Results of NRMs

4.3.1 TIN EMCs in Underdrain Effluent

The EMCs of TIN in underdrain effluent from lab test and simulation results of 7 models (SWQ, SP-0, SP-1. SP-m, 3P-0, 3P-1, 3P-m) calibrated with FD columns are plotted in Figure 4. 5, in which each box contains TIN EMCs of all 12 events from columns with the same control rule (4 FD columns, 4 IWS columns, 5 SM columns, and 5 VC columns). Except for SP-0, all models simulate TIN EMCs within the 0-2.0 mgN/L range, which is consistent with the lab test results. For FD columns used for calibration, 3P-1 demonstrates the best accuracy in estimating average TIN EMCs with a -8.3% error, while SP-0 performs the worst with a -55.6% error. For the other three types of columns used for validation, SWQ overestimates average TIN EMCs from IWS and VC columns by 89.9% and 87.7%, respectively, and underestimates the average TIN EMCs from SM columns by 32.1%. In contrast, the estimation of average TIN EMCs from NRM except for SP-0 fall within the error range of -19.2% to 21.4%. In particular, 3P-m performs the best with only -2.5%, 0.6%, and 8.3% error for IWS, SM, and VC columns, respectively. Additional information on average TIN EMCs from lab tests and model simulations, along with the percent errors of simulated average TIN EMCs, can be found in Table S 3 in the supplementary material. The TIN EMCs for each event from lab test and model simulations are plotted in Figure S 1 in the supplementary material.

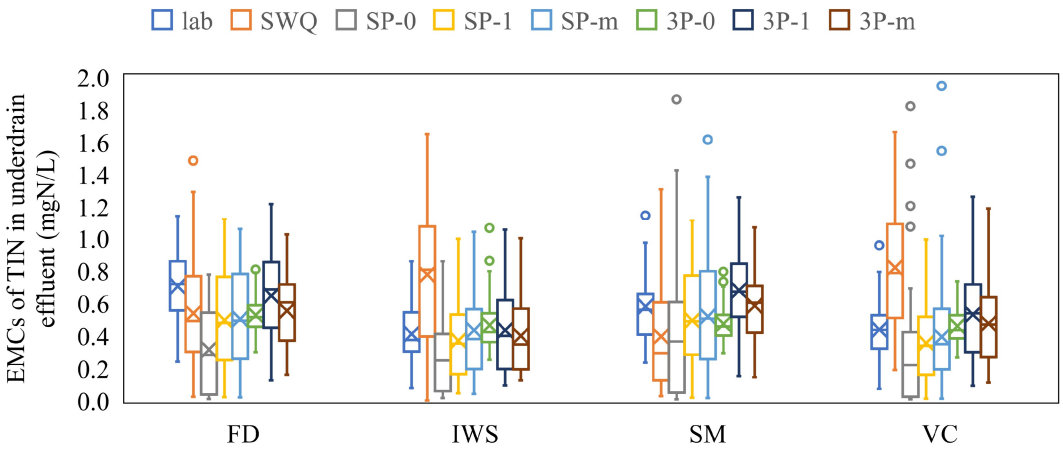

Figure 4. 5 Box plots of TIN EMCs in underdrain effluent from laboratory tests and simulation results calibrated with FD columns, with outliers from SP-0 simulations excluded.

The NRMs have especially significant improvement on IWS and VC columns when compared to SWQ. As the main difference between the IWS and VC columns versus the FD and SM columns is that the former two have a higher soil saturation rate during dry periods, these results suggest that this improvement contributes to the saturation rate factor f_{sat} as they account for the impact of soil saturation rate on nitrogen transformations in the soil media layer. The description of impacts of saturation rate is absent in SWMM LID module.

It should be noted that in the boxes of SP-0 model for IWS, SM, and VC columns, the marks of average are not shown in Figure 4. 5. This is because SP-0 predicted extremely high TIN EMCs for the first events in IWS, SM, and VC columns. Figure 4. 6 shows boxplot of TIN EMCs for the first event from lab test, from SP-0 model calibrated with FD columns, and from SP-0 model calibrated with IWS columns. When SP-0 is calibrated with IWS columns instead of FD columns, this error is greatly reduced. It is also observed that the SP-0 predicted maximum nitrogen removal rates through gas emission and plant uptake are significantly different when calibrated with FD columns (2.6 mg N/kg soil/hour) and IWS columns (5.1 mg N/kg soil/hour). These results show that SP-0 is not accurate unless it is trained with high saturation conditions and is thus not functional in term of evaluating alternative bioretention system designs. In addition, SP-0 tends to underestimate TIN EMCs for the rest events. This is because nitrogen removal

rates do not decrease with lower mass of TN in the soil. Due to these limitations, SP-0 model is considered ineffective and is not included in further analysis.

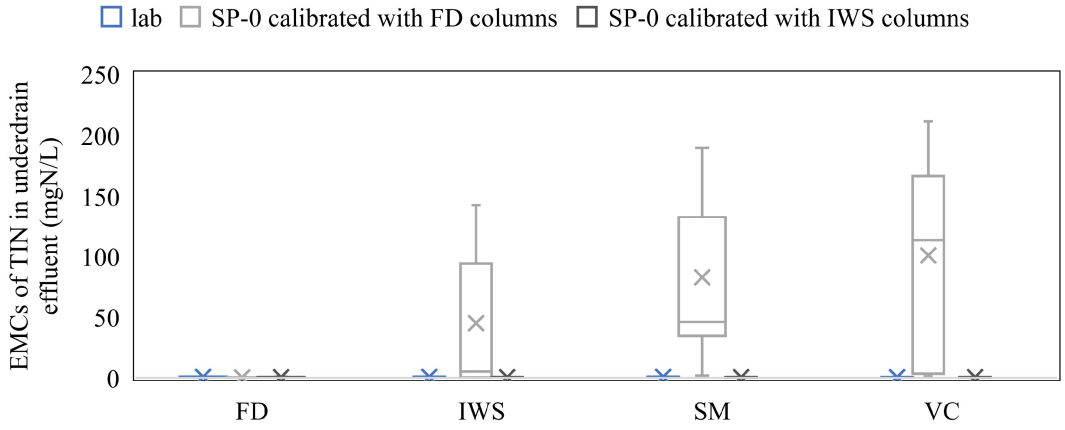

Figure 4. 6 Box plots of TIN EMCs in underdrain effluent from laboratory tests, SP-0 model calibrated with FD columns, and SP-0 model calibrated with IWS columns.

4.3.2 Percent of Good Prediction (PGP) for TIN EMCs

To better evaluate the accuracy of predicted TIN EMCs, a performance measure of Percent of Good Prediction (PGP) is calculated by the following steps. First, the average simulated TIN concentration in the underdrain effluent ($\overline{EMCTIN_{eff,sim}}$) is calculated over the five calibration runs for each event in each column type. Then, an acceptable error range around the simulated average is estimated as three times the standard deviation of lab-observed data ($3 \times std(EMCTIN_{eff,lab})$) for each event in each column type, giving a predicted range of underdrain effluent EMC as $\overline{EMCTIN_{eff,sim}} \pm 3 \times std(EMCTIN_{eff,lab})$. Lastly, the PGP value is calculated as the percentage of lab-observed datapoints that fall into the predicted range. In this way, the process of using the NRM and SWQ models as predictive tools in the real engineering field is mimicked, and PGP can represent the likelihood of successfully predicting real TIN EMCs with a given error range.

PGP values of the SWQ model and the five versions of NRM (SP-0 excluded) are listed in Table 4. 3. The models tend to have higher PGP values for SM columns when compared to IWS and VC columns. The Soil Moisture RTC rule maintained the SM column near field capacity and thus created soil saturation conditions similar to the FD

columns that were used for model calibration. This can lead to better model performances. In the final column, one can see over all types of validation columns, the 3P models improves prediction accuracy by 15-20% when compared to SWQ. SP-m does provide 10.8% improvement when compared to SWQ with much simpler model structure than the 3P models, while improvements brought by SP-1 is less significant.

Table 4. 3 PGP of effluent TIN concentration from SWQ and the 5 NRMs

	FD	IWS	SM	VC	Validation Columns
SWQ	37.5%	20.8%	84.7%	30.0%	46.7%
SP-1	52.1%	47.9%	62.7%	40.0%	50.3%
SP-m	52.1%	50.0%	54.2%	66.7%	57.5%
3P-0	41.7%	58.3%	79.7%	65.0%	68.3%
3P-1	75.0%	50.0%	79.7%	53.3%	61.7%
3P-m	56.3%	56.3%	89.8%	55.0%	67.7%

4.3.3 Percent Removal of Total Load

The percent removal of total load TIN ($PRL_{TIN,\ total}$) is calculated with equation 4.5 for each column:

$$\boldsymbol{PRL_{TIN,cumu}} = \frac{\sum_{i=1}^{n_{event}}(EMCTIN_{inflow} \times V_{inflow}) - \sum_{i=1}^{n_{event}}(EMCTIN_{eff} \times V_{eff})}{\sum_{i=1}^{n_{event}}(EMCTIN_{in} \times V_{inflow})} \quad \textbf{Equation 4. 5}$$

where $EMCTIN_{inflow}$ and $EMCTIN_{eff}$ are the TIN EMCs in stormwater inflow and underdrain effluent, respectively.

The absolute error of the average $PRL_{TIN,\ total}$ compared to labs observations are shown in Figure 4. 7. SWQ shows good prediction results for the SM columns, which have similar hydrologic conditions with the FD columns, but fails to predict $PRL_{TIN,\ total}$ of the VC and IWS columns. Lab data shows that VC and IWS columns are more effective in TIN mass removal, but SWQ predicts the opposite. In comparison, the errors of predicted average $PRL_{TIN,\ total}$ from SP-m, 3P-1, and 3P-m are limited to the range of -8.2% to 6.7%, which is comparable to the variance of lab observed $PRL_{TIN,\ total}$ (in the range of 4.7% to 9.6% among 4 or 5 columns for all four types of columns). When compared to SWQ, SP-1, SP-m, 3P-1, and 3P-m models have comparable performances

for FD columns, acceptable to good performances for SM columns, and reduce absolute error of $PRL_{TIN,\ total}$ by 16.4% to 21.8% for IWS and VC columns.

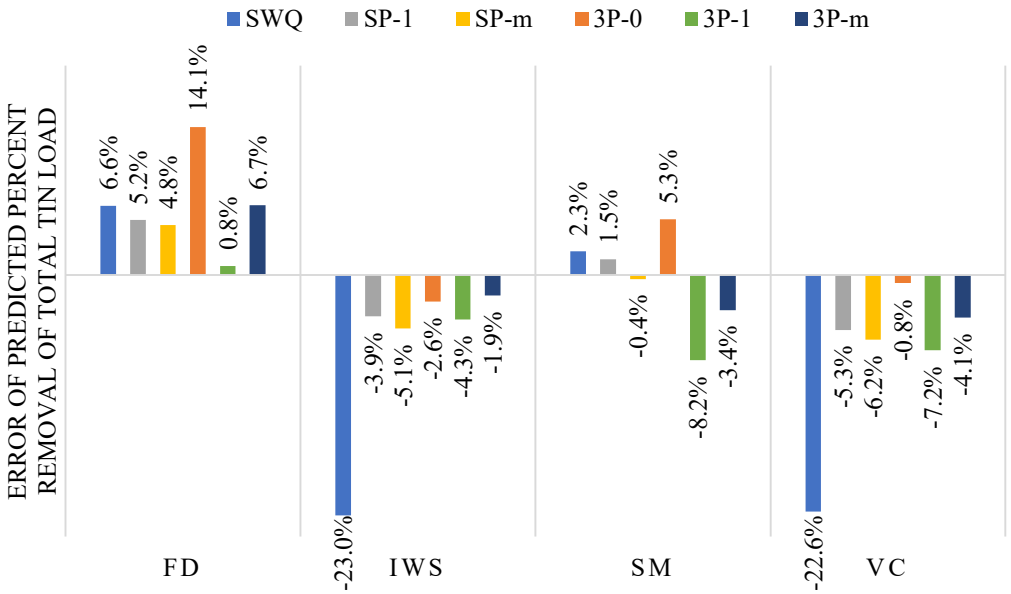

Figure 4. 7 Error of predicted percent removal of total TIN loads.

To understand the reason for 3P-0 to overestimate $R_{TIN,\ cumu}$ for FD and SM columns, the time series of 3P-0 predicted content and denitrification rate are plotted in Figure 4. 8. Since biochemical reaction rates in a zero-order model are not influenced by reactant content, the calibrated value of optimal reaction rates of denitrification and plant uptake need to be large enough to avoid any accumulation of nitrate in the soil layer and avoid continuously increasing NO_3-N concentration in the layer effluent over time. For the same reason, when weight content of NO_3-N decreases, the rates of denitrification and plant uptake would not decrease accordingly. As a result, in the 3P-0 predicted time series, NO_3-N content in soil does not accumulate during dry periods, the underdrain effluent TIN EMCs are underestimated, and the percent of mass removal are overestimated. For the drier columns and rain events with higher inflow NO_3-N concentrations, this error of prediction is greater. Thus, 3P-0 is not an effective model and is excluded from further analysis.

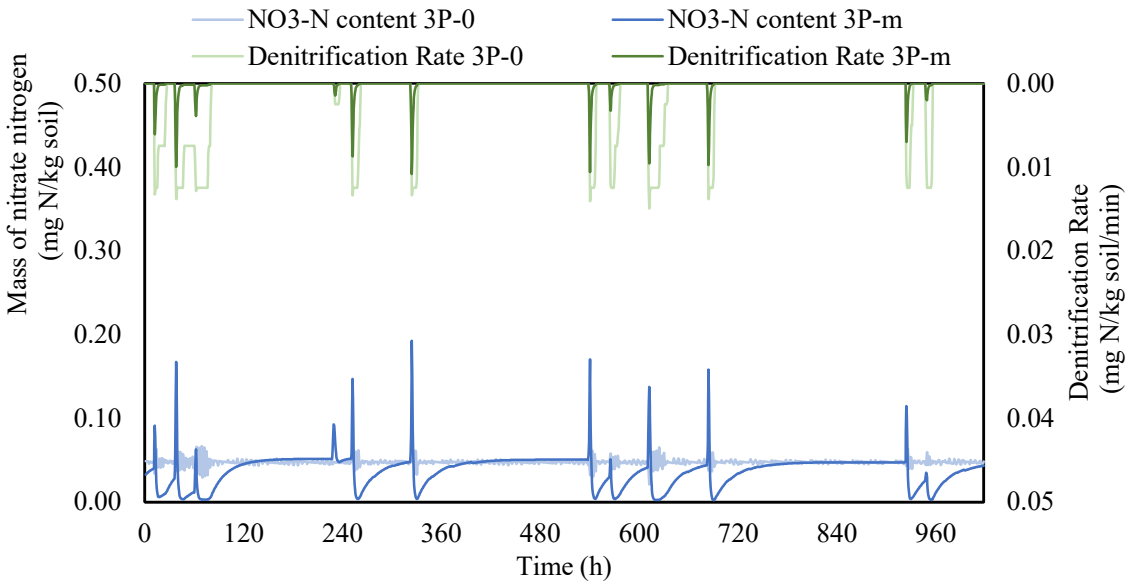

Figure 4. 8 Timeseries of mass of nitrate nitrogen and denitrification rate in FD columns predicted by 3P-0 and 3P-m models.

4.3.4 Description of Impactful Environmental Factors and Operational Conditions

Statistical analysis can be used to determine the significance of the correlation between nitrogen removal rates and environmental factors or operational conditions. Evaluating whether the statistical correlations from NRM predictions agree with those from lab-observed data provides an indication of whether the NRMs correctly capture the impacts of key influencing factors. Previous research has found that the presence of IWS, effective vegetation, depth of mulch layer, and temperature all have statistically significant positive correlation with total inorganic nitrogen removal rate in bioretention systems, while higher flow rate can have a significant negative impact [10], [11].

In this study, 16 factors describing the total volume of stormwater inflow and underdrain effluent, maximum flow rates, antecedent dry periods, soil saturation condition in the top, bottom, middle layers, and average soil moisture condition of the entire soil columns were selected for Kendall's Rank analysis [12] with datasets from lab experiment and model simulation results. Significant correlations were found between TIN mass removal and 6 analyzed parameters, which are: volume of underdrain effluent (Veff), maximum flow rate of underdrain effluent (MaxReff), maximum flow rate of interlayer flow (MaxRint), TIN EMC in stormwater inflow (TINin), duration of period

when saturation rate of the entire column is higher than 0.7 (SAveHigh) and duration of period when saturation rate of the entire column is lower than 60% (SAveLow). The p values and signs of correlation with statistical significance for the lab data and model results are listed in Table 4. 4.

Table 4. 4 The p values from Kendall's Rank analysis with signs in parentheses showing positive (+) or negative (-) correlation with percent removal of TIN load.

	Veff	MaxReff	MaxRint	TINin	SAveHigh	SAveLow
lab	(-) 3.50E-09	(-) 2.70E-04	(-) 1.90E-05	(+) 3.41E-15	--	--
SWQ	(-) <2.2E-16	(-) <2.2E-16	(-) <2.2E-16	--	(-) <2.2E-16	(+) <2.2E-16
SP-1	--	--	--	(+) <2.2E-16	(+) 1.45E-03	(-) 4.91E-04
SP-m	--	(+) 4.23E-03	(+) 5.61E-03	(+) <2.2E-16	--	--
3P-1	(-) 1.50E-04	(-) 7.74E-03	(-) 5.99E-05	(+) <2.2E-16	(+) 8.13E-13	(-) 1.60E-09
3P-m	(-) 1.42E-04	(-) 3.83E-03	(-) 4.83E-05	(+) <2.2E-16	(+) 1.35E-10	(-) 4.07E-09

Note: colors of the cell indicate sign of correlation and the confidence level; light red: positive correlatoin with 95% conficence level; dark red: positive correlatoin with 99% conficence level; light blue: negative correlatoin with 95% conficence level; dark blue: negative correlatoin with 99% conficence level

For the lab-observed dataset, the volume of underdrain flow (Veff) is negatively correlated with percent removal of total inorganic nitrogen load (PRL_{TIN}) because volume reduction (via deep infiltration or evapotranspiration) is a major mechanism of nitrogen removal in bioretention systems. The maximum flow rate of underdrain effluent (MaxReff) and maximum flow rate of interlayer flow (MaxRint), are negatively correlated with R_{TIN}. Other researchers [10], [13] have suggested that high flow rates can limit contact time for soil filtering and can flush out the originally absorbed nutrients. Events with higher TIN_{in} have higher R_{TIN}. The same results were found in one previous data-driven study [14]. This can be explained by the mixing of cleaner old water (i.e. water retained from previous events), and the increase of biochemical reaction rates with higher TIN concentrations. Theoretically, longer durations of wet conditions can benefit nitrogen removal through continuous denitrification. Thus, it is expected that the duration of period when saturation rate of the entire column is higher than 0.7 (SAveHigh) and duration of period when saturation rate of the entire column is lower than 60% (SAveLow) would be positively and negatively correlated with TIN removal,

respectively. However, the correlations between TIN removal rates and SAveHigh or SAveLow are not significant in this lab-observed dataset (N=216).

3P-1 and 3P-m are the best performing modules as they predict the same directions of correlation, when compared to lab tested data, between PRL_{TIN} and the first 4 factors. They also predicted the expected positive correlation between PRL_{TIN} and SAveHigh and the expected negative correlation between PRL_{TIN} and SAveLow. SP-1 has satisfactory performance at characterizing the impacts of inflow TIN concentrations and of the durations of high and low saturation conditions. As a comparison, SWQ and SP-m predicts opposite directions for saturation conditions (SAveHigh and SAveLow) and hydrological factors (Veffluent, MaxREff, and MaxRInter).

Accurate descriptions of impacts from environmental factors and operational conditions, such as soil saturation rates, total inflow volumes, inflow concentrations, and maximum flow rates, provide good evidence that the models are correctly describing the biochemical processes in soil columns or bioretention systems. These models should then provide accurate predictions when these environmental factors or operational conditions change in the future. Based on the results obtained in this section, it can be concluded that 3P-1 and 3P-m are more reliable in this perspective.

4.3.5 Stability of Calibration Results

To evaluate and compare the stability of calibration results of the four selected versions of NRM, the time series of TN mass in each column is predicted with five calibration runs from each NRM. Euclidian Distance (ED) values are calculated with equation 4.6 for each calibration run in each column and each NRM. In equation 4.6, WTN_{run} is the mass of TN in the column predicted by each calibration run in each time step. WTN_{ave} is the average of predicted mass of TN among five calibration runs.

$$\boldsymbol{ED_{run} = \sqrt{\sum_{m=1}^{n_{step}} (WTN_{run} - WTN_{ave})^2 / n_{step}}} \qquad \textbf{Equation 4. 6}$$

As shown in Figure 4. 9, the magnitude of the variations of TN content time series are irrelevant of column type, but only dependent on the type of NRMs. 3P-1 has the largest ED value among the four NRMs, but the ED values are limited to 1.8 mg N/kg soil, which is only 0.25% of 3P-1 simulated TN weight content at the end of the

simulated period. ED values of other three NRMs are limited to 0.8 mg N/kg soil. This means that the multiple sets of calibration results provide consistent descriptions of nitrogen removal or nitrogen transformations in the soil columns.

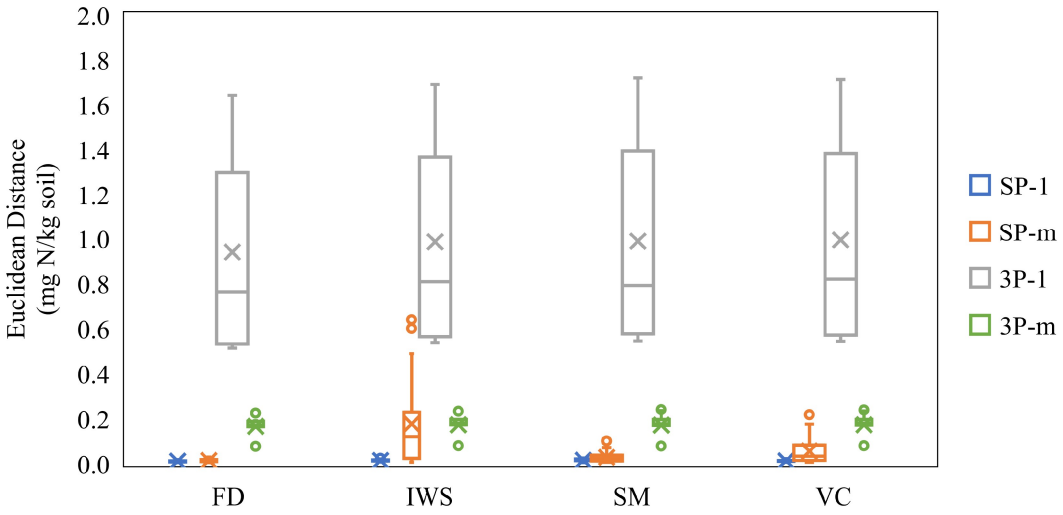

Figure 4. 9 Box plots of the Euclidian distances between simulated time series of TN mass from 5 sets of calibration results and their averages.

4.4 Predicted Time Series

Aside from event mean concentrations and cumulative TIN mass removal rates, the four selected models can generate time series that provide more information on nitrogen removal and transformation processes. Time series are of great potential of application in the engineering design, and of great significance in research about nitrogen cycling in bioretention systems. For instance, the time series of TIN concentration and discharged TIN load in underdrain effluent can help decide the best hydraulic retention time for the IWS layer that aims to enhance nitrogen removal while preventing flooding. Visualizing and comparing time series of environmental conditions and reaction rates can help us understand the interactions between nitrogen-related biochemical processes and might shed lights on the mechanisms of nitrogen cycling. It is often difficult to obtain such time series in lab experiments or through field work due to the extremely high costs of people and hours required, and field challenges. Thus, the models predicted time series are of great value. In addition, by comparing time series predicted by SP and 3P models, we can understand the impacts of model structure on simulation results and summarize potential

improvements to the current versions. In this section, time series predicted by the four selected models are plotted and analyzed to provide examples for the previously stated applications.

4.4.1 Time Series of TIN Concentration and Loads in Underdrain Effluent

Figure 4. 10 (a) shows the time series of TIN concentration in the underdrain effluent from the VC columns throughout the experiment period. The volume control (VC) columns were chosen as an example for analysis here because they are under the real-time control rule to maintain a 30 cm saturated zone. As a result, their soil moisture conditions fluctuate the most and are different from those in the FD columns used for model calibration. (TIN effluent concentration time series for other column types are provided in Figure S 2 in the supplementary materials.) In Figure 4. 10, each line represents the average of time series of all columns of the same type from 5 calibration runs (average of 25 values for each point on the line) predicted by the corresponding model. The yellow dots mark out the lab-tested TIN EMCs in underdrain effluent from the 5 VC columns for each event. All four models predict that TIN concentration in underdrain effluent reaches a peak within 6 hours after each event starts and fall back to below 0.2 mg/L within 12 hours.

To take a closer look at these time series, TIN effluent concentrations from VC columns from Aug 23rd to Aug 29th are plotted in Figure 4. 10 (b). The results show that 3P models predict higher and slightly earlier peak of effluent TIN concentrations than SP models, particularly for larger events after long dry periods. The difference in predictions can be attributed to the different model structures used for each model type. 3P models calculate organic nitrogen (OrgN), NH_4-N, and NO_3-N with three different nitrogen pools. During dry periods, organic nitrogen is converted to NO_3-N through decomposition and nitrification processes. Since there is limited denitrification in aerobic conditions, the weight content of NO_3-N accumulates over time, leading to an increase in the weight content of total inorganic nitrogen during dry periods. On the other hand, SP models only simulate total nitrogen removal due to plant uptake and limited denitrification during dry periods, leading to a slow decrease in weight content of total nitrogen over time during dry periods. In this dataset, TN content is used to estimate TIN

content in SP models. Therefore, TIN effluent concentrations during dry periods tend to be higher in 3P models predictions than SP models predictions. Additionally, initial TIN content in the soil column is higher at the start of events after dry periods in 3P models compared to SP models, which explains the higher and earlier peak of TIN underdrain effluent concentration predicted by 3P models.

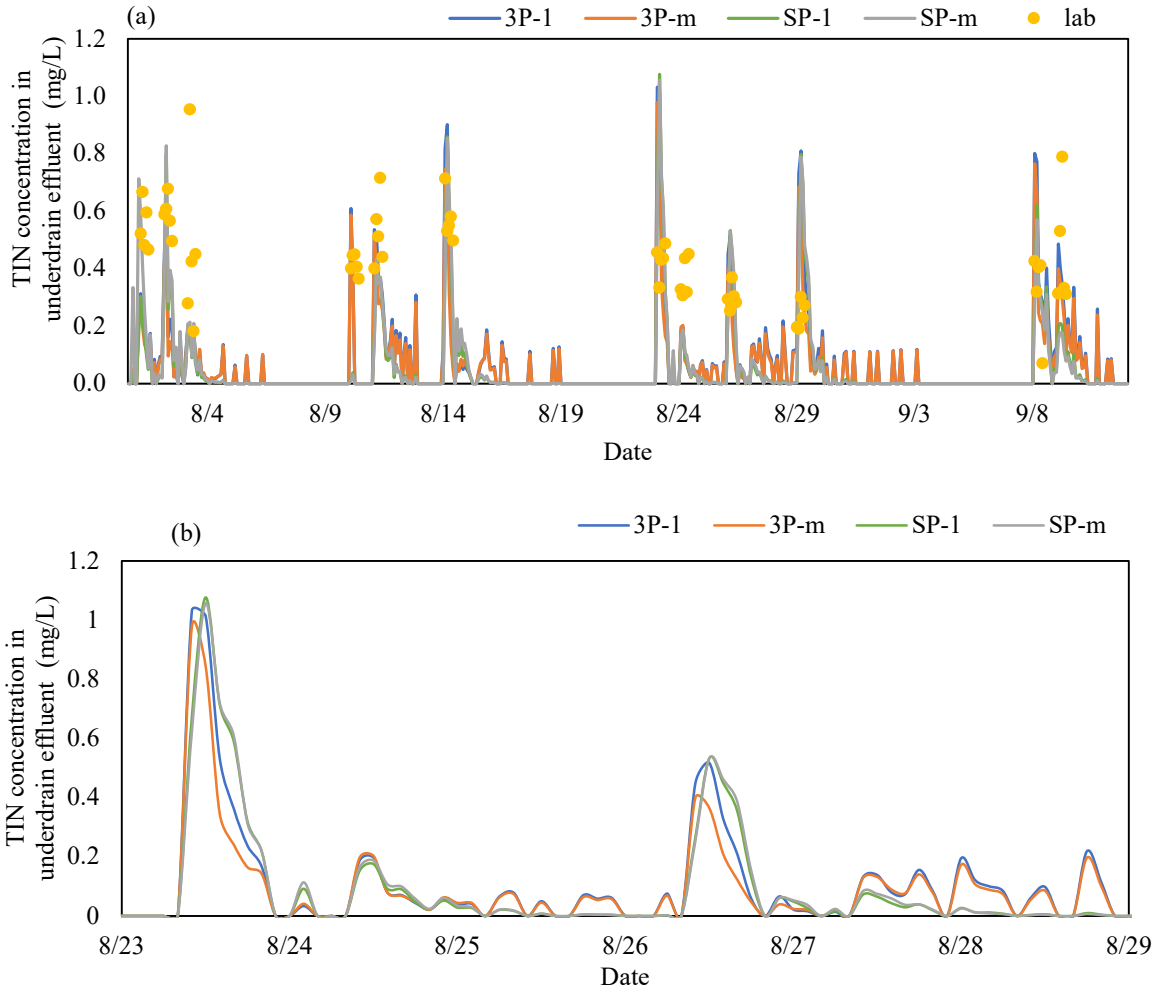

Figure 4. 10 Time series of TIN concentration in underdrain effluent from VC columns (a) for the entire experimental period, (b) from Aug 11th to Aug 19th.

4.4.2 Time Series of Mass of TN and NO_3-N in Soil Column

The predicted time series of mass of TN and NO_3-N in VC soil columns are plotted in Figure 4. 11. The TN and NO_3-N content time series predicted by the same type of models (SP or 3P) are very similar, while those time series predicted by different types of models are disparate. The fact that the models with first order kinetics and Michaelis-

Menten equations predict very similar time series for NO_3-N and TN mass indicate that both of these kinetics fit nitrogen transformations in bioretention systems, and that most of the time, the biochemical reactions are limited by mass of reactants. The SP models predicted TN time series are distinct from 3P models predicted TN time series but are similar to the 3P models predicted NO_3-N time series. This is again caused by different structures of the two types of models and the lack of calibration for organic nitrogen concentrations in the underdrain effluent. In 3P models, OrgN, NO_3-N, and NH_4-N pools are calculated separately. It is estimated that 3% of OrgN in soil column is dissolved in the liquid phase and lost through underdrain effluent in each time step. Thus, the decrease of OrgN mass in soil column is slow, leading to a higher predicted mass of TN at the end of simulated period when compared to predictions from SP models. On the other hand, in SP models, the sum of OrgN, NO_3-N and NH_4-N is simulated with the TN pool, and the SP simulated TN concentration is calibrated with the lab-tested TIN concentration, assuming negligible OrgN concentration in underdrain effluent in this experiment. Thus, TN content dropped quickly at the beginning of the simulated period and remained low. Availability of lab measurements of the OrgN concentration in the underdrain effluent or soil TN-content for calibration could make these predicted time series more accurate.

There are small differences between 3P predicted time series of NO_3-N mass and SP predicted time series of TN mass. In 3P models, the NO_3-N content accumulates after events, and becomes stable afterwards. During rain events, inflow water brings in higher concentration of NH_4-N, leading to higher rates of nitrification and accumulation of NO_3-N. When NH_4-N from inflow water is nitrified, NH_4-N is only supplied through decomposition, nitrification rate decreases, and the accumulation of NO_3-N through nitrification reaches a balance with the loss of NO_3-N through plant uptake and denitrification. In SP models, the accumulation of NO_3-N is not simulated, and the TN content remains constant after rain events.

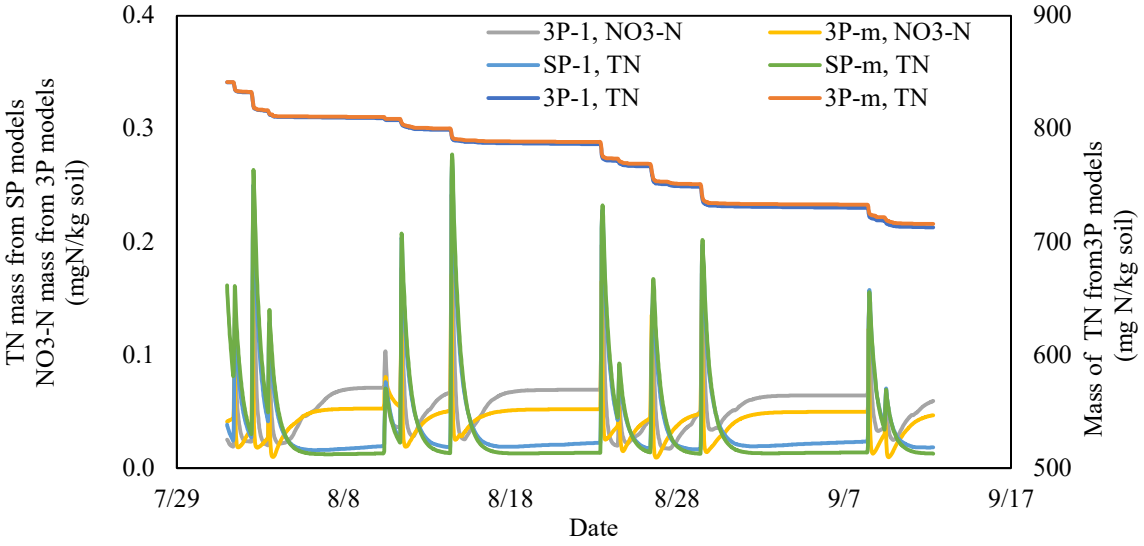

Figure 4. 11 Time series of average mass of TN and NO_3-N in VC columns predicted by the four selected NRMs.

Time series of mass of TN and NO_3-N for other column types display similar trends, with slight differences resulting from distinct control rules and soil moisture conditions. Figure 4. 12 illustrates the NO_3-N weight content from 3P-m models in FD and IWS columns. Two observations are made. Firstly, NO_3-N weight content in the soil layer has higher peaks during events and drops more slowly after events in IWS columns than FD columns. This is due to the higher water content in IWS columns with the 45-cm saturated zone. The IWS layer stores rainwater at the beginning and end of events, while NO_3-N dissolved in water discharged through the underdrain pipe in the FD columns. Secondly, mass of NO_3-N rises more quickly in FD columns during dry periods. However, during prolonged dry periods, NO_3-N weight content becomes similar in FD and IWS columns. This is expected as shortly after rain events, high saturation rate in the 45-cm saturated zone enhances denitrification and keeps NO_3-N accumulation at a lower speed. Once the saturation rate in the IWS layer drops due to plant water uptake and evaporation, denitrification ceases, and the accumulation of NO_3-N accelerates. Moreover, these time series curves reveal that there is a balance between NO_3-N accumulation and depletion in the soil layer during dry periods, and NO_3-N weight content is most influenced by stormwater inflow. Further details on time series of TN and NO_3-N mass in all four column types can be found in Figure S 3.

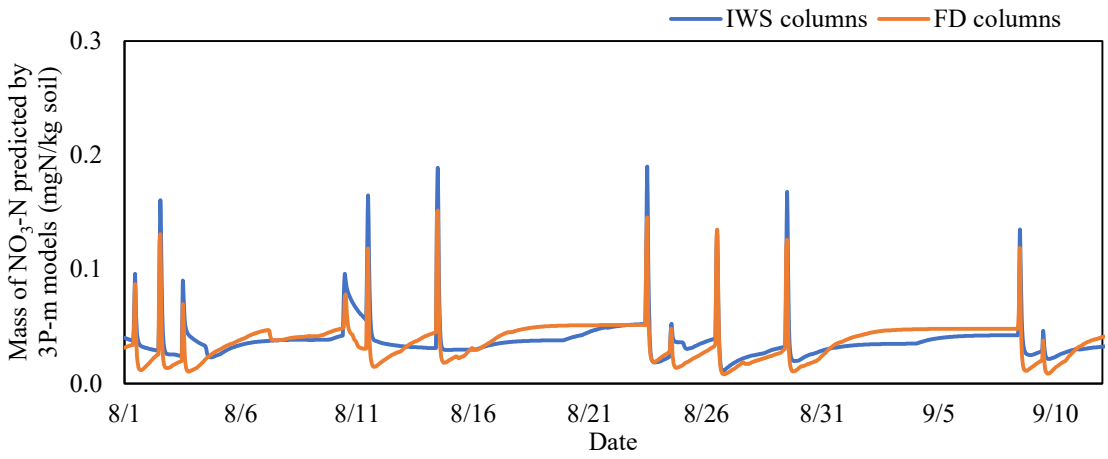

Figure 4. 12 Time series of mass of NO_3-N simulated by 3P-m for IWS and FD columns.

4.4.3 Reaction Rates Predicted by 3P-1 and 3P-m

The time series of nitrification and denitrification rates for VC columns predicted by 3P-1 and 3P-m models are plotted in Figure 4. 13, together with records of precipitation and soil saturation rates. In Figure 4. 13 (a), the solid lines represent the average denitrification rates over five VC columns, while the orange and green shades represent the ranges of predicted denitrification rates for the five columns from 3P-1 and 3P-m, respectively. The results indicate that the calibrated reaction rates for nitrification are highly stable in both 3P-1 and 3P-m models.

Both nitrification and denitrification rates peak during rain events due to the significant increase in reactant mass resulting from stormwater transport. The nitrification and denitrification rates predicted by the two 3P models are comparable, though 3P-1 shows higher increase in nitrification rate during events. This can be attributed to the characteristics of first order reaction kinetics, which cause reaction rates to increase proportionally with an increase in reactant mass. Time series of nitrification and denitrification rates predicted by the 3P models are included in supplementary materials as Figure S 4 and Figure S 5.

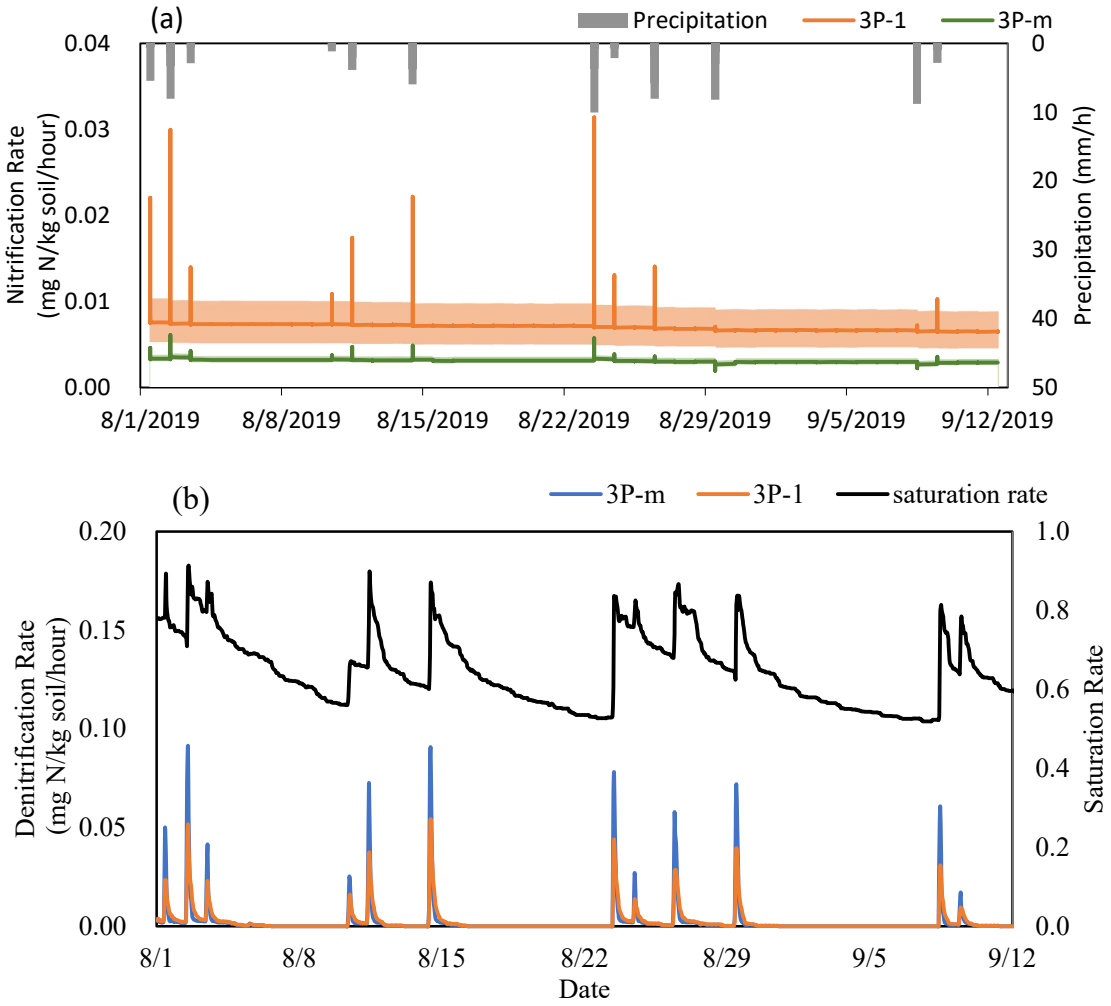

Figure 4. 13 Time series of (a) nitrification rates and precipitation and (b) denitrification rates and soil column saturation rates in VC columns generated by 3P-1 and 3P-m.

Table 4. 5 lists the reaction rates predicted by both 3P-1 and 3P-m models. The 3P-m predicted reaction rates are comparable to what's reported in previous literature, while 3P-1 predicted reaction rates are slightly higher.

Table 4. 5 Biochemical reaction rates from 3P models prediction and previous literature

	3P-1	3P-m	Previous Literature
Decomposition Rate (mg C/kg soil/h)	0.08-0.20	0.06-0.09	0.017-0.042 [15]
Nitrification Rate (mg N/kg soil/h)	0.00-0.04	0.00-0.01	0.016-0.019 [16]
Denitrification Rate (mg N/kg soil/h)	0.000-0.068 (average 0.02)	0.000-0.132 (average 0.002)	0.0065 [15]

Figure 4. 14 summarizes and plots the denitrification rate predicted for four types of columns, with solid lines indicating average values over the same type of columns, and shades showing the variance of predicted values. To better illustrate denitrification rates during dry periods, Y-axis is limited to 0.00 to 0.01 mg N/kg soil/h. 3P-1 model exhibits limited variances, while 3P-m model shows negligible variances, indicating highly stable calibration results. Both 3P-1 and 3P-m models suggest that IWS and VC columns exhibit higher denitrification rates than the dryer FD and SM columns, indicating a consistent expected trend.

N_2O gas emission rates are estimated as 1% of nitrogen that went through denitrification. Over the 46 days simulated period, nitrogen emitted as N_2O gas fall in the range of 7.9 to 14.7 mg according to 3P-m, and in the range of 11.5 to 21.5 mg according to 3P-1. Using these values as yearly average, N_2O emission rate from these simulated bioretention systems can be roughly estimated as 8.8 to 23.9 kg N/ Hectare / year, which is at the upper limit of what's reported for agricultural fields and grasslands [17]–[20]. Better estimation of N_2O emission from bioretention system can be reached if there is data available for model calibration from field tests or lab experiments.

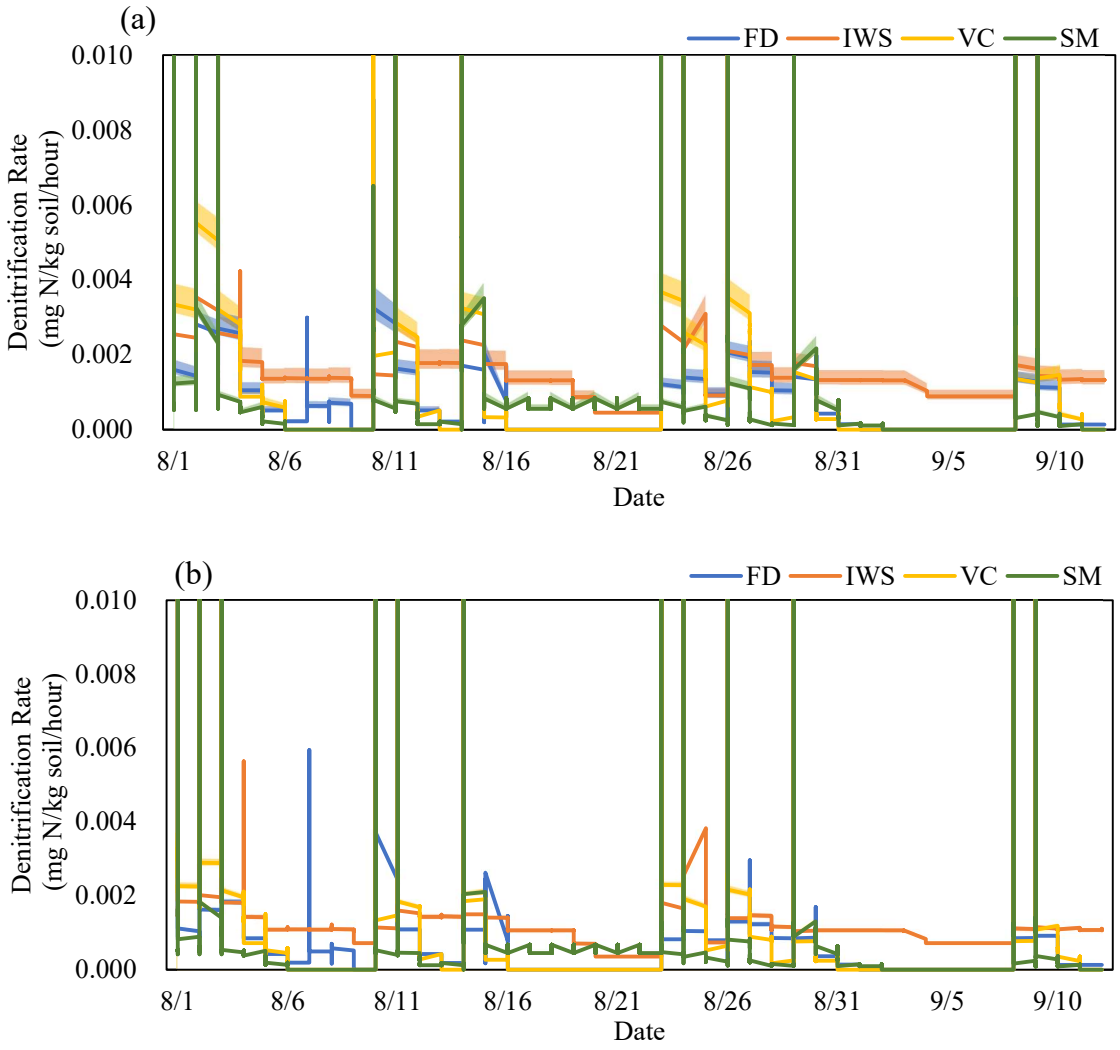

Figure 4. 14 Denitrification rates simulated for four types of columns by (a) 3P-1 model and (b) 3P-m model.

4.5 Discussion and Conclusions

In this research, using a laboratory dataset, the 6 versions of NRM are calibrated to free drainage column data and validated with three other types of columns with internal water storage layers or real time control rules.

Results show that for both SP and 3P models, 0 order kinetics is not suitable for simulating nitrogen removal in bioretention systems. With the same complexity level, models using first order kinetics and the Michaelis Menten equation have similar performances. Which reaction kinetics is more suitable for NRM need to be decided with further model validation.

SP-1, SP-m, 3P-1, and 3P-m models all greatly improve prediction accuracy of percent removal of TIN load and TIN EMCs in the underdrain effluent when compared to the SWMM water quality model (SWQ). Absolute error of predicted percent removal of TIN load over the experimental period (PRL_{total}) from the four models are limited to -8.2% to 6.7% for all four types of columns. In comparison, SWQ underestimate PRL_{total} in IWS and VC columns by 23.0% and 22.6%, respectively.

SWQ predicted average TIN EMCs have 89.9%, -32.1%, and 87.7% error for IWS, SM, and VC columns, while the four NRMs reduce this error to -19.2% to 21.4%. 3P-m has the best performance, with only -2.5%, 0.6%, and 8.3% bias. SP-1, SP-m, 3P-1, and 3P-m models provide accurate prediction of effluent TIN EMCs for 3.6%, 10.8%, 15.0%, and 21.0% more events than SWQ. The four selected models' significantly higher prediction accuracy, especially for IWS and VC columns, suggest that, unlike SWQ, these four NRMs can predict the impact of higher soil moisture conditions on nitrogen removal in bioretention system with IWS layers or valve control strategies, even when only calibrated with data from conventional bioretention systems.

The 3P-1 and 3P-m models outperform other models in accurately describing environmental factors and operational conditions. Specifically, these models capture the direction of impacts of four operational conditions that have statistically significant correlations with TIN removal rates in the lab-tested dataset. This finding supports the PBN models' ability to make accurate predictions when soil saturation rates or flow rates are changed under future climate conditions or by valve control rules.

The TIN effluent concentration time series for all four models indicate that peak concentration is reached within 6 hours of the start of events and drops below 0.2 mg/L within 12 hours. These findings suggest that retaining water for 12 hours could be sufficient to encourage denitrification in these columns. This demonstrates how NRMs can assist in the design of valve control strategies for bioretention systems.

Analyzing the time series generated by the NRM models provided valuable insights into their functionality. In this specific case study, OrgN concentrations in underdrain effluent are not available. As a result, SP models overlook OrgN content, and predicted low TN content throughout the experimental period. In contrast, OrgN content in soil

layer is simulated by the 3P models, and the predicted TN content is much higher than that predicted by the SP models. In comparison to SP models, 3P models also offer the advantage of providing detailed information on biochemical reaction rates and mass of nitrogen species in the soil column. Consequently, 3P models capture the accumulation of NO_3-N during dry periods. Additionally, 3P-1 and 3P-m models predict decomposition, nitrification, and denitrification reaction rates that generally align with previous literature.

Given the stated advantages of 3P-1 and 3P-m models, they are selected as the two best performing versions of NRM. Further validation with field data would assist their generalization and future applications.

References

[1] P. P. Persaud, A. A. Akin, B. Kerkez, D. T. McCarthy, and J. M. Hathaway, "Real time control schemes for improving water quality from bioretention cells," *Blue-Green Systems*, vol. 1, no. 1, pp. 55–71, Aug. 2019, doi: 10.2166/bgs.2019.924.

[2] Cornell Composting Science and Engineering, "Compost Chemistry," 1996. https://compost.css.cornell.edu/chemistry.html (accessed Jan. 15, 2023).

[3] California Water Boards, "MS4 Permit for Discharges from the City of Long Beach Attachment H. Bioretention/biofiltration Design Criteria." 2014. Accessed: Jan. 15, 2023. [Online]. Available: https://www.waterboards.ca.gov/losangeles/water_issues/programs/stormwater/municipal/ms4_permits/long_beach/2014/Attachment%20H_final.pdf

[4] USDA Natural Resource Conservation Service, "Soil Quality Indicators," Oct. 2009. https://www.nrcs.usda.gov/Internet/FSE_DOCUMENTS/nrcs143_019177.pdf (accessed Jan. 25, 2022).

[5] P. Shrestha, S. E. Hurley, and E. C. Adair, "Soil Media CO2 and N2O Fluxes Dynamics from Sand-Based Roadside Bioretention Systems," *Water (Basel)*, vol. 10, no. 2, 2018, doi: 10.3390/w10020185.

[6] A. L. Wright, T. L. Provin, F. M. Hons, D. A. Zuberer, and R. H. White, "Dissolved Organic Carbon in Soil from Compost-amended Bermudagrass Turf," *HortScience HortSci*, vol. 40, no. 3, pp. 830–835, 2005, doi: 10.21273/HORTSCI.40.3.830.

[7] X. M. Zou, H. H. Ruan, Y. Fu, X. D. Yang, and L. Q. Sha, "Estimating soil labile organic carbon and potential turnover rates using a sequential fumigation–incubation procedure," *Soil Biol Biochem*, vol. 37, no. 10, pp. 1923–1928, 2005, doi: https://doi.org/10.1016/j.soilbio.2005.02.028.

[8] Y. Galletti *et al.*, "Atmospheric deposition of organic matter at a remote site in the central Mediterranean Sea: implications for the marine ecosystem," *Biogeosciences*, vol. 17, no. 13, pp. 3669–3684, 2020, doi: 10.5194/bg-17-3669-2020.

[9] K. B. Kim, H.-H. Kwon, and D. Han, "Exploration of warm-up period in conceptual hydrological modelling," *J Hydrol (Amst)*, vol. 556, pp. 194–210, 2018, doi: https://doi.org/10.1016/j.jhydrol.2017.11.015.

[10] R. Wang, X. Zhang, and M.-H. Li, "Predicting bioretention pollutant removal efficiency with design features: A data-driven approach," *J Environ Manage*, vol. 242, pp. 403–414, 2019, doi: https://doi.org/10.1016/j.jenvman.2019.04.064.

[11] B. J. Koch, "Nitrogen Removal by Stormwater Management Structures: A Data Synthesis," *J Am Water Resour Assoc*, vol. 50, no. 6, pp. 1594–1607, Dec. 2014.

[12] M. G. KENDALL, "A NEW MEASURE OF RANK CORRELATION," *Biometrika*, vol. 30, no. 1–2, pp. 81–93, Jun. 1938, doi: 10.1093/biomet/30.1-2.81.

[13] F. K. F. Geronimo, M. C. Maniquiz-Redillas, and L.-H. Kim, “Fate and removal of nutrients in bioretention systems,” *Desalination Water Treat*, vol. 53, no. 11, pp. 3072–3079, 2015, doi: 10.1080/19443994.2014.922308.

[14] J. K. McNett, W. F. Hunt, and A. P. Davis, “Influent Pollutant Concentrations as Predictors of Effluent Pollutant Concentrations for Mid-Atlantic Bioretention,” *Journal of Environmental Engineering*, vol. 137, no. 9, pp. 790–799, 2011, doi: 10.1061/(ASCE)EE.1943-7870.0000373.

[15] L. Liu, F. Wang, S. Xu, W. Sun, Y. Wang, and M. Ji, “Woodchips bioretention column for stormwater treatment: Nitrogen removal performance, carbon source and microbial community analysis,” *Chemosphere*, vol. 285, p. 131519, 2021, doi: https://doi.org/10.1016/j.chemosphere.2021.131519.

[16] J. Wang, L. H. C. Chua, and P. Shanahan, “Modeling and designing for nitrogen removal in bioretention basins,” *Environmental Modelling & Software*, vol. 146, p. 105212, 2021, doi: https://doi.org/10.1016/j.envsoft.2021.105212.

[17] N. C. Lawrence, C. G. Tenesaca, A. VanLoocke, and S. J. Hall, “Nitrous oxide emissions from agricultural soils challenge climate sustainability in the US Corn Belt,” *Proceedings of the National Academy of Sciences*, vol. 118, no. 46, p. e2112108118, Nov. 2021, doi: 10.1073/pnas.2112108118.

[18] A. Mendoza Beltran, K. Jepsen, M. Rufí-Salís, S. Ventura, C. Madrid Lopez, and G. Villalba, “Mapping direct N2O emissions from peri-urban agriculture: The case of the Metropolitan Area of Barcelona,” *Science of The Total Environment*, vol. 822, p. 153514, 2022, doi: https://doi.org/10.1016/j.scitotenv.2022.153514.

[19] J. G. Koops, M. L. van Beusichem, and O. Oenema, “Nitrogen loss from grassland on peat soils through nitrous oxide production,” *Plant Soil*, vol. 188, no. 1, pp. 119–130, 1997, doi: 10.1023/A:1004252012290.

[20] G. Braker, P. Dorsch, and L. R. Bakken, “Genetic characterization of denitrifier communities with contrasting intrinsic functional traits,” *FEMS Microbiol Ecol*, vol. 79, no. 2, pp. 542–554, 2012, doi: 10.1111/j.1574-6941.2011.01237.x.

5 Updates and Validation of 3P-1 and 3P-m with Field-Scale Bioretention Data[4]

5.1 Introduction

In the previous chapter, SP-1, SP-m, 3P-1, and 3P-m were proven to improve prediction accuracy of nitrogen effluent concentration of SWMM. Compared to the SP models, 3P models can better describe the impacts of environmental factors and operational conditions and provide more information through time series of reaction rates. Before they are applied to simulate the impacts of various designs or valve control rules on bioretention systems, the 3P-1 and 3P-m models still need to be further validated with field-scale bioretention systems to confirm their performance for more complicated real systems. In addition, validation results from the last chapter did not provide strong evidence to decide which of 3P-1 and 3P-m performs better.

Thus, in this chapter, the 3P-1 and 3P-m models are applied to simulate a dataset from a field bioretention system. The dataset was divided into four different calibration and validation sets to understand the models' sensitivity to rainfall characteristics and environmental conditions. Performances of 3P-1 and 3P-m are measured using the prediction accuracy of effluent loads and by the accurate description of impacts of environmental factors. Time series from the two models are also analyzed to provide further insights to the models themselves as well as nitrogen cycling in bioretention systems.

5.2 Updated 3P-1 and 3P-m

The original 3P-1 and 3P-m models have several limitations with respect to simulating more complicated field bioretention systems. First, the 3P-1 and 3P-m models were primarily developed to describe nitrogen transformations within the soil column. Real bioretention systems have other components that affect the hydraulics, such as a

[4] This chapter is planned to be published in part in: J. Li, T. B. Culver, C. R. Burgis, W. Zhang, and J. A. Smith, "Validating Nitrogen Removal Models with Field Bioretention Data," (in preperation)

forebay, the ponding layer, and the storage layer. Second, the description of saturation factor in 3P-1 and 3P-m remain coarse and can be updated. Third, the practice of simulating the soil media layer with several horizontal layers relies heavily on available soil moisture or saturation rate data, which is not commonly available for field bioretention systems.

Accordingly, the 3P-1 and 3P-m models developed in chapter 3 are updated in the following manner. First, the forebay, ponding layer, soil layer, and storge layer were each simulated as a unique layer in the 3P models. If a raised outlet is present to keep an internal water storage layer in the bioretention cell, the soil layer is separated into a dry soil media layer and a submerged layer to improve simulation accuracy. It is assumed that the dissolved contaminants in each layer are immediately completely mixed in the liquid phase. To account for biochemical processes in the storage layer, available reactants are now described with their concentration in the liquid phase in units of mg/L instead of mg reactant per kg soil as in the previous chapters. Biochemical reactions in the forebay and the ponding layer are assumed to be negligible given their short hydraulic retention time.

Previous studies have shown that up to 36% of organic carbon in stormwater runoff exists in the form of particulate matter [1], [2], and that up to 58% of total nitrogen (TN) in stormwater runoff exists in the form of Organic Nitrogen (ON) [3]. This means that removal of total organic carbon (TOC) in the forebay through particulate settlement should not be neglected. Removal of particulate organic matter through settling in the forebay is simulated with equation 5.1, where effluent total organic carbon concentration ($CTOC_{out}$) increases with increased inflow concentrations ($CTOC_0$) and decreased flow rates of forebay inflow, and the curve is adjusted by a calibrated parameter f_{sed}.

$$\boldsymbol{CTOC_{out} = CTOC_0 \times \left(1 - \frac{2}{1+\exp(inflow \times f_{sed})}\right)} \qquad \textbf{Equation 5. 1}$$

Given that the organic nitrogen concentration is simulated with a preset organic carbon to organic nitrogen ratio (CNR), equation 5.1 also impacts the total organic nitrogen concentration in the water flow from forebay to the ponding layer. It is assumed that the settling of particles is effective in the forebay and that the total organic carbon that flows into the ponding layer can be taken as a good estimation of dissolved organic carbon

(DOC). Thus, the only process calculated for the ponding layer is the mass balance after immediate complete mixing.

Biochemical processes including decomposition, nitrification, denitrification, and plant uptake are simulated in the drier soil media layer, the submerged layer, and the storage layer. Reaction rates are calculated with first-order reaction kinetics and Michaelis-Menten equations in the 3P-1 and 3P-m models, respectively. Equations 5.2 and 5.3 are used to calculate biochemical reactions in the soil media layers (including drier soil media layer and the submerged layer) in the 3P-1 and 3P-m, respectively, while reaction rates in the storage layer are estimated with equation 5.4 and 5.5:

$$\boldsymbol{R_{soil} = C_{soil} \times f_{sat} \times (1 - \exp(-k_{bio} \times TS \times f_{tem}))} \quad \textbf{Equation 5. 2}$$

$$\boldsymbol{R_{soil} = C_{soil} \times k_{bio} \times f_{sat} \times f_{tem} \times TS / (C_{soil} + k_{mbio})} \quad \textbf{Equation 5. 3}$$

$$\boldsymbol{R_{storage} = F_{storage} \times C_{storage} \times f_{sat} \times (1 - \exp(-k_{bio} \times TS \times f_{tem}))} \quad \textbf{Equation 5. 4}$$

$$\boldsymbol{R_{storage} = F_{storage} \times C_{storage} \times f_{sat} \times f_{tem} \times TS \times k_{bio} / (C_{storage} + k_{Mbio})} \quad \textbf{Equation 5. 5}$$

In these equations, R is the hourly reaction rate of a simulated biochemical process in unit of mg C/L/h for decomposition, or mg N/L/h for nitrification, denitrification, and plant uptake processes. C represents the initial concentration of DOC with units of mg C/L, or ammonia-nitrogen (NH_4-N) or nitrate-nitrogen (NO_3-N) in units of mg N/L. k_{bio} and k_{Mbio} are the optimal hourly reaction rates (mg C/L/h or mg N/L/h) and the Michaelis-Menten constant (mg C/L or mg N/L) for the given simulated biochemical process, respectively. TS is the length of time step in units of minutes. Subscripts *soil* and *storage* indicate the layer in which the calculated biochemical reaction happens, and the subscript k indicate which biochemical reaction is calculated. Optimal reaction rates in the storage layer are estimated as a constant fraction of the optimal reaction rate in the soil media layer, and the fraction $F_{storage}$ is calibrated.

Adopted from the Water and Nitrogen Management Model (WNMM) [4], equations 5.6 to 5.10 are used to calculate the temperature factor f_{tem} and the saturation rate factor f_{sat} in 3P-1 and 3P-m models. These equations are selected because they describe the impacts using only soil hydraulic characteristics and do not add additional parameters for calibration. Curves of f_{tem} and f_{sat} are provided in Figure 5. 1.

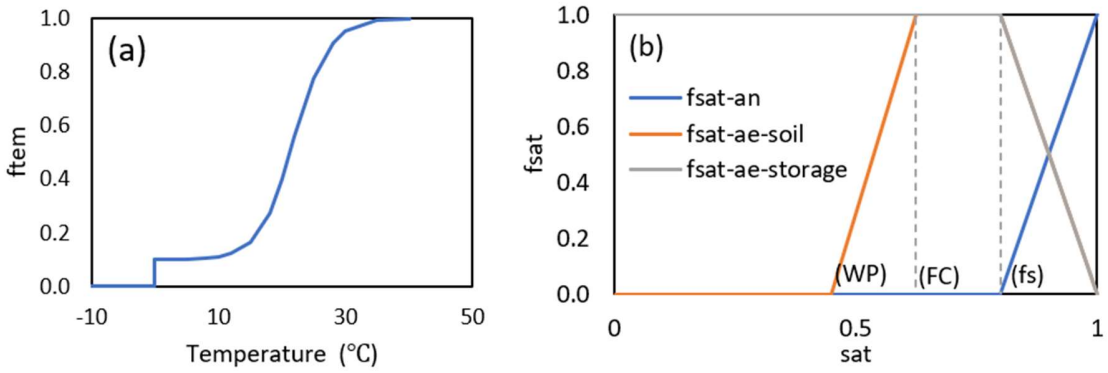

Figure 5. 1 Curves of (a) the temperature factor and (b) soil saturation rate factors

The temperature factor f_{tem} is determined via equation 5.6 in both the soil media and the storage layer. All biochemical reactions cease when temperature drops below 0 ℃.

$$f_{tem} = 0.1 + \frac{0.9T}{T+\exp(9.93-0.312T)} \qquad \textbf{Equation 5. 6}$$

The saturation rate factor used in chapter 3 is updated to describe the impacts of saturation rates on biochemical reactions more precisely. For denitrification, which is an anaerobic process, the saturation rate factor is calculated with equation 5.7 in the soil layer, and equation 5.8 in the storage layer, where *fs* is a threshold of saturation rate to initiate denitrification, set to 0.8. *theta, nmax, DST,* and *DSTmax* are volumetric moisture content in the soil media layer, soil porosity, depth of standing water in the storage layer, and maximum depth of storage layer, respectively. In both the soil media layer and the storage layer, denitrification does not start until water occupies 80% of all pores. After this threshold is reached, the saturation rate factor increases linearly with water content.

$$f_{sat-an-soil} = \begin{cases} \frac{theta-fs\times n_{max}}{n_{max}-fs\times n_{max}} & theta \geq fs \times n_{max} \\ 0 & theta < fs \times n_{max} \end{cases} \qquad \textbf{Equation 5. 7}$$

$$f_{sat-an-storage} = \begin{cases} \frac{DST-fs\times DST_{max}}{DST_{max}-fs\times DST_{max}} & DST \geq fs \times DST_{max} \\ 0 & DST < fs \times DST_{max} \end{cases} \qquad \textbf{Equation 5. 8}$$

For all other biochemical processes, which are aerobic, the soil saturation rate factor is calculated with equation 5.9 in the soil layer and equation 5.10 in the storage layer.

$$f_{sat-ae-soil} = \begin{cases} \frac{n_{max}-theta}{n_{max}-fs\times n_{max}} & fs \times n_{max} < theta \leq n_{max} \\ 1 & FC < theta \leq fs \times n_{max} \\ \frac{theta-WP}{FC-WP} & WP \leq theta \leq FC \\ 0 & theta < WP \end{cases} \qquad \textbf{Equation 5. 9}$$

$$f_{sat-ae-storage} = \begin{cases} \frac{DST_{max} - DST}{DST_{max} - fs \times DST_{max}} & DST > fs \times DST_{max} \\ 1 & DST \leq fs \times DST_{max} \end{cases} \quad \textbf{Equation 5. 10}$$

In the soil media layer, when the soil moisture content is situated between field capacity (*FC*) and the threshold for denitrification (where $theta = fs \times n_{max}$), aerobic biochemical processes operate at optimum rates. As soil moisture content moves away from this range in either direction, reactions slow down progressively until ceasing at 100% saturation or the wilting point (*WP*). In the storage layer, it is assumed that aerobic biochemical processes have optimal saturation conditions whenever the saturation rate is smaller than *fs*. DST_{max} can be found in the bioretention system's design graph, while n_{max}, *FC,* and *WP* are hydraulic characteristics of the soil media layer that can be determined by either soil hydraulic characteristic tests or SWMM model calibration. Time series of *theta* and *DST* are required as inputs to the 3P-1 and 3P-m models and can be obtained from the SWMM LID report.

5.3 The Field Bioretention System

In this chapter, the updated 3P-1 and 3P-m models are used to simulate a bioretention system located in Fairfax County, Virginia to validate their performance on simulating bioretention systems in the field. The bioretention system was designed to manage stormwater collected from Lorton Road, which carries 100,000 vehicles per day. The Bioretention systems was constructed in 2017 and serves a drainage area of 47,753 m^2 with 35% impervious surfaces. The system design includes one forebay, measuring 150 m^2, connected via a 24-inch pipe to the bioretention cell, which measures 862 m^2. To prevent flooding during events larger than the 1-year 24-hour design event, there is a bypass channel located to the north of the forebay. The bioretention cell features a 6-inch ponding layer, a 30-inch layer of engineering soil media, and a 12-inch unsealed storage layer with its underdrain outlet raised to the top of the storage layer to enhance denitrification. Additionally, the forebay and the bioretention cell have been planted with vegetation such as shrubs and sedges, which are maintained twice a year in springtime and fall.

In a previous study, 24 events between April 2018 and June 2019 were monitored. Data collected during monitoring includes flow rate time series of total inflow to forebay

(forebay inflow), bypass from bypass channel (bypass), and outflow through the underdrain pipe (underdrain effluent). Event-mean concentrations of nitrate-nitrogen (NO_3-N), total dissolved nitrogen (TDN), and dissolved organic carbon (DOC) in forebay inflow, bypass, and underdrain effluent were tested. This field study has several advantages for our modeling work. There is a record of precipitation events for over a year, including warm and cold temperatures and snow events. This provides a good opportunity to validate the effectiveness of the temperature factor used in 3P models. A second advantage is that both inorganic and organic nitrogen concentrations are available, which would greatly facilitate the calibration process. Thirdly, isotopic testing was also conducted to determine the level of denitrification that was present. Comparing the model simulations with isotopic test data would provide strong evidence on whether the 3P models have good description on mechanisms of nitrogen transformations in a real-world scenario. More detailed description of the bioretention systems and the monitoring study can be found in previous publications [5], [6].

To establish the 3P-1 and 3P-m models, it is assumed that the soil media layer contains 5% organic matter by weight [7]. The initial mass of organic nitrogen was determined based on the initial organic carbon content (33%) and the carbon to nitrogen ratio (15.7:1) of the applied soil amendments according to lab test results. Initial mass of NO_3-N (2.2 mg /kg) and NH_4-N (3700 mg /kg) were also determined with laboratory test. To reduce the uncertainty brought by estimated initial contents and better estimate the condition of the bioretention system after 1 year of operation, historical events between Oct 1st and April 15th, 2018, are also simulated as a warm-up period, but not included in model calibration or validation. Time series of precipitation and temperature at the closest weather station (Washington Dulles International Airports) [8] were downloaded at hourly time step and used as inputs to the SWMM hydraulic model.

5.4 Calibration and Validation of the Modeling System

Figure 5. 2 shows the workflow of this modeling study. First, a ***SWMM hydraulic model*** was used to simulate the hydrology and hydraulics of the contributing drainage area and the bioretention system. The SWMM hydraulic model was developed and calibrated to generate time series of water flows into, within, and out of the bioretention

system, in 10-min time steps. Second, the ***SWMM stormwater quality model*** was calibrated to generate time series of contaminant concentration in stormwater runoff that flows into the forebay. Third, the time series of water flows and contaminant concentrations generated by the two previous models were used as inputs to the 3P-1 and 3P-m models. The 3P models were calibrated and validated with loads of contaminants discharged from the underdrain outlet of the bioretention cell in the field. Lastly, a ***SWMM LID water quality model (SWMM LID)*** was calibrated and validated as a comparison to the 3P-1 and 3P-m models. Detailed practices are explained in the following sections.

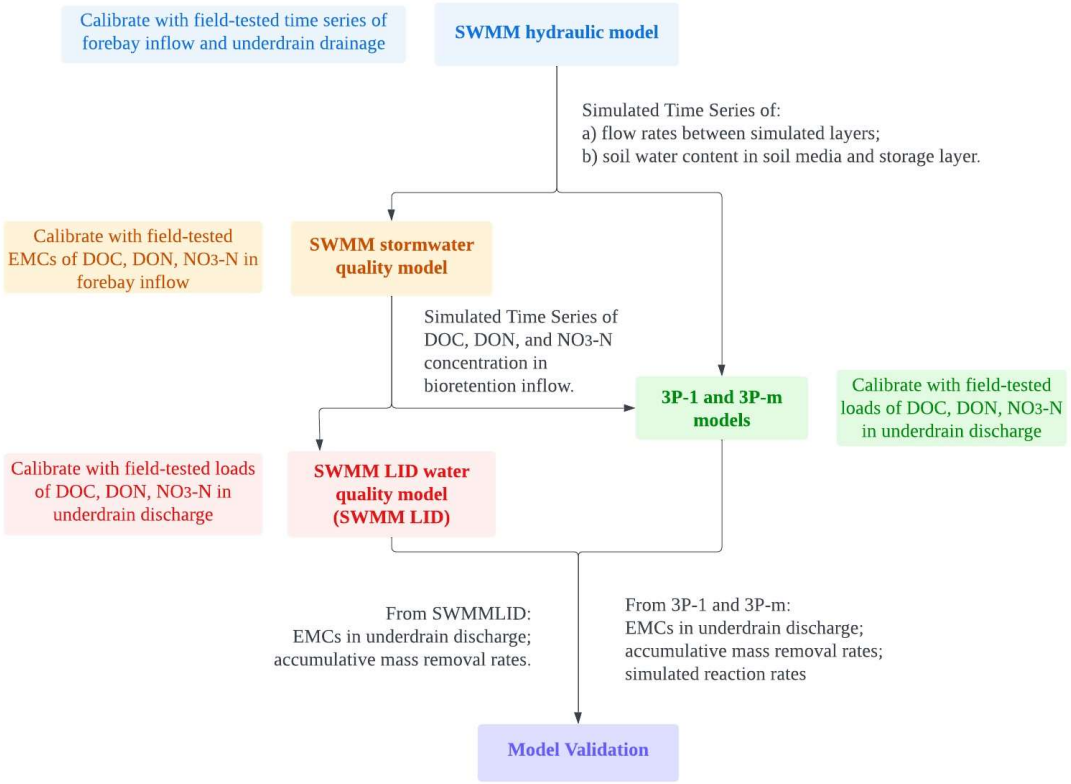

Figure 5. 2 Workflow of this modeling study

5.4.1 Calibration of SWMM Hydraulic Model

Stormwater runoff from the contributing drainage area (CDA) first flows into the forebay, which in the SWMM model is represented as an unsealed storage unit. Dimensions of the contributing drainage area, the storage unit, and the bioretention cell

were taken from the design diagrams of the bioretention system. Time series of precipitation and temperature at the closest weather station (Washington Dulles International Airports) were downloaded at hourly time step and used as inputs to the SWMM hydraulic model. A total of 15 parameters were calibrated to maximize the average Normalized Nash-Sutcliff Efficiency coefficient (NNSE) for both forebay inflow and underdrain effluent, which were calculated with equations 5.11 and 5.12. In these equations, the subscript p denotes the calibrated waterflow. Q_{obs} and Q_{sim} are water flow rates in each time step from field record and SWMM simulation, respectively. The parameter of n_{event} is the number of calibrated events (equals to 24). ti and Ti are the start and end time of event i.

$$\boldsymbol{NSE_{i,p} = 1 - \frac{\sum_{ti}^{Ti}(Q_{obs,p} - Q_{sim,p})^2}{\sum_{ti}^{Ti}(Q_{obs,p} - \overline{Q_{obs,p}})^2}} \qquad \textbf{Equation 5. 11}$$

$$\boldsymbol{\overline{NNSE_p} = \frac{\sum_{i=1}^{n_{event}}(\frac{1}{2 - NSE_{i,p}})}{n_{event}}} \qquad \textbf{Equation 5. 12}$$

The NNSE ranges between 0 and 1 (1.0 inclusive), with increasing value indicating a better fit. NNSE=0.5 corresponds to NSE=0, where model simulation results have the same predictive skills as the average of observed time series. NNSE = 0.67 corresponds to NSE=0.5, where calibration results are considered satisfactory for daily hydrological simulations [9]–[11]. The $\overline{NNSE_p}$ for forebay inflow, and underdrain effluent are 0.74, and 0.66, respectively, indicating generally satisfactory reproductions of the recorded time series of flow rates at hourly time steps.

The field measured and SWMM simulated time series of flow rates are shown in Figure 5. 3. The SWMM hydraulic model produces reliable simulations of flow rates for forebay inflow and bioretention cell underdrain effluent. In addition to the 24 calibrated events, some storm flows appear in the SWMM simulations. This is because for these historical events, no field data was collected from the bioretention field. Nonetheless, these events were modeled in the SWMM hydraulic model to generate a more precise representation of soil moisture conditions for the subsequent events that are calibrated.

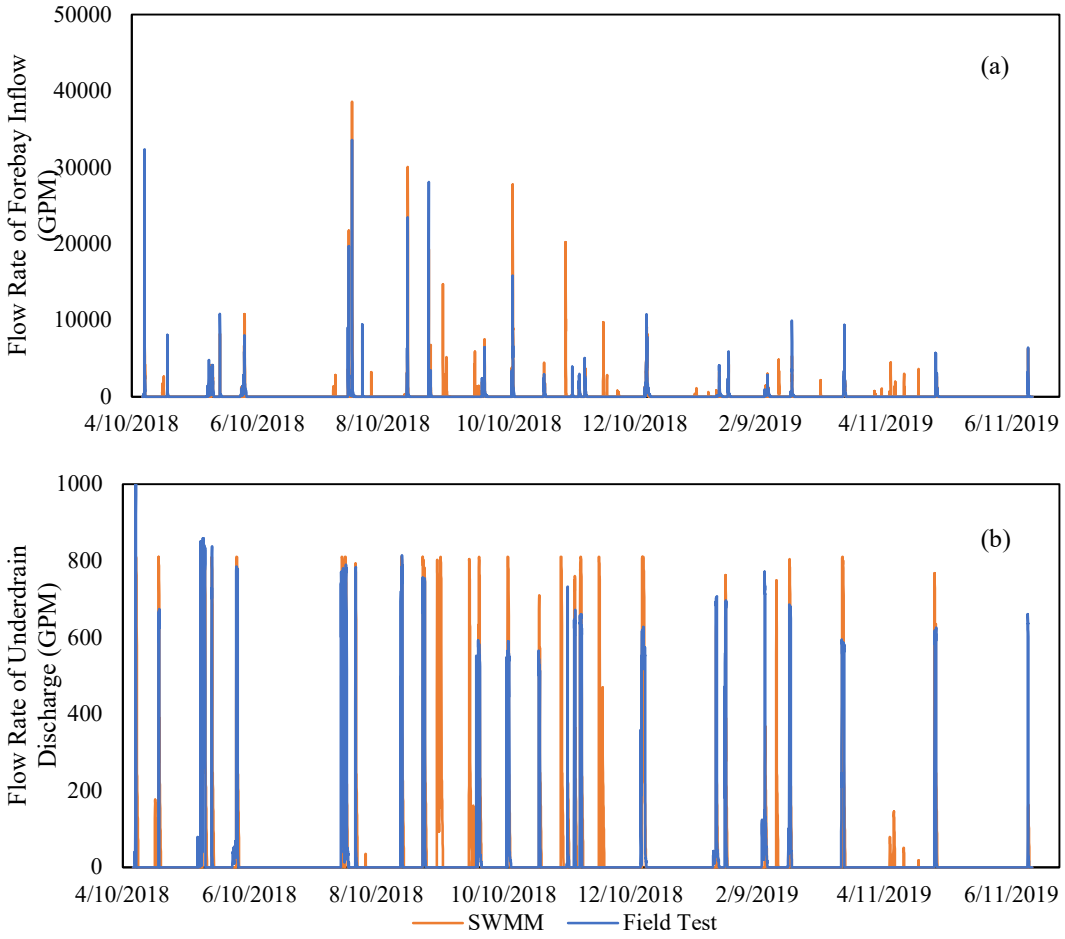

Figure 5. 3 Time series of flow rates from field record and SWMM hydraulic model of (a) forebay inflow and (b) underdrain effluent

5.4.2 Calibration of SWMM Stormwater Quality Model

Next, a SWMM stormwater quality model was developed and calibrated to simulate DOC, DON, and NO_3-N concentrations in the forebay inflow. Linear regression analysis is first applied to field EMCs to select quantitative relationships suitable for each contaminant in the SWMM stormwater quality model. Results show that EMC of DOC in forebay inflow increases linearly with antecedent dry periods, and that NO_3-N EMC is negatively correlated with maximum flow rates. Neither antecedent dry periods nor maximum flow rates are correlated with NO_3-N EMCs. Thus, a power buildup function (equation 5.13) and an exponential wash-off function (equation 5.14) were selected to calculate DOC load in the forebay inflow. The EMC function (equation 5.15) and Rating

Curve wash off function (equation 5.16) were used to calibrate for DON and NO_3-N loads, respectively.

$$\textbf{DOC build-up: } B = Min(A_1, A_2 t^{A_3}) \qquad \textbf{Equation 5. 13}$$

$$\textbf{DOC wash-off: } W = E_1 \times q^{E_2} \times B \qquad \textbf{Equation 5. 14}$$

$$\textbf{DON wash-off: } W = E_1 \times Q \qquad \textbf{Equation 5. 15}$$

$$\textbf{NO3-N wash-off: } W = E_1 \times Q^{E_2} \qquad \textbf{Equation 5. 16}$$

In the build-up functions, A_1 is maximum build up possible in unit of mass per unit area, A_2 is the build-up rate constant, and A_3 is the time exponent. A_1, A_2, and A_3 are calibrated. In the wash-off functions, W is the wash-off load, Q and q are runoff rates in GPM and inch/hour respectively. B is pollutant buildup over the watershed in mg. E_1 and E_2 are wash-off coefficient and wash-off exponent and are calibrated.

For each pollutant, parameters were calibrated to minimize RMSE of inflow loads of the monitored events calculated with equation 5.17, with subscript j representing the calibrated contaminant (DOC, DON, or NO3-N), and n_{event} equals to 24.

$$RMSE_j = \sqrt{\frac{\sum_i^{n_{event}} (Load_{in,sim} - Load_{in,field})^2}{n_{event}}} \qquad \textbf{Equation 5. 17}$$

RMSE of inflow loads of DOC, DON, and NO_3-N are 32.4, 5.1, and 6.3 g, and the RMSE of inflow EMCs are 0.19, 0.18, and 0.84 mg/L, respectively. In comparison, the average inflow load of DOC, DON, and NO_3-N are 158.7, 9.5, and 12.2 g, and the average inflow EMCs are 5.4, 0.38, and 0.43 mg/L, respectively. All RMSE values are 15-54% of corresponding average values, indicating acceptable calibration results. As shown in Figure 5. 4, the SWMM simulated EMCs of DOC and NO_3-N also have similar regression results with antecedent dry periods and maximum flow rates when compared to the field dataset.

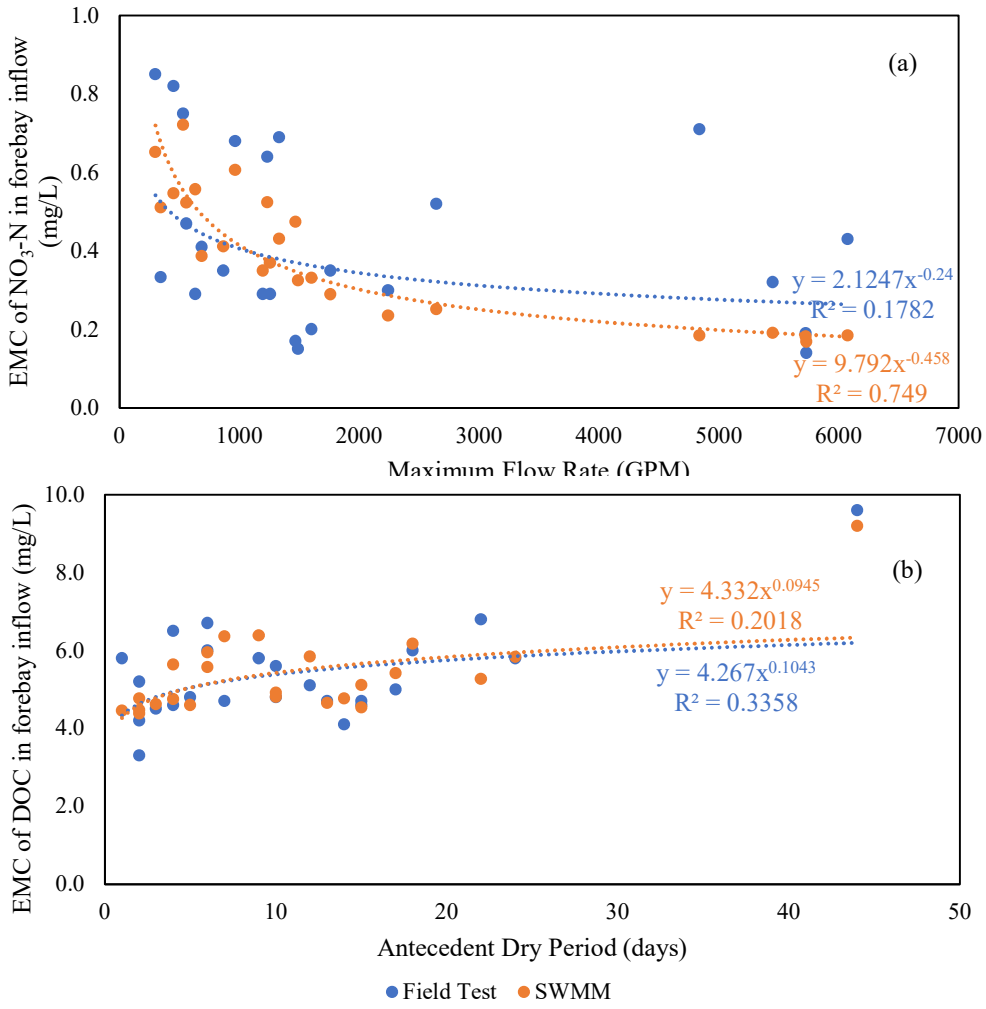

Figure 5. 4 Linear regression analysis of field and SWMM simulated results, (a) NO_3-N EMCs with maximum flow rates, and (b) DOC EMCs with antecedent dry days.

5.4.3 Calibration of the 3P-1 and 3P-m Models

The time series of flowrates and contaminant concentrations from the calibrated SWMM hydraulic model and SWMM stormwater quality model were used as inputs to the 3P-1 and 3P-m models. Four different rules were used to create four different sets of calibration and validation events. In all cases, the 24 recorded events were divided evenly into 12 calibration events and 12 validation events. The first selection rule randomly finds 12 events for calibration (the Random set), while the other three rules select 12 events with highest daily average temperature (the Summer set), 12 events with highest total precipitation (the Large Events set), and 12 events with longest antecedent dry periods

(the Drier set) for calibration. Robustness of 3P models to the uncertainty brought by characteristics of events sampled for calibration were analyzed by comparing validation results from these four calibration sets. The events selected for calibration and validation in each set are listed in Table S 4, together with their total precipitation, daily average temperature, and numbers of antecedent dry days. For each set of events, calibration was repeated three times, using Dynamically Dimensioned Search (DDS) [12] with 500 iterations. This higher number of iteration times was selected based on the observation that the convergence speed is slower for this dataset. The calibrated parameters are listed in Table 5. 1.

Table 5. 1 The symbols and meanings of calibrated parameters in the updated 3P-1 and 3P-m models.

symbol	meaning	calibrated for model
k_{deco}	optimal reaction rate of decomposition	3P-1, 3P-m
k_{nitr}	optimal reaction rate of nitrification	3P-1, 3P-m
k_{deni}	optimal reaction rate of denitrification	3P-1, 3P-m
k_{plant}	optimal reaction rate of plant uptake	3P-1, 3P-m
F_{ST}	reaction rate factor for storage layer	3P-1, 3P-m
p_{DOM}	percent of organic matter that is dissolved	3P-1, 3P-m
R_{OCSP}	rate of organic matter supply	3P-1, 3P-m
f_{sed}	factor of particulate matter sedimentation in forebay	3P-1, 3P-m
k_{Mdeco}	Michaelis Menten constant of decomposition	3P-m
k_{Mnitr}	Michaelis Menten constant of nitrification	3P-m
k_{Mdeni}	Michaelis Menten constant of denitrification	3P-m
k_{Mplant}	Michaelis Menten constant of plant uptake	3P-m

8 and 12 parameters are calibrated in the updated 3P-1 and 3P-m models, respectively. Given that in the field, managing the total nitrogen load discharged from bioretention systems is more important than predicting the event mean concentrations of individual events, the models are calibrated to minimize the Sum of Square Error of Loads (SSEL) calculated with equations 3.19 and 3.21, which were previously explained in chapter 3.

$$SSEL_k = \sum_{s}^{forms\ of\ nitrogen} (RMSE\ of\ Load_{k,s}/(\max(Load_{k,s}) - \min(Load_{k,s}))$$

Equation 3.19

$$RMSE\ of\ Load_{k,s} = \sqrt{\sum_{i=1}^{n_{event}} (Load_{k,s,obs} - Load_{k,s,sim})^2 / n_{event}}$$

Equation 3.21

Aside from the loads of DON and NO_3-N, the loads of DOC and NH_4-N were also included in the calibration. NH_4-N was not detected in forebay inflow, underdrain effluent, or bypass in any of the 24 recorded events. Thus, the average of field-tested NH_4-N load was assumed to be 0.04 mg NH_4-N/L, which is half of the lower detection limit of NH_4-N concentration.

5.4.4 Calibration of the SWMM LID Water Quality Model

Finally, a SWMM LID water quality model (referred to as the SWMM LID model thereafter) was calibrated and validated as a comparison to the 3P models. To be consistent with the 3P-1 and 3P-m models, organic matter settling with particulates in the forebay was simulated with equation 5.1 in the storage unit in SWMM. Then, a single parameter, the percent removal rate in the SWMM LID model, was calibrated for each of the four calibration sets for DOC, DON, NO_3-N, and NH_4-N with equation 5.17.

5.5 Model Validation Results

5.5.1 Percent Removal of Contaminant Loads

The prediction accuracy of the SWMM LID model, 3P-1, and 3P-m models are first evaluated with percent removal of total load (PRL_{total}) of TDN, NO_3-N, and DOC of all validated events, which was calculated with equation 5.18 and plotted in Figure 5. 5.

$$PRL_{total,j} = 100\% \times (\sum Load_{j,sim} - \sum Load_{j,field}) / \sum Load_{j,field} \quad \textbf{Equation 5. 18}$$

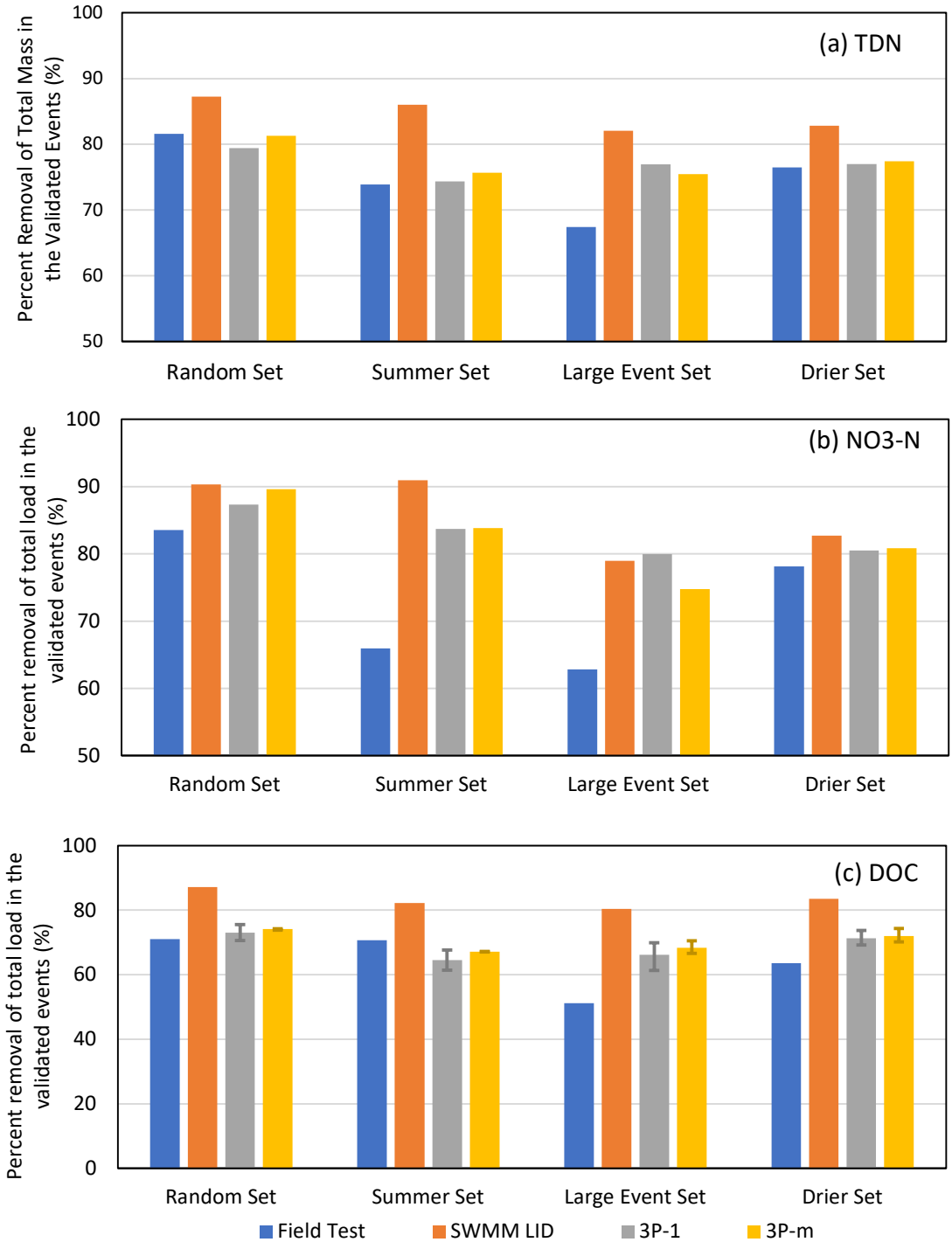

Figure 5. 5 Percent removal of total mass of (a) TDN, (b) NO_3-N, and (c) DOC of validated events from four calibration sets, error bars showing variance from three repeated calibration

In Figure 5. 5, the error bars represent the range of results obtained from three calibration runs of each calibration set for 3P-1 and 3P-m. When compared to the SWMM LID model, both 3P-1 and 3P-m significantly improved the accuracy of TDN and DOC PRL_{total} predictions for all four calibration sets. 3P-1 and 3P-m predicted TDN PRL_{total} with errors ranging from -2.6% to 3.2%, while the SWMM LID overestimated PRL_{total} by 5.6% to 12.1% among the four validation sets. Similarly, for DOC, 3P-1 and 3P-m predicted PRL_{total} with errors ranging from -9.2% to 10.8%, while the SWMM LID has errors ranging from 11.6% to 20.1%. This can be attributed to the SWMM LID model's inability to simulate the bioretention system as a source of organic matter, as the field-tested DOC EMC in underdrain discharge is often higher than that in forebay inflow during many events. The PRL_{total} prediction accuracy for NO_3-N was found to be similar among the three models, with better predictions for the Random Set and Drier Set.

The Larger Event Set was found to have lower accuracy among the three models for all three contaminants, indicating an error source not related to nitrogen cycling simulation but rather hydraulic simulations and model structure. This issue may arise from the assumption that contaminant concentrations are the same from top to bottom of the soil media layer. Studies [13], [14] have shown that actual DOC and TN concentration in the top layer of the soil may be much higher than the average concentrations in the entire soil media layer. With high DOC concentration, rapid decomposition and nitrification processes can lead to rapid increase of NO_3-N concentrations. For smaller events, the denitrification process is limited during short periods of high saturation. As a result, field data shows that smaller events have significantly higher NO_3-N EMC in underdrain effluent (as shown in Figure 5.6 (b)) and lower TDN mass removal rates than in larger events, whereas this difference is not captured by the 3P models. To mitigate this issue, it is suggested that 3P models treat the soil media layer as multiple layers whenever soil moisture data is available or include a range of events with varying precipitation amounts and rainfall intensities in model calibration.

The 3P-1, 3P-m, and SWMM LID models significantly overestimate PRL_{total} for validated events in the Summer set. However, the accurate prediction results from the

Random and Drier sets indicate that 3P models can describe nitrogen transformations under warmer or colder conditions when events with various temperature conditions are included in the calibrated set. These results suggest that significant differences between warmer and colder conditions in the field is impacting nitrogen transformation processes but are not captured by the current 3P models.

To understand the results from the Summer set, field data are divided according to the calibration sets and plotted in Figure 5. 6. As expected, total effluent volume in the calibrated and validated events in the Larger Event set are different. The Drier set also has different total effluent volumes in the calibrated and validated events. In this dataset, longer antecedent dry periods are positively correlated with larger volumes of stormwater inflow. Total underdrain volumes for calibrated and validated events in the Random and Summer sets are similar.

The relative difference between average EMCs of NO_3-N, DON, and DOC in calibrated and validated events (RD_{EMC}) are calculated with equation 5.19, where subscripts *valid* and *calib* represents the validated and calibrated events, respectively.

$$RD_{EMC,j,set} = \frac{\overline{EMC_{j,set,valid}} - \overline{EMC_{j,set,calib}}}{\overline{EMC_{j,set,calib}}} \times 100\% \quad \textbf{Equation 5. 19}$$

For NO_3-N, RD_{EMC} for the Random, Summer, Large Event, and Drier sets are 7.3%, 172.4%, 48.2%, and 3.2%, respectively. For DON, RD_{EMC} for the four sets are 10.2%, -47.3%, 23.5%, and 23.6%, respectively. For TDN, RD_{EMC} for the summer set is only 0.4%. It is apparent that the field bioretention system has significantly higher EMC for NO_3-N, lower EMC for DON in winter than in summer, but similar EMC for TDN in the summer and winter seasons. This explains good prediction accuracy for TDN PRL_{total} for the Summer set despite the error for NO_3-N and DON PRL_{total}. The differences in NO_3-N and DON effluent EMCs can be explained by two reasons. First, the supply of external organic matter is lower in winter due to less plant activity and less animal waste, which explains the lower effluent EMCs of DOC and DON. Although the external organic nitrogen supply rate (*ONSP*) is multiplied with the temperature factor in the 3P models, the *ONSP* value may be overestimated when winter conditions are not included in calibration. Second, it may be possible that the activity of aerobic and anaerobic bacteria is unevenly impacted by temperature. Different levels of inhibition to soil biomass in

winter could result from a lower temperature itself or other seasonal factors like the deep frost lines, freeze-thaw cycle, or higher concentrations of road salts [15]. The impacts of these factors are not represented in the 3P models when winter events are not included in the calibrated set of events, which could explain the lower validation performance for the Summer set. Further research is needed to understand the reasons that lead to the distinct EMCs of NO_3-N and DON in warmer and colder conditions. It is also suggested that the temperature factor for the denitrification process can be adjusted or calibrated separately to better describe the impacts of temperature and provide more insights on the mechanisms of seasonality of nitrogen transformation processes. Box plots of field tested and model simulated EMC and discharged loads of NO_3-N, DON, TDN, and DOC are provided in Figure S 6 to Figure S 9 in the supplementary materials.

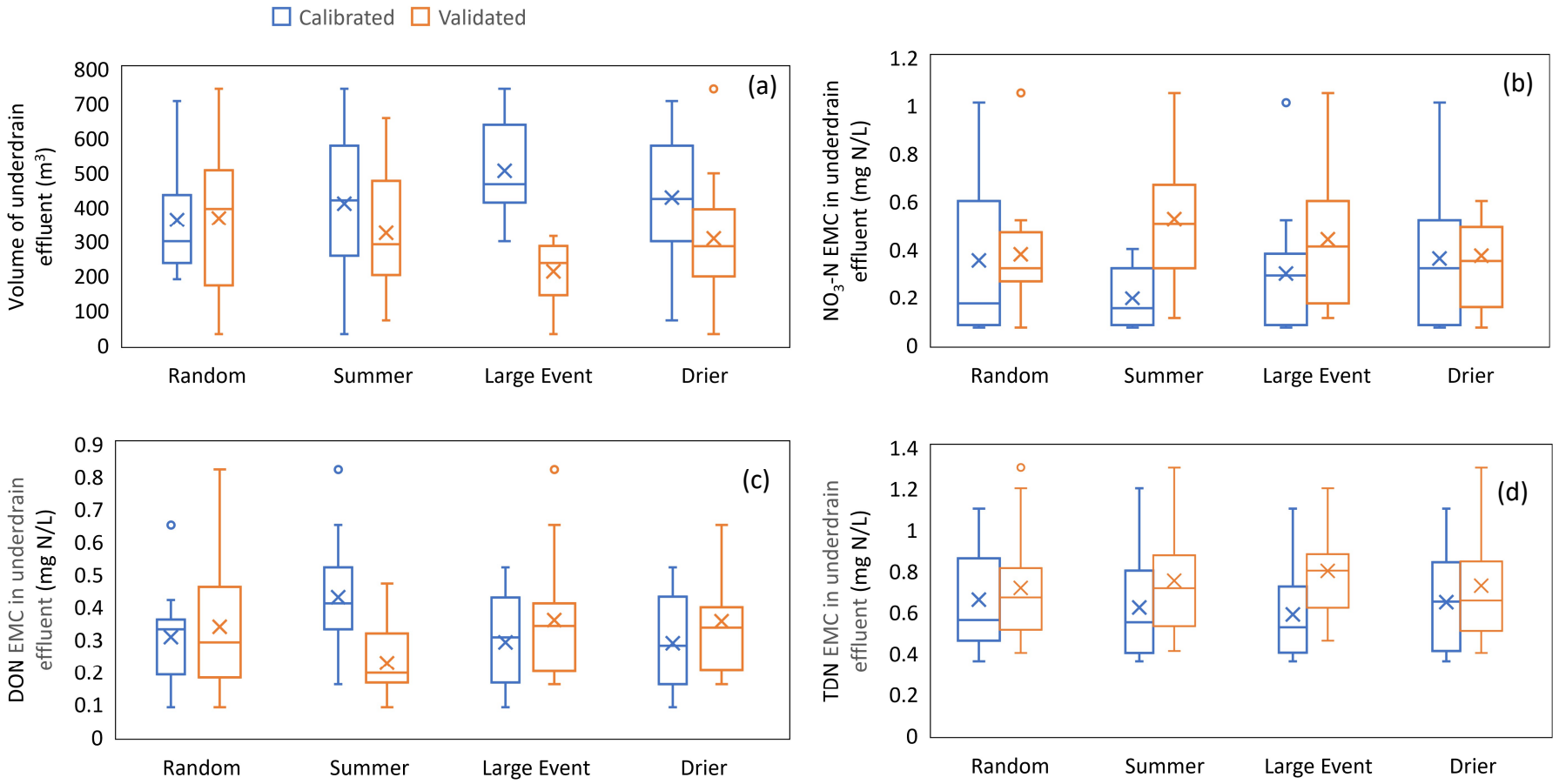

Figure 5. 6 Box plots of data from field test, separated into calibrated and validated events according to four calibration sets for (a) volume of underdrain effluent, (b) NO_3-N EMCs in underdrain effluent; (c) DON EMCs in underdrain effluent, and (d) TDN EMCs in underdrain effluent.

5.5.2 Scaled RMSE of Contaminant Loads

The parameter of scaled RMSE (SRMSE) is used to evaluate the accuracy of predicted contaminant loads in the underdrain effluent of each event. RMSE of discharged load of the validated events is scaled to the average discharged load of all 24 events for each contaminant for easier comparison of prediction accuracy among the three contaminants, as shown in equation 5.20.

$$SRMSE_j = \frac{RMSE_{j,valid}}{Load_{all\ event}} \qquad \textbf{Equation 5. 20}$$

The results are plotted in Figure 5. 7,with error bars showing the results from three repetitive calibration runs for each calibration set. 3P-m model has lower SRMSE than SWMM LID regardless of simulated contaminant, calibration sets, or calibration runs. On average, 3P-m model reduced RMSE by 27.9 g for TDN, 17.3 g for NO_3-N, and 61.6 g for DOC, corresponding to 27.1%, 20.1%, and 41.6% of SRMSE from SWMM LID results. For the best calibration runs, 3P-1 model can also reduce SRMSE by 6.2% to 36.2%, 4.6% to 43.7%, and 40.0% to 54.7% for TDN, NO_3-N, and DOC depending on the calibration set. However, the performances among calibration runs can be less stable for 3P-1, and results from some calibration runs do not have significant improvement to the SWMM LID predictions. These results indicated that higher DDS iteration numbers or multiple times of calibration should be used for 3P-1 to find the best calibrated parameters.

When comparing the SRMSE among calibration sets, it's interesting to observe that SRMSE of NO_3-N in the Summer Set from all three models are larger than the other three calibration sets. This, combined with the large error of predicted percent removal of total mass for the Summer Set, reinforces that including events with various temperature conditions in the calibration set is crucial to successfully training the current 3P models. It should also be noted that the SRMSE values of TDN for the Summer Set are comparable to other calibration sets. Again, this is caused by the similar TDN EMCs under warmer and colder conditions as shown in Figure 5. 6 (d).

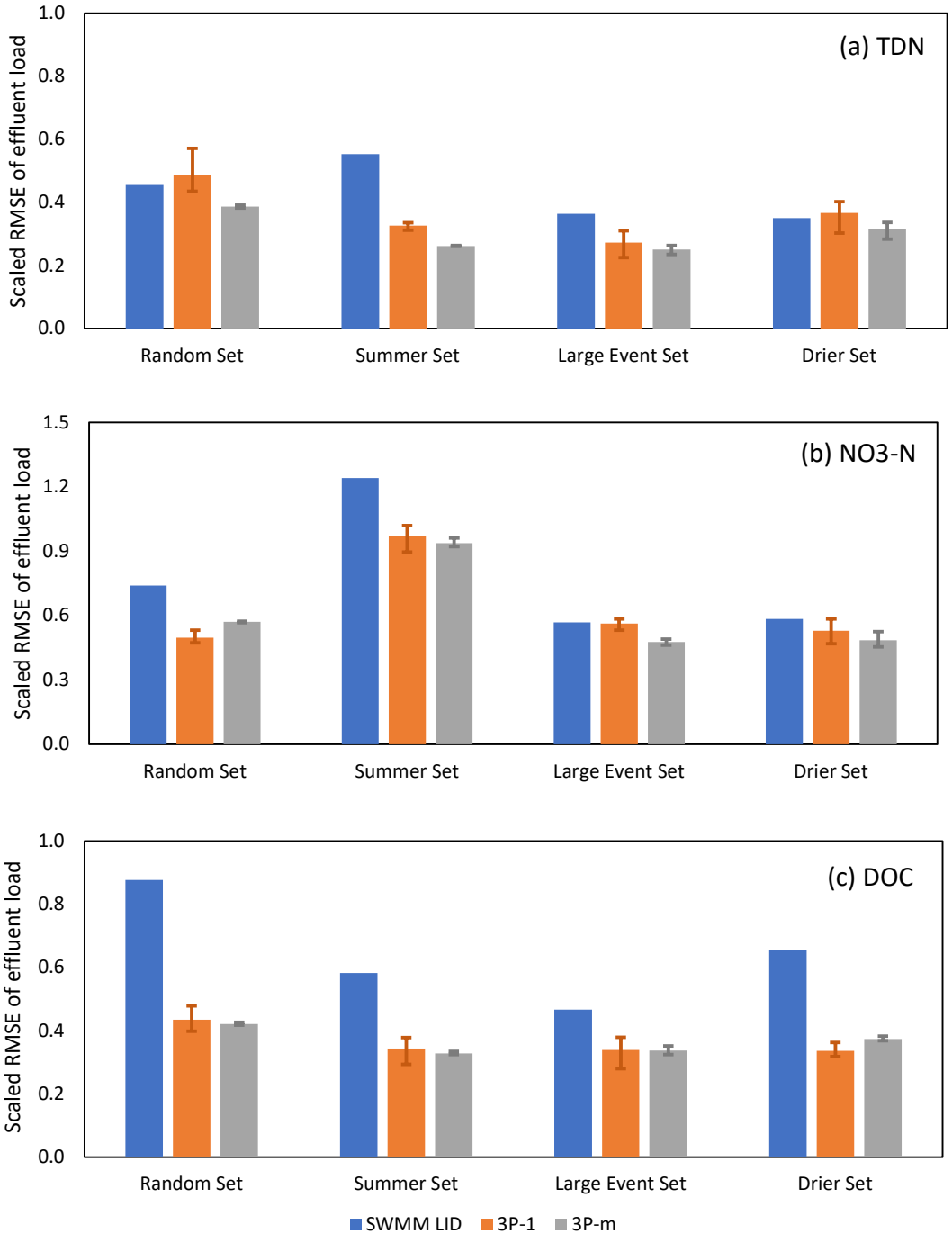

Figure 5. 7 Scaled RMSE of underdrain effluent loads of (a) TDN, (b) NO_3-N, and (c) DOC from 4 calibration sets, error bars showing variance from three times repeated calibration.

5.5.3 Statistical Analysis

The field and model simulated results were first compared with the Kolmogorov-Smirnov test [16] to see if they follow the same distribution over the 24 events. The tested parameters were percent removal of load and EMCs of NO_3-N and TDN. SWMM LID model has p values smaller than 0.05 for all four tested parameters. On the other hand, 3P-m had p values of around 0.12 for NO_3-N EMCs and percent of mass removal, and p values of 0.32 and 0.73 for TDN EMCs and percent of mass removal. The 3P-1 results showed different distributions than field-tested data for NO_3-N EMC based on a p value of 0.04, but similarity for the other three parameters was observed with p values in the range of 0.20 to 0.84. These results reveal that SWMM LID has a markedly different distribution than field-tested data while the 3P models simulated results match field-tested data with 95% confidence level for all parameters except NO_3-N EMC in 3P-1.

The correlation between various environmental factors on NO_3-N and TDN EMCs in underdrain discharge were then analyzed using Kendall's Rank test [17]. Kendall's Rank test was first applied to the field dataset. At a 95% confidence level, 7 factors had a statistically significant correlation with NO_3-N EMCs, and 11 factors had a significant correlation with TDN EMCs. In the second step, Kendall's Rank test was applied to determine the correlation between these impactful factors and the NO_3-N and TDN effluent EMCs simulated by the 3P and SWMM LID models. Based on prediction accuracy of PRL_{total} and SRMSE, the best calibration run of each calibration set from the 3P-1 and 3P-m models were selected to form the dataset from these two models.

Results are listed in Table 5. 2, with colors of the cell indicate sign of correlation and the confidence level. Light red and dark red represents positive correlation with 95% and 99% confidence level, while light blue and dark blue represent negative correlation with 95% and 99% confidence level. In the field data, higher NO_3-N EMC in the forebay inflow was found to be positively correlated with NO_3-N EMC in underdrain effluent. Temperature, maximum flow rates in forebay and the bioretention cell, average depth of pounding water in the forebay, and duration of high saturation conditions in the soil media layer are negatively correlated with NO_3-N EMC in underdrain effluent. Similarly, NO_3-N and TDN EMCs in the forebay inflow was found to be positively correlated with

TDN EMC in underdrain effluent. Temperature, maximum flow rates, and longer duration of high saturation conditions in both soil and storage layers are significantly correlated to the opposite direction. In addition, higher total volume of forebay inflow leads to lower TDN EMC in underdrain effluent, which is consistent with results from other bioretention systems reported by Koch [18].

The findings of Kendall's Rank test, as listed in Table 5. 2 and plotted in Figure 5. 8, demonstrate that 3P-1 and 3P-m models have effectively captured the impact of all the seven significant factors on NO_3-N effluent EMC. Conversely, only 43% of the 7 impactful factors for NO_3-N effluent EMCs were found statistically correlated in the SWMM LID simulated dataset.

Table 5. 2 The p values and signs of correlation from Kendall's Rank test for 7 factors with NO_3-N effluent EMC and 11 factors with TDN underdrain EMCs in the field and models simulated datasets.

for NO_3-N underdrain EMC	Field Tested	SWMMLID	3P-1	3P-m
NO_3-N EMC in BR cell inflow	(+) 0.0323	--	(+) 0.003	(+) 2.59E-06
Average temperature	(-) 1.91E-05	(-) 3.52E-08	(-) 1.65E-11	(-) 9.16E-11
Maximum flowrate of forebay inflow	(-) 5.02E-04	(-) 3.88E-05	(-) 4.08E-12	(-) 1.39E-14
Maximum flowrate of soil infiltration	(-) 0.005	(-) 3.23E-05	(-) 1.59E-10	(-) 8.16E-12
Maximum flowrate of inter-layer flow	(-) 0.032	--	(-) 1.16E-04	(-) 7.05E-11
Average depth of pounding water in forebay	(-) 0.012	--	(-) 0.001	(-) 5.23E-10
Duration of very high saturation in soil layer (>90%)	(-) 0.044	--	(-) 0.006	(-) 8.55E-09
for TDN underdrain EMC	**Field Tested**	**SWMMLID**	**3P-1**	**3P-m**
NO_3-N EMC in stormwater inflow	(+) 0.050	--	--	--
TDN EMC in BR cell inflow	(+) 0.027	--	--	(+) 2.62E-4
Volume of underdrain effluent	(-) 0.014	(+) 1.07E-6	--	(-) 8.40E-05
Average temperature	(-) 0.005	(-) 1.24E-10	(-) 0.010	(-) 2.31E-07
Maximum flowrate of forebay inflow	(-) 0.005	(-) 0.001	--	(-) 1.13E-05
Maximum flowrate of inter-layer flow	(-) 0.008	--	(-) 0.008	(-) 7.65E-08
Average depth of pounding water in forebay	(-) 7.08E-04	(+) 0.007	--	(-) 2.97E-06
Duration of high saturation in soil layer (>80%)	(-) 0.029	(+) 8.02E-08	--	(-) 3.92E-04
Duration of very high saturation in soil layer (>90%)	(-) 0.003	(+) 4.74E-04	--	(-) 1.13E-05
Duration of very high saturation in storage layer (>90%)	(-) 0.035	(+) 5.89E-09	--	(-) 6.24E-04
Duration of saturated storage layer	(-) 0.047	(+) 1.76E-08	--	(-) 4.46E-04

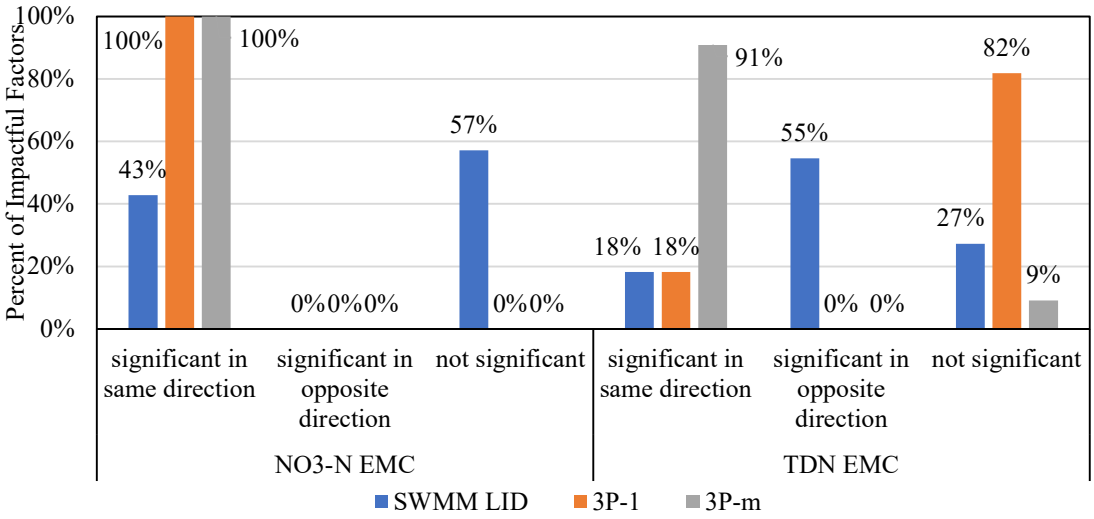

Figure 5. 8 Percentage of parameters found impactful for NO_3-N and TDN effluent EMCs in field dataset that is correctly and incorrectly captured by SWMM LID, 3P-1, and 3P-m models.

In terms of TDN, the results indicate that 3P-m has the best performance and SWMM LID the worst. Specifically, 3P-m accurately described the influence of ten out of the eleven impactful factors. The eleventh factor is NO_3-N EMC in forebay inflow, which has no significant correlation with TDN effluent EMC in the 3P-m predicted dataset. Likewise, 3P-1 successfully described the negative correlation between temperature, maximum inter-layer flow rates and TDN effluent EMCs. However, the correlations between the remaining nine impactful factors and TDN effluent EMCs were not captured. While SWMM LID also captured the negative correlation between temperature, maximum forebay inflow flow rates and TDN effluent EMCs, it also predicts significant correlations between six other impactful factors and TDN effluent EMCs to the opposite direction as the field set.

Similar to what's shown in the chapter 4, these results again reveal that SWMM LID is not capable of accurately capturing the impacts of environmental or operational conditions on nitrogen transformations in stormwater bioretention systems. Consequently, its prediction results for bioretention nitrogen removal given future weather conditions or under the valve control strategies are unreliable. Furthermore, although both 3P-1 and 3P-m demonstrated similar prediction accuracy in terms of PRL_{total} and SRMSE, 3P-m provided more accurate descriptions of the impacts of flow rates and saturation rates.

It is worthing noting that in the field dataset, maximum flow rates are negatively correlated with TDN percent mass removal, but their correlations with NO_3-N mass removal rates are not significant. Same observation has also been reported in other papers [19], [20]. For example, in a long-term field test, Lopez et al. [21] observed that when hydraulic loading rate (HLR) increased from 4.1 cm/h to 13.9 cm/h, TN removal rates in a bioretention with IWS decreased from 90% to 52%. For a bioretention system without IWS layers, TN removal rates decreased from 59% to 14% when HLR increased from 4.1 to 13.9 cm/h. HLR has not significant impacts on NO_3-N mass removal rates in the conventional system. These impacts are more significant as HLR further increase. There is no conclusive agreement on the mechanism behind this phenomenon. Given the differences between TDN and NO_3-N, it is probably reasonable to assume that organic nitrogen is the key to explanation. It is possible that higher flow rates flushed out more organic matters and caused the decrease in TDN removal rates, while NO_3-N removal rates are less impacted by flow rates as NO_3-N is readily dissolved in the liquid phase.

5.6 Predicted Time Series

The 3P-1 and 3P-m models can provide crucial insights into the simulated nitrogen cycling through their generated time series. Time series of underdrain discharged TDN loads, denitrification rates, and mass of NO_3-N in the soil layer are generated with the best calibration run of each calibration set from 3P-1 and 3P-m. Average of these time series are plotted in Figure 5. 9, together with records of precipitation, temperature, and saturation rate of the soil layer generated by the SWMM hydraulic model.

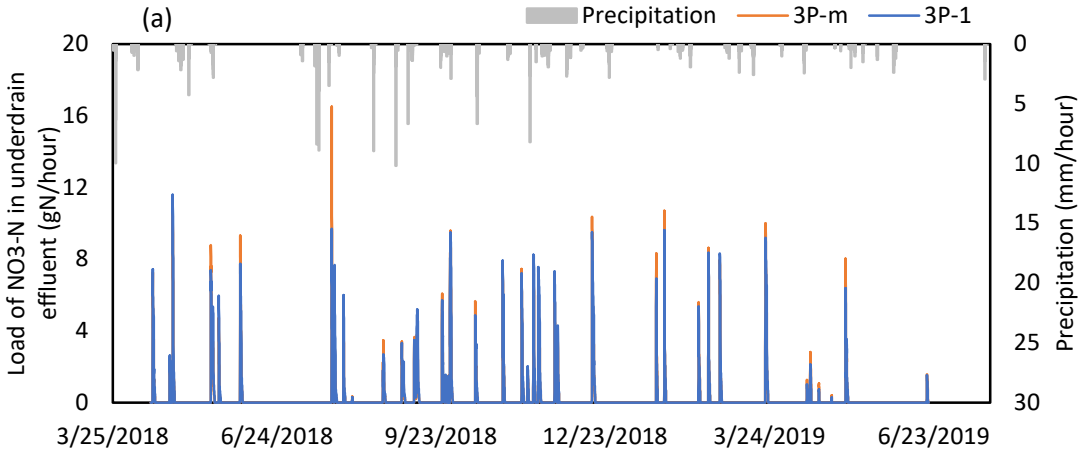

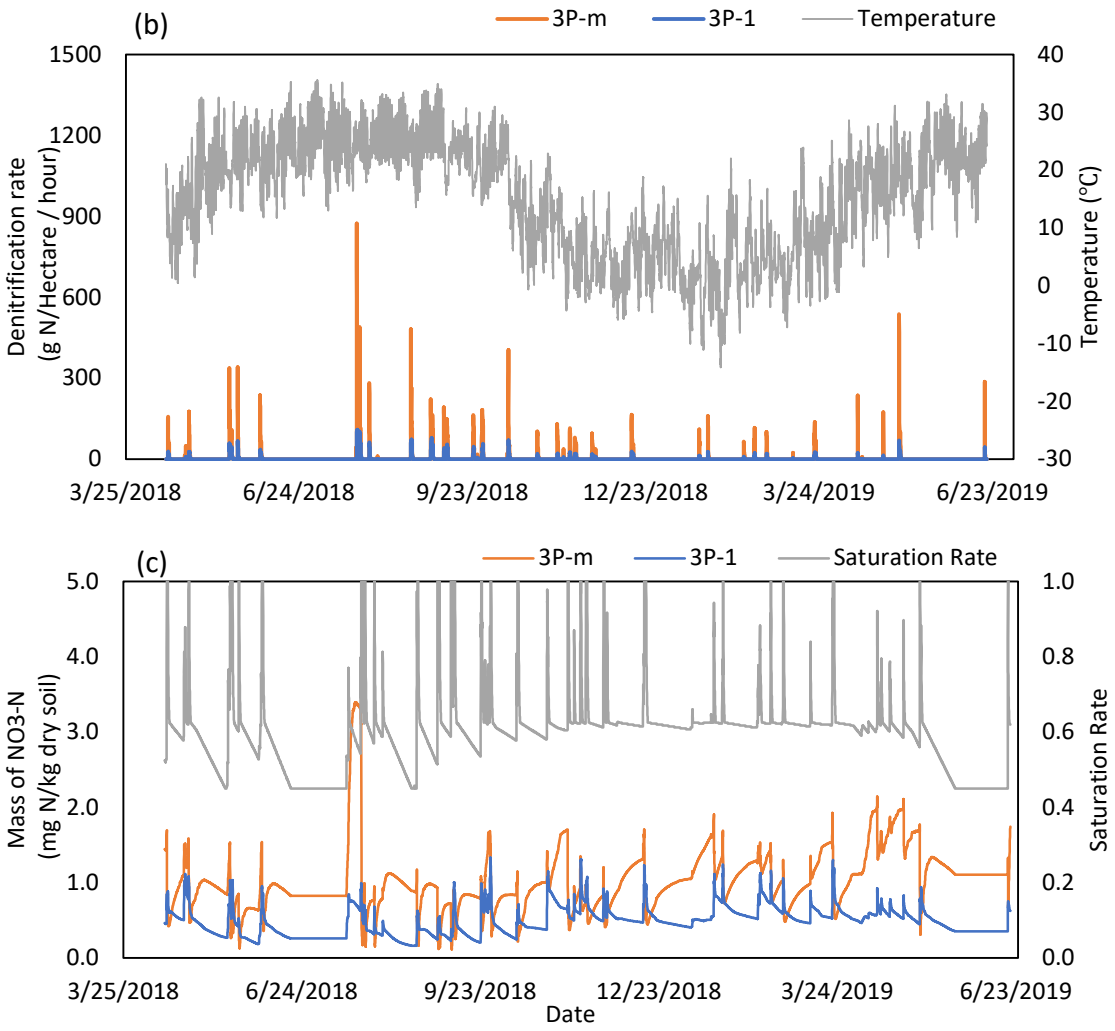

Figure 5. 9 3P-1 and 3P-m models simulated time series of (a) TDN load in underdrain effluent and precipitation (b) denitrification rate and temperature, and (c) mass of NO_3-N in soil media layer and soil saturation rate for the entire simulated period

As shown in Figure 5. 9 (a), the predicted time series of discharged NO_3-N load from the two bioretention system models are similar. Figure 5. 9 (b) illustrates that the temperature factor in 3P-1 and 3P-m models significantly impacts the reaction rates of denitrification, with higher peaks occurring in July than January. Decomposition, nitrification, organic matter supply, and plant uptake rates are similarly impacted by temperature. The peak denitrification rate from 3P-m is 8 time larger than that from 3P-1, and the average denitrification rate throughout the simulated periods from 3P-m is 3 time of that from 3P-1. Figure 5.9 (c) depicts that the 3P-1 and 3P-m models generally agree

on the range of NO_3-N mass in the soil layer, and that it is significantly impacted by rain events. However, during dry periods, the time series differ markedly.

To better understand the differences between the model predicted time series of NO_3-N mass in the soil layer, the time series from the best calibration run of each calibration sets are plotted in Figure 5. 10. The 3P-m model's projected time series under four calibration sets exhibit the same shapes and trends during precipitation events and dry periods. In contrast, the 3P-1 model's estimated time series for four calibration sets show distinct differences from one another. These findings indicate a lower level of stability of calibration results for the 3P-1 model. For this bioretention site, 3P-1 does not provide conclusive predictions on whether NO_3-N accumulates or depletes during the dry periods. Thus, the insights provided by analyzing time series predicted by 3P-1 carry a lower level of confidence.

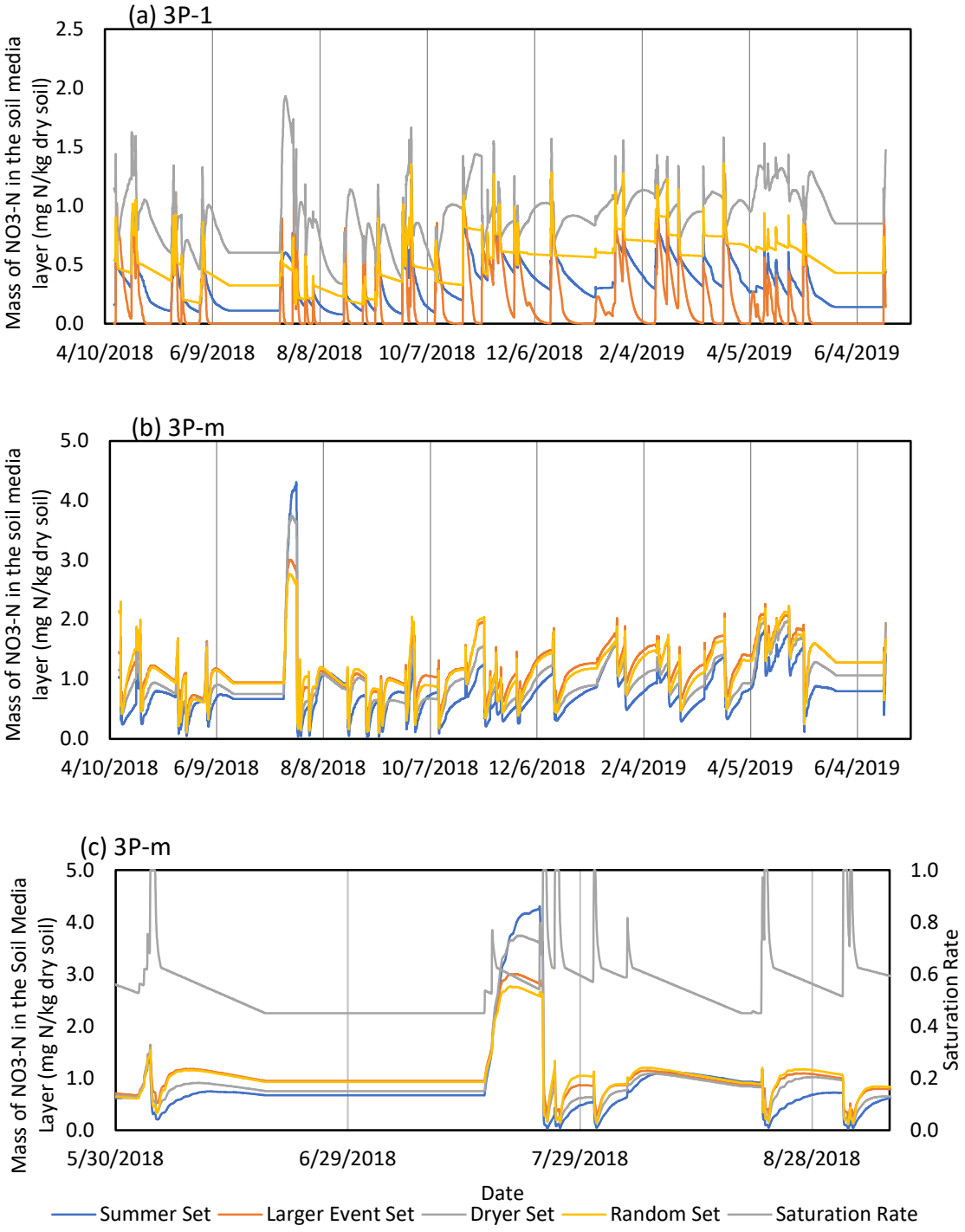

Figure 5. 10 Time series of mass of NO_3-N predicted from the best run of each calibration set from (a) 3P-1 and (b) 3P-m, and (c) 3P-m from May 30th to Sep 7th.

To look at fluctuations in more detail, Figure 5. 10 (c) displays the time series from May 30th to Sep 7th of the mass of NO_3-N in the soil layer as predicted by 3P-m. According to 3P-m simulations, mass of NO_3-N reaches peaks during rain events and falls rapidly after rain events when the saturation rate exceeds 80%. During dry periods, NO_3-N mass initially increases as the saturation rate decreases from 80% to field capacity (62.5%), before decreasing again as the saturation rate drops to the wilting point (45%). During the one-month dry period from Jun 19th and July 18th, NO_3-N mass remains constant. These trends were not the same as in chapter 4 which did not adjust the saturation rate factor, as described in Figure 5. 1 (b). Although the rates of NO_3-N accumulation and depletion during dry periods differ slightly, the overall trend remains consistent between calibration sets.

Further details on time series of discharged NO_3-N loads, decomposition, nitrification, denitrification, and plant uptake rates predicted by the 3P-1 and 3P-m models are provided with Figure S 10 to Figure S 14 in the supplementary materials. These figures reveal that the 3P-1 model's predicted rates of decomposition, nitrification, and plant uptake vary widely across calibration sets, while those of 3P-m remain consistent. For 3P-m, the average predicted denitrification rate is 600 times greater than the average plant uptake rate, indicating that denitrification dominates NO_3-N removal. Due to the low stability of calibration results, 3P-1 is considered less effective than 3P-m and is not discussed in the following sections. Detailed time series from 3P-m with best calibration run of each calibration set are plotted with temperature and soil saturation conditions in Figure S 15 to Figure S 18 in the supplementary materials.

Accurate predictions of the NO_3-N load in the underdrain effluent with small time steps are valuable for supporting the design of valve control rules. Figure 5. 11 illustrates the accumulated NO_3-N load in underdrain effluent from events with varying rainfall characteristics, along with the accumulated volume of underdrain effluent. In Figure 5. 11 (a), the two events in July, 60% of the total discharged NO_3-N load was carried by the first 20% of effluent volume. Thus, retaining stormwater inflow at the beginning of events is effective for NO_3-N removal. In Figure 5. 11 (b), the two events in September differ from the Type II event which is typically used to simulate design events in Virginia

[22], [23]. For the event on Sep 23rd, the last 10% of underdrain effluent carries 20% of total discharged NO_3-N load. For the event on Sep 27th, over 80% of the NO_3-N load was discharged after the first four hours. For these two events, retaining stormwater as soon as rain events start might not be the most effective way to improve nitrogen mass removal. These figures underscore the importance of precise predictions regarding precipitation event characteristics and nitrogen transformations in small time steps and suggest that real-time valve control rules should be designed not only based on stormwater management objectives but should also consider the impacts of antecedent dry periods, temperature, and rainfall intensity distribution within events.

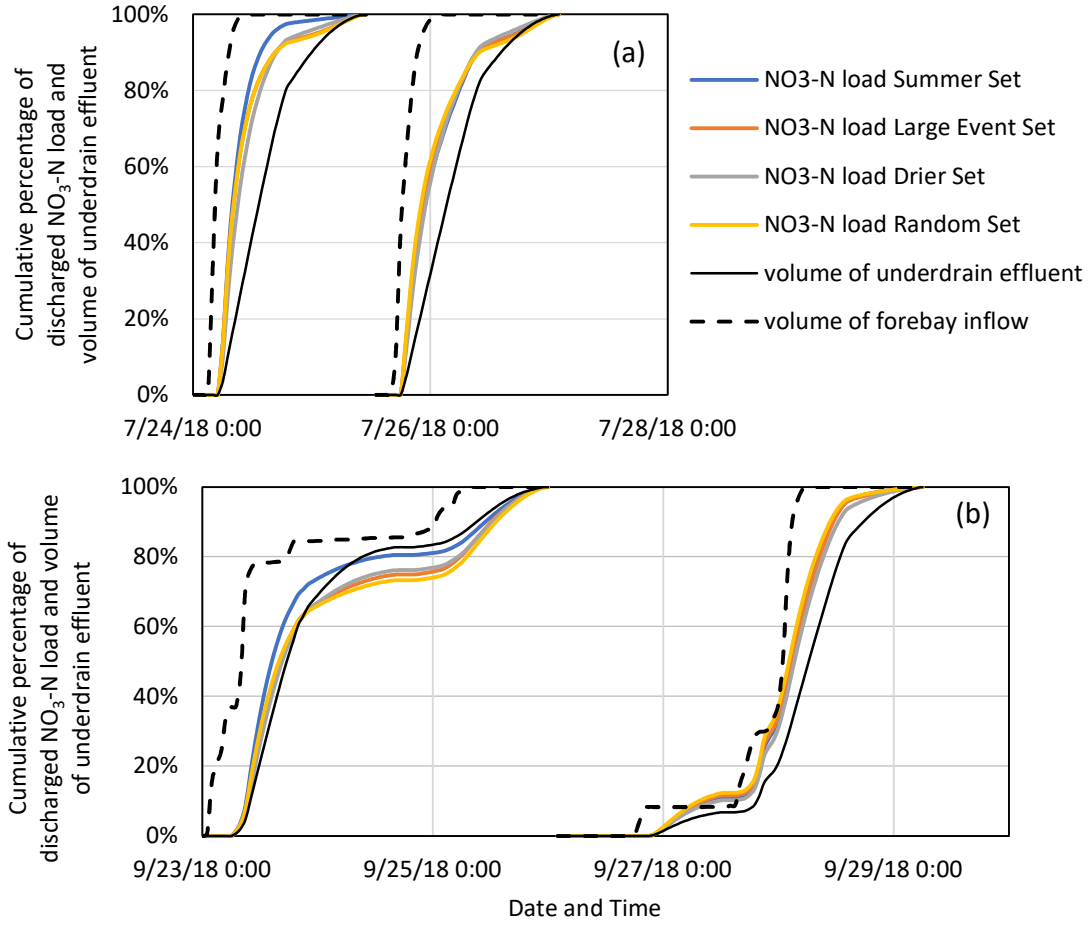

Figure 5. 11 Cumulative percentages of NO_3-N load discharged through underdrain effluent, volume of underdrain effluent, and volume of forebay inflow for (a) two events in July and (b) two events in September predicted by 3P-m model.

5.7 NO_3-N Sources and Sinks

This section examines the percentage contribution of each source and sink of NO_3-N in the bioretention cell, based on 3P-m simulations using the Random Set's best calibration run. The two sources of NO_3-N were identified as forebay inflow and nitrification, while the four sinks of NO_3-N were identified as denitrification, underdrain discharge, loss via bypass or infiltration into deeper groundwater, and plant uptake. The total amount of NO_3-N from each of the two sources and the amount of NO_3-N lost through each of the four sinks from the end of the preceding event until the end of each simulated event were calculated. The resulting percentages for both the sources and sinks are plotted in Figure 5. 12. The results show that the contributions of immobilization and underdrain discharge to NO_3-N loss are negligible for all events, and that most NO_3-N in bioretention cell are lost through volume reduction (including bypass and deep infiltration) or denitrification. As a source, nitrification contributes to 43% of NO_3-N on average. Contribution from nitrification and denitrification to NO_3-N accumulation and loss in bioretention cell are higher from May to October, reflecting higher biochemical activity during summertime. This result is consistent with the field isotope test, which revealed an enrichment of N^{15}-NO_3 from bioretention system inlet to outlet in eight out of eleven events that occurred from May to October, but only in two of the remaining thirteen events during the colder months [5]. This alignment of results provides strong evidence of the reliability of the 3P-m model in describing nitrogen cycling in bioretention systems.

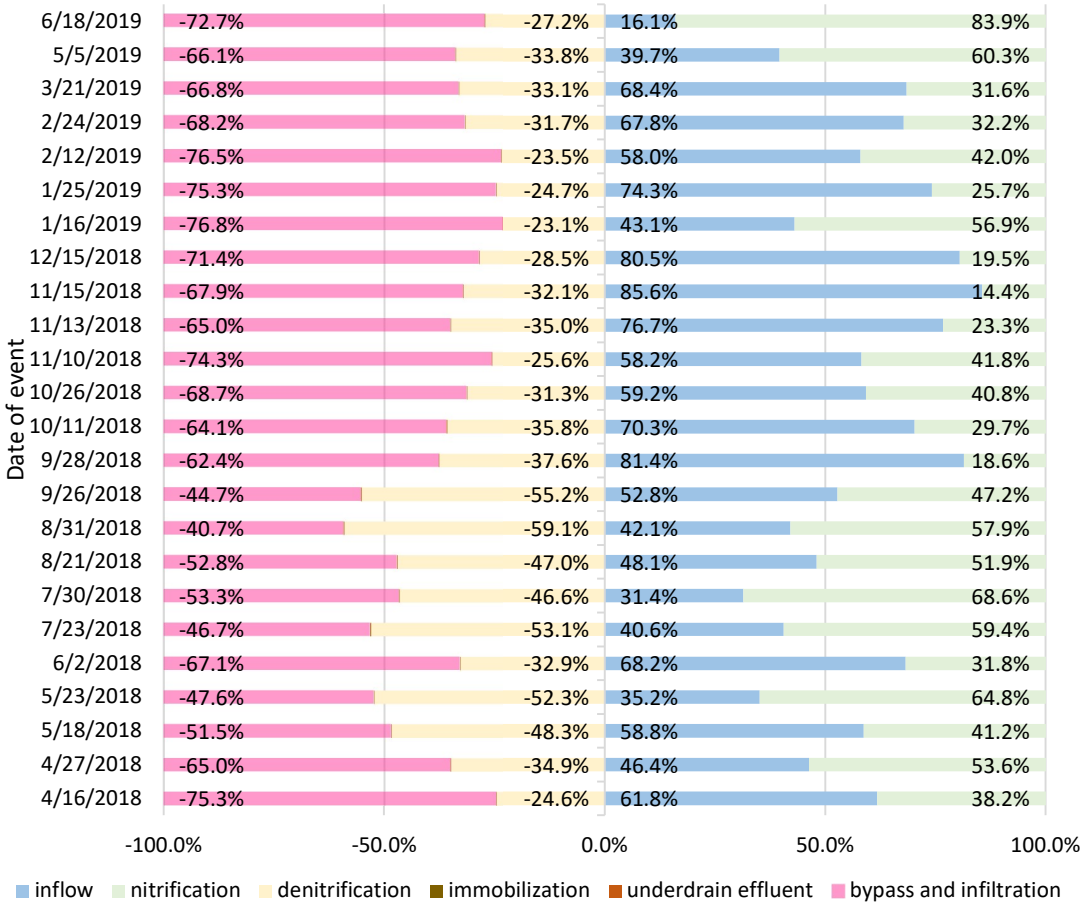

Figure 5. 12 Percent contribution of NO_3-N sources and sinks predicted by 3P-m

5.8 Discussion and Conclusions

In this chapter, the 3P-1 and 3P-m model are used to simulate the nitrogen transformations in a field bioretention system. The models were updated to describe the nitrogen-related processes in the forebay and the storage layer and provide more detailed description of the saturation rate factor. Calibration and validation results show that 3P-m model can improve prediction accuracy of percent removal of TDN load over 12 validated events by 5.5% to 10.6% and reduce SRMSE of TDN load in underdrain effluent by 16.2% to 53.0% when compared to SWMM water quality model, varying with calibration set. The improvements on prediction accuracy of DOC discharge load are even more significant. For the best calibration run in each calibration set, the 3P-1 model can also improve prediction accuracy and even outperform 3P-m. However, the 3P-1 model has less stable calibration results than 3P-m, and its predicted time series of

biochemical reaction rates and nitrogen content are not reliable. Time series analysis further suggests that precise simulations of discharged NO_3-N loads with smaller time steps are beneficial for designing bioretention valve control rules. Additionally, antecedent dry periods, temperature, as well as intensity and duration of rain events should all be considered when designing bioretention systems for nitrogen removal.

Statistical analysis shows that 3P-m generated NO_3-N and TDN percent mass removal and EMCs have the same distribution over the 24 monitored events with field-tested data, while all these four parameters predicted by SWMM have distinct distributions. Kendall's Rank test shows that the 3P models have correct descriptions on the impacts of temperature, inflow EMCs, maximum flow rates, total inflow volume, and soil saturation rate on NO_3-N EMCs in underdrain discharge, which SWMM water quality model fails to do. When it comes to TDN, 3P-m has the best performance as it successfully captures 10 out of 11 impactful factors. 3P-1 missed the correlation between soil saturation conditions and TDN EMCs in underdrain discharge, but still outperforms SWMM which predicts the impacts of 6 of the 11 factors to the opposite direction.

According to 3P-m simulations, nitrification and denitrification are more active during summertime and takes up higher percentages of NO_3-N sources and sinks in the soil media layer. These results agree with field isotope tests, providing strong evidence that the 3P-m model correctly describe the seasonality of physical processes in nitrogen cycling.

In general, when compared to the field results, the 3P-m model is shown to be stable and reliable in simulating nitrogen loads and EMCs in bioretention underdrain discharge with good accuracy and 10-min time steps. It also describes nitrogen transformation processes under the impacts of time-varying environmental conditions including soil saturation conditions, temperature, organic contents, and precipitation characteristics.

References

[1] K. M. McCabe, E. M. Smith, S. Q. Lang, C. L. Osburn, and C. R. Benitez-Nelson, "Particulate and Dissolved Organic Matter in Stormwater Runoff Influences Oxygen Demand in Urbanized Headwater Catchments," *Environ Sci Technol*, vol. 55, no. 2, pp. 952–961, 2021, doi: 10.1021/acs.est.0c04502.

[2] S. Kalev and G. S. Toor, "Concentrations and Loads of Dissolved and Particulate Organic Carbon in Urban Stormwater Runoff," *Water (Basel)*, vol. 12, no. 4, 2020, doi: 10.3390/w12041031.

[3] S. T. Pamuru, E. Forgione, K. Croft, B. V Kjellerup, and A. P. Davis, "Chemical characterization of urban stormwater: Traditional and emerging contaminants," *Science of The Total Environment*, vol. 813, p. 151887, 2022, doi: https://doi.org/10.1016/j.scitotenv.2021.151887.

[4] Y. Li *et al.*, "A spatially referenced water and nitrogen management model (WNMM) for (irrigated) intensive cropping systems in the North China Plain," *Ecol Modell*, vol. 203, no. 3, pp. 395–423, 2007, doi: https://doi.org/10.1016/j.ecolmodel.2006.12.011.

[5] C. R. Burgis, G. M. Hayes, W. Zhang, D. A. Henderson, S. A. Macko, and J. A. Smith, "Tracking denitrification in green stormwater infrastructure with dual nitrate stable isotopes," *Science of The Total Environment*, vol. 747, p. 141281, 2020, doi: https://doi.org/10.1016/j.scitotenv.2020.141281.

[6] C. R. Burgis, G. M. Hayes, D. A. Henderson, W. H. Zhang, and J. A. Smith, "Green stormwater infrastructure redirects deicing salt from surface water to groundwater," *SCIENCE OF THE TOTAL ENVIRONMENT*, vol. 729, 2020, doi: 10.1016/j.scitotenv.2020.138736.

[7] "Virginia DEQ Stormwater Design Specification vol. No.9 Bioretention," Mar. 2011. Accessed: Dec. 21, 2021. [Online]. Available: https://www.swbmp.vwrrc.vt.edu/wp-content/uploads/2017/11/BMP-Spec-No-9_BIORETENTION_v1-9_03012011.pdf

[8] "Weather Underground." https://www.wunderground.com/history/daily/KDCA/date/2018-6-29 (accessed Jun. 28, 2023).

[9] D. N. Moriasi, M. W. Gitau, N. Pai, and P. Daggupati, "Hydrologic and Water Quality Models: Performance Measures and Evaluation Criteria," *Trans ASABE*, vol. 58, no. 6, pp. 1763–1785, 2015, doi: https://doi.org/10.13031/trans.58.10715.

[10] F. Kachholz and J. Tranckner, "Long-Term Modelling of an Agricultural and Urban River Catchment with SWMM Upgraded by the Evapotranspiration Model UrbanEVA," *Water (Basel)*, vol. 12, no. 11, 2020, doi: 10.3390/w12113089.

[11] C. Santhi, J. G. Arnold, J. R. Williams, W. A. Dugas, R. Srinivasan, and L. M. Hauck, "Validation of the SWAT Model on a Large RWER Basin with Point and Nonpoint

Sources," *JAWRA Journal of the American Water Resources Association*, vol. 37, no. 5, pp. 1169–1188, Oct. 2001, doi: https://doi.org/10.1111/j.1752-1688.2001.tb03630.x.

[12] B. A. Tolson and C. A. Shoemake, "Dynamically dimensioned search algorithm for computationally efficient watershed model calibration DYNAMICALLY DIMENSIONED SEARCH ALGORITHM," *Water Resour Res*, vol. 43, no. 1, Jan. 2007.

[13] E. Kavehei, G. A. Jenkins, C. Lemckert, and M. F. Adame, "Carbon stocks and sequestration of stormwater bioretention/biofiltration basins," *Ecol Eng*, vol. 138, pp. 227–236, 2019, doi: 10.1016/j.ecoleng.2019.07.006.

[14] E. Kavehei, B. S. Farahani, G. A. Jenkins, C. Lemckert, and M. F. Adame, "Soil nitrogen accumulation, denitrification potential, and carbon source tracing in bioretention basins," *Water Res*, vol. 188, 2021, doi: 10.1016/j.watres.2020.116511.

[15] H. Kratky, Z. Li, Y. Chen, C. Wang, X. Li, and T. Yu, "A critical literature review of bioretention research for stormwater management in cold climate and future research recommendations," *Front Environ Sci Eng*, vol. 11, no. 4, p. 16, 2017, doi: 10.1007/s11783-017-0982-y.

[16] Hubert W. Lilliefors, "On the Kolmogorov-Smirnov Test for the Exponential Distribution with Mean Unknown," *J Am Stat Assoc*, vol. 64, no. 325, 1969.

[17] M. G. KENDALL, "A NEW MEASURE OF RANK CORRELATION," *Biometrika*, vol. 30, no. 1–2, pp. 81–93, Jun. 1938, doi: 10.1093/biomet/30.1-2.81.

[18] B. J. Koch, "Nitrogen Removal by Stormwater Management Structures: A Data Synthesis," *J Am Water Resour Assoc*, vol. 50, no. 6, pp. 1594–1607, Dec. 2014.

[19] S. Igielski, "Understanding urban stormwater denitrification in bioretention internal water storage zones," *Water environment research*, vol. 91, no. 1, pp. 32–44, Jan. 2019.

[20] E. V Lopez-Ponnada, T. J. Lynn, M. Peterson, S. J. Ergas, and J. R. Mihelcic, "Application of denitrifying wood chip bioreactors for management of residential non-point sources of nitrogen," *J Biol Eng*, vol. 11, no. 1, p. 16, 2017, doi: 10.1186/s13036-017-0057-4.

[21] E. V Lopez-Ponnada, T. J. Lynn, S. J. Ergas, and J. R. Mihelcic, "Long-term field performance of a conventional and modified bioretention system for removing dissolved nitrogen species in stormwater runoff," *Water Res*, vol. 170, p. 115336, 2020, doi: https://doi.org/10.1016/j.watres.2019.115336.

[22] United States Department of Agriculture, "National Engineering Handbook Part 630 Hydrology Chapter 4 Storm Rainfall Depth and Distribution," 2019. https://directives.sc.egov.usda.gov/OpenNonWebContent.aspx?content=43924.wba (accessed Jul. 01, 2023).

[23] United States Department of Agriculture, “USDA Technical Release 55 Urban Hydrology for Small Watersheds,” 1986. https://www.nrc.gov/docs/ML1421/ML14219A437.pdf (accessed Jul. 01, 2023).

6 Conclusions and Future Research Opportunities

In this dissertation, six version of Nitrogen Removal Model (NRM) are developed and tested with laboratory and field-tested datasets. Results show that:

a) 0-order kinetics is not suitable for NRM.

b) The SP and 3P models with first order kinetics and Michaelis Menten equations significantly improve prediction accuracy for percent removal of nitrogen loads and event mean concentrations compared to the widely applied Storm Water Management Model (SWMM).

c) The more complex structure of the 3P models allows them to capture environmental factors and operational conditions, according to statistical analysis results.

d) Validation with the field dataset reveals that the 3P-m model outperforms the 3P-1 model in terms of stability of calibration results and reliability of generated time series.

e) Our study generates time series of effluent concentrations, discharged loads, and biochemical reaction rates using the 3P-m model, providing insights into nitrogen removal processes in bioretention systems. These insights can assist in designing physical structures, operational conditions, and valve control rules with simulation results as evidence.

Overall, our research demonstrates the potential of 3P-m in predicting nitrogen removal and concentrations accurately. The 3P-m model offers stable calibration results and reliable time series, making it a valuable tool for designing bioretention systems and valve control strategies in bioretention systems.

During development and validation processes of NRM, we also recognized some limitations:

a) To simplify the development process, the first order kinetics and Michaelis-Menten equation was applied to all biochemical processes in 3P-1 and 3P-m, respectively. However, it is possible that different biochemical processes are best fitted with different kinetics.

b) The sensitivity of initial conditions, pre-set parameter values, and warm up period has not been tested.

c) Estimating N_2O emission rates remains challenging due to the scarcity of field-tested data from urban environments and bioretention systems. As such, our current estimation method remains coarse.

Given great potential and limitations of NRM 3P-m, the following topics are recommended as future research opportunities:

a) Assisting in the design of valve control strategies: Developing NRM was motivated by the need to assist in designing valve control strategies. With validation results from chapters 4 and 5, we believe that 3P-m can provide reliable predictions for bioretention nitrogen removal rates under various valve control strategies. With the help of 3P-m, it would be exciting to test different valve control strategies and assess whether they can meet specifics goals of volume reduction and nitrogen removal. This will help to create general rules of thumb for stormwater management practices oriented towards flood prevention, water resource recovery, or a balance between these two goals under current and future climate conditions.

b) Further updates and validations of NRM: Further validation with datasets from field bioretention systems will be essential in understanding the hidden strengths and weaknesses of 3P-m and expanding its application scenarios. Validations will also facilitate possible upgrades of the SP-1, SP-m, or 3P-1 model.

Although it is currently challenging to simulate N_2O emissions and plant activities with equations describing relevant biochemical processes, the seasonality of plant impacts can potentially be better estimated with an empirical factor. Empirical equations describing gas emissions are also provided by agricultural models. With filed-tested data from urban environments provided, they can be leveraged for the NRMs.

c) Sensitivity test on calibrated parameters, pre-set parameters, initial conditions, and warm-up periods is helpful for further understandings on the functionality and characteristics of the current NRMs. As none of these sensitivity tests is practiced in this dissertation due to the limited time, they are suggested for future research.

d) Integrating NRM with SWMM: The current NRM has been developed as a stand-alone extension Python package to SWMM that focuses on nitrogen removal and transformations. Integrating this package with SWMM will offer exciting opportunities for interactions between hydraulic analysis and nitrogen simulations, opening doors for new and innovative research. Such integration can also enhance the prediction accuracy of SWMM and other stormwater models in terms of nitrogen transformation and removal. Ultimately, integrating NRM with other stormwater models will contribute to building more comprehensive and accurate models for sustainable stormwater management practices.

Supplementary Materials

Summary:

3 tables and 18 graphs

Chapter 3

Table S 1 Meaning of math symbols used in section 2.5.

Symbols	Meaning	Unit
C_p	Changes of carbon content over time, with subscript p describing the relevant process.	$Mass \cdot Mass^{-1} \cdot Time^{-1}$ $Mass \cdot Area^{-1} \cdot Time^{-1}$ $Mass \cdot Volume^{-1} \cdot Time^{-1}$
N_p	Changes of nitrogen content over time, with subscript p describing the relevant process.	$Mass \cdot Mass^{-1} \cdot Time^{-1}$ $Mass \cdot Area^{-1} \cdot Time^{-1}$ $Mass \cdot Volume^{-1} \cdot Time^{-1}$
k_p	Optimal reaction rate constant, with subscript p describing the relevant reaction.	Units of reaction rate for 0-order, 1st-order, or Michaelis-Menten kinetics
f_{en}	Parameter of comprehensive environmental factor representing the limitation of restrictive environmental conditions	dimensionless
$f_{z,p}$	Parameter of one specific limiting environmental factor, with subscript z and p representing the environmental factor and relevant process.	dimensionless
CNR	Carbon to Nitrogen ratio in soil layer, sub organic matter pools, or biomass.	dimensionless
NH_4, NO_3 InN	Concentration of ammonium-nitrogen, nitrate-nitrogen, and inorganic nitrogen.	$Mass \cdot Mass^{-1}$ $Mass \cdot Area^{-1}$ $Mass \cdot Volume^{-1}$
N_aO_b	Concentration of nitrogen in species including nitrate (NO_3^-), nitrite (NO_2^-), nitric oxide (NO), and nitrous oxide (N_2O).	$Mass \cdot Mass^{-1}$
$N_xO_{y,p}$	Emission rates of nitrogen oxide gases in the possible forms of N_2O, NO, and N_2.	$Mass \cdot Mass^{-1} \cdot Time^{-1}$ $Mass \cdot Area^{-1} \cdot Time^{-1}$
TNO	Total concentration of nitrogen in oxides.	$Mass \cdot Mass^{-1}$
μ	Relative growth rate of denitrifying bacteria, varies with nitrogen species.	$Time^{-1}$
Y	Maximum growth rate of denitrifying bacteria, varies with nitrogen species.	$kg\ C \cdot kg\ N^{-1}$
M	Maintenance coefficient of denitrifying bacteria, varies with nitrogen species.	$kg\ N \cdot kg^{-1} \cdot h^{-1}$
α_p	Maximum fraction of nitrogen that can be emitted as N_2O. Subscript p describes the relevant process.	dimensionless
B_p	Total microbial biomass, with subscript indicating the species of bacteria evolved in certain process.	$Mass$

Table S1 (cont.) Meaning of math symbols used in section 2.5.

Symbols	Meaning	Unit
AD, D	Coefficients for adsorption and diffusion.	dimensionless
CLAY, $CLAY_{max}$	Real-time and maximum possible clay content of the simulated soil. (by default, $CLAY_{max}$ = 0.63)	dimensionless
K_{NH_4}, K_{H_2O}	Dissociation constants for the NH_4^+: NH_3 and H^+: OH^- equilibrium.	$Mass \cdot Volume^{-1}$
$\beta_{N_xO_y}$	Empirical coefficients for production, with subscript indicating the produced nitrogen oxide.	dimensionless
γ	Empirical factor reflecting the resistance to NH_3 transport from soil surface to the atmosphere.	dimensionless
R_f	Retardation factor for ammonia.	dimensionless
s	Soil saturation rate.	dimensionless
θ	Soil moisture content.	dimensionless
Z	Depth from soil surface.	$Length$
FR	Amount of flat residue.	$Mass \cdot Area^{-1}$
NP_{FR}	Nitrogen concentration in crop residues.	$Mass \cdot Mass^{-1}$
$NP_{opt,day}$, $NP_{opt,day-1}$, $NP_{act,day-1}$	Optimal nitrogen concentration in plant at current and previous day of the year; and actual nitrogen concentration in plant at the precious day.	$Mass \cdot Mass^{-1}$
NP_{grain}, NP_{shoot}, NP_{root}	Nitrogen content in plant, with subscriptions indicating the part of crop plant.	percentage
PB_{day}, PB_{day-1}	Content of plant biomass (roots and above ground) at current and previous day of the year.	$Mass \cdot Area^{-1}$
WU_{day}	Water taken by plant at current day of the year.	$Length$
WP	Wilting point.	dimensionless
E_{micro}	Empirical coefficient of microbial efficiency of assimilating carbon released from decomposition.	dimensionless
α_{imm}	Mass fraction of decomposition released carbon that is immobilized.	dimensionless
InN_{max}	The amount of inorganic nitrogen	$Mass \cdot Volume^{-1}$
YLD	Crop yield.	$Mass \cdot Area^{-1}$
HI	Plant harvest index.	dimensionless
RSR	The root-to-shoot ratio of plant at maturity.	dimensionless
N_{mde}, N_{pde}	Nitrogen demand for microbe and plant growth.	$Mass \cdot Area^{-1} \cdot Time^{-1}$

Chapter 4

Table S 2 Summary of mass balance calculations from lab experiment and SWMM simulations for the four columns over entire experimental period

	Total Inflow (L)			Effluent (L)			Total EVT (L)			Internal Flow	
Column	lab	SWMM	VE%	lab	SWMM	VE%	lab	SWMM	VE%	Flow1	Flow2
FD1	160.43	160.76	0.21	149.81	150.24	0.29	11.91	12.28	3.11	157.44	153.93
FD2	160.43	160.82	0.24	154.40	154.86	0.30	8.27	8.37	1.21	158.93	156.94
FD4	160.43	160.76	0.21	130.45	130.88	0.33	29.98	30.51	1.77	151.02	141.02
FD5	160.43	160.74	0.19	145.46	145.49	0.02	16.90	17.22	1.89	155.93	150.85
FD average	160.43	160.77	0.21	145.03	145.37	0.23	16.77	17.10	1.99		
IWS1	145.28	145.49	0.14	121.13	120.65	-0.40	28.33	29.07	2.61	133.14	
IWS2	145.28	145.51	0.16	109.95	110.23	0.25	37.26	37.99	1.96	128.59	
IWS3	145.28	145.44	0.11	128.18	129.28	0.86	18.71	19.35	3.42	137.87	
IWS4	145.28	145.27	-0.01	119.42	118.19	-1.03	29.73	30.62	2.99	131.56	
IWS average	145.28	145.43	0.10	119.67	119.59	-0.08	28.51	29.26	2.75		
SM1	160.43	160.70	0.17	143.62	144.62	0.70	18.41	18.86	2.44	155.14	149.84
SM2	160.43	160.73	0.19	122.02	122.20	0.15	39.37	40.55	3.00	147.96	135.38
SM3	145.28	145.31	0.02	119.25	120.27	0.86	27.65	28.29	2.31	136.73	128.62
SM4	145.28	145.59	0.21	118.51	118.32	-0.16	28.70	29.40	2.44	136.68	127.67
SM5	145.28	145.41	0.09	106.38	106.34	-0.04	40.20	40.95	1.87	132.99	120.01
SM average	151.34	151.55	0.14	121.96	122.35	0.30	30.87	31.61	2.41		
VC1	145.28	145.25	-0.02	108.53	108.24	-0.27	40.93	42.18	3.05	132.35	119.49
VC2	143.39	143.41	0.01	140.64	141.73	0.78	4.36	9.17	110.32	141.90	140.43
VC3	145.28	145.39	0.08	131.33	131.76	0.32	18.14	18.69	3.01	140.40	135.41
VC4	145.28	145.42	0.10	117.78	118.90	0.95	29.43	29.69	0.88	136.58	127.74
VC5	145.28	145.41	0.09	133.92	134.16	0.18	13.94	14.26	2.30	141.50	137.60
VC average	144.90	144.98	0.05	126.44	126.96	0.39	21.36	22.80	23.91		

Table S 3 Average TIN EMCs from lab test and model simulations, and percent error of simulated average TIN EMCs from 7 models

	Average TIN EMC (mg N/L)				Percent Error (%)			
	FD	IWS	SM	VC	FD	IWS	SM	VC
lab	0.70	0.41	0.58	0.44				
SWQ	0.54	0.77	0.39	0.82	-23.55	89.91	-32.11	87.68
SP-0	0.31	3.94	7.17	8.60	-55.56	867.13	1138.03	1874.36
SP-1	0.49	0.37	0.49	0.35	-29.55	-9.50	-15.10	-19.18
SP-m	0.50	0.43	0.52	0.39	-28.43	5.87	-10.72	-10.34
3P-0	0.53	0.46	0.47	0.46	-25.14	13.47	-18.82	5.06
3P-1	0.64	0.43	0.68	0.53	-8.30	5.77	17.09	21.35
3P-m	0.55	0.40	0.58	0.47	-21.31	-2.48	0.61	8.29

Chapter 5

Table S 4 Events selected for calibration and validation sets in Chapter 5, together with their total precipitation (P), daily average temperature (T), and number of antecedent dry days (ADP).

Date	Random Set	Summer Set	T (°C)	Large Event Set	P (mm)	Drier Set	ADP (d)
4/16/2018	V	V	12.5	C	94.5	C	24
4/27/2018	C	V	14.1	V	26.4	V	2
5/18/2018	C	C	17.2	C	93.5	C	22
5/23/2018	V	C	23.5	V	21.8	V	4
6/2/2018	C	C	25.0	C	51.1	C	10
7/23/2018	V	C	26.0	C	104.9	V	6
7/30/2018	C	C	23.3	V	24.4	V	5
8/21/2018	V	C	25.1	C	72.1	C	17
8/31/2018	C	C	27.9	C	72.6	C	10
9/26/2018	V	C	24.2	V	7.4	V	1
9/28/2018	C	C	17.6	C	39.9	V	2
10/11/2018	V	C	24.7	C	86.1	C	13
10/26/2018	C	V	9.0	V	39.6	C	15
11/10/2018	V	V	5.9	V	14.0	C	15
11/13/2018	V	V	8.0	V	32.0	V	3
11/15/2018	V	V	2.7	C	43.7	V	2
12/15/2018	V	V	11.1	C	103.6	C	14
1/16/2019	V	V	2.0	V	24.1	V	7
1/25/2019	C	V	2.9	V	27.4	V	6
2/12/2019	C	V	3.5	V	15.2	C	18
2/24/2019	C	V	7.1	V	32.8	V	4
3/21/2019	V	V	8.0	C	64.8	C	12
5/5/2019	C	C	18.1	C	78.7	V	9
6/18/2019	C	C	23.9	V	19.1	C	44

Note: in this table ‘V’ marks out events used for validation, while ‘C’ represents Calibrated events.

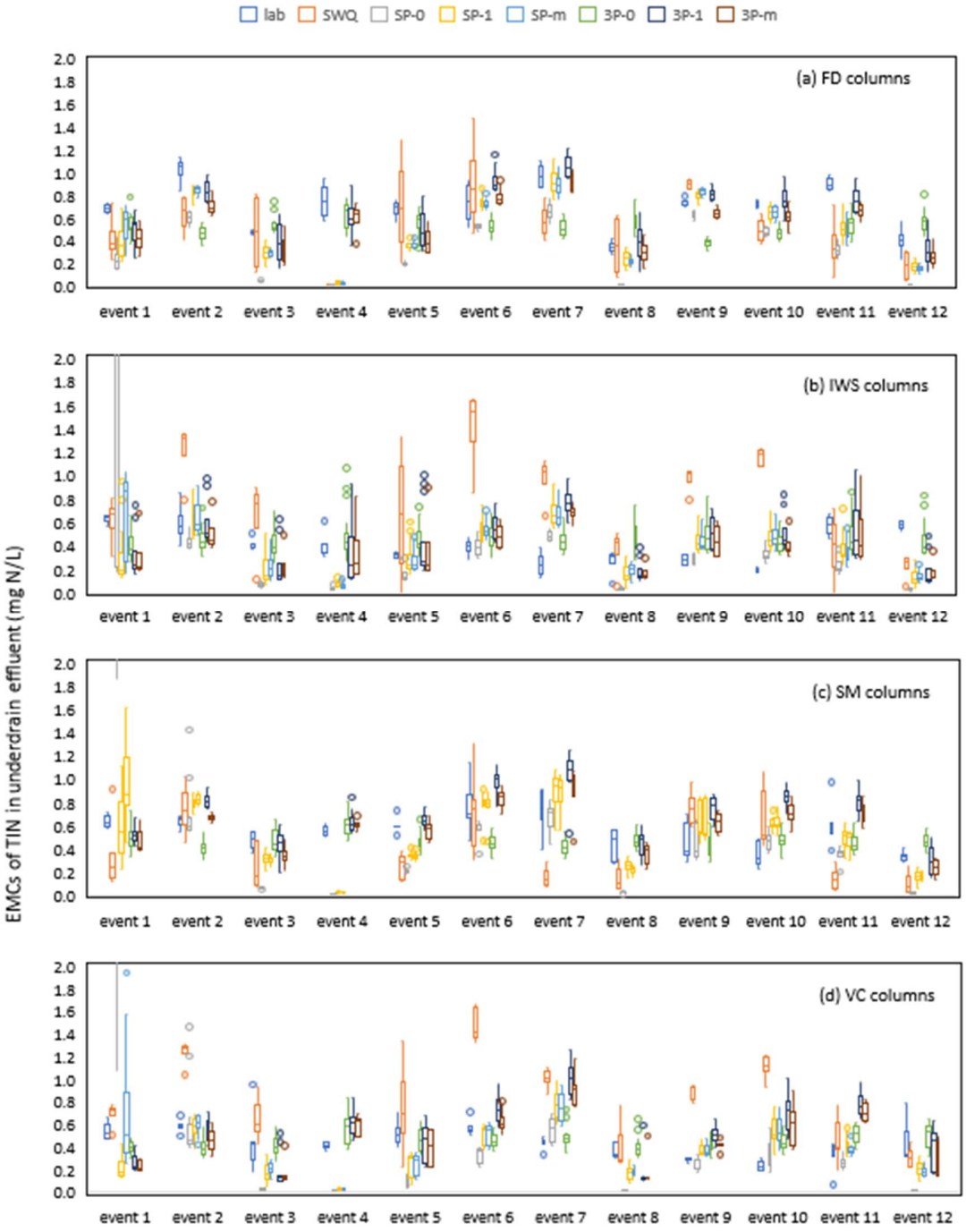

Figure S 1 Boxplots of lab tested, and models simulated TIN EMCs in underdrain effluent for each event in (a) FD columns, (b) IWS columns, (c) SM columns, (d) VC columns, values higher than 2 mg/L are not shown.

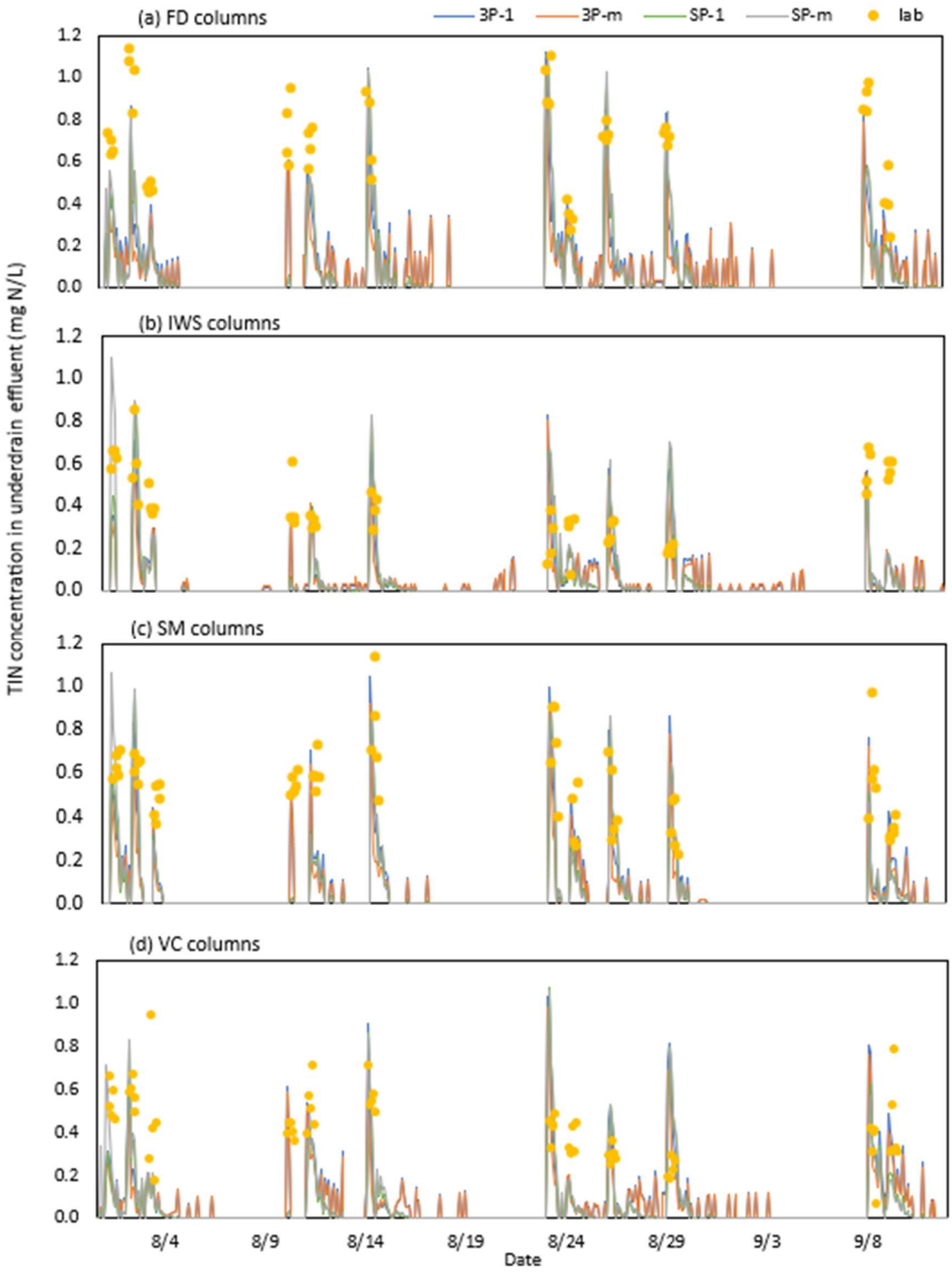

Figure S 2 Timeseries of TIN concentration in underdrain effluent generated by SP-1, SP-m, 3P-1, and 3P-m models, for (a) FD, (b) IWS, (c) SM, and (d) VC columns.

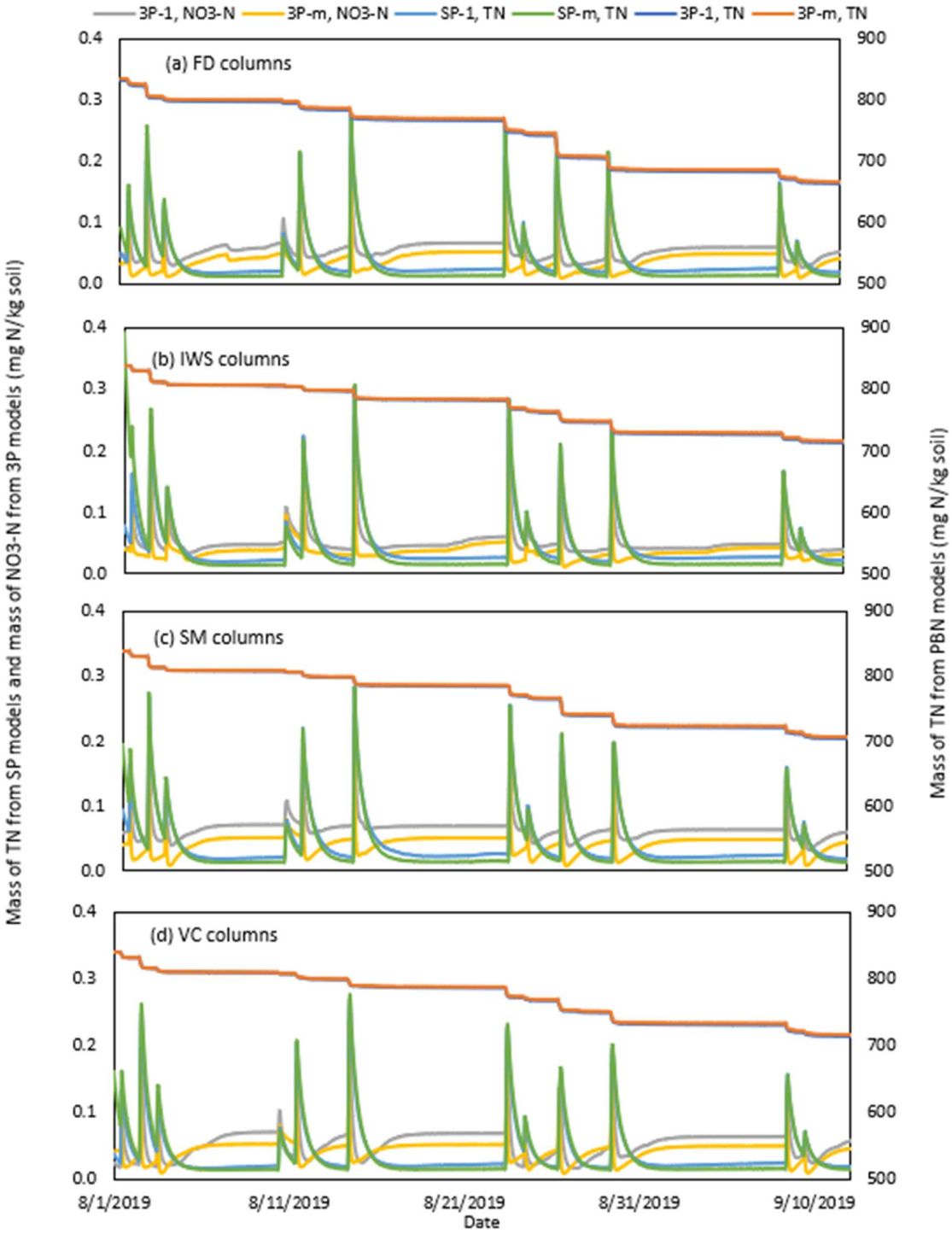

Figure S 3 Timeseries of mass of TN and NO_3-N predicted by SP-1, SP-m, 3P-1, 3P-m models for (a) FD, (b) IWS, (c) SM, and (d) VC columns.

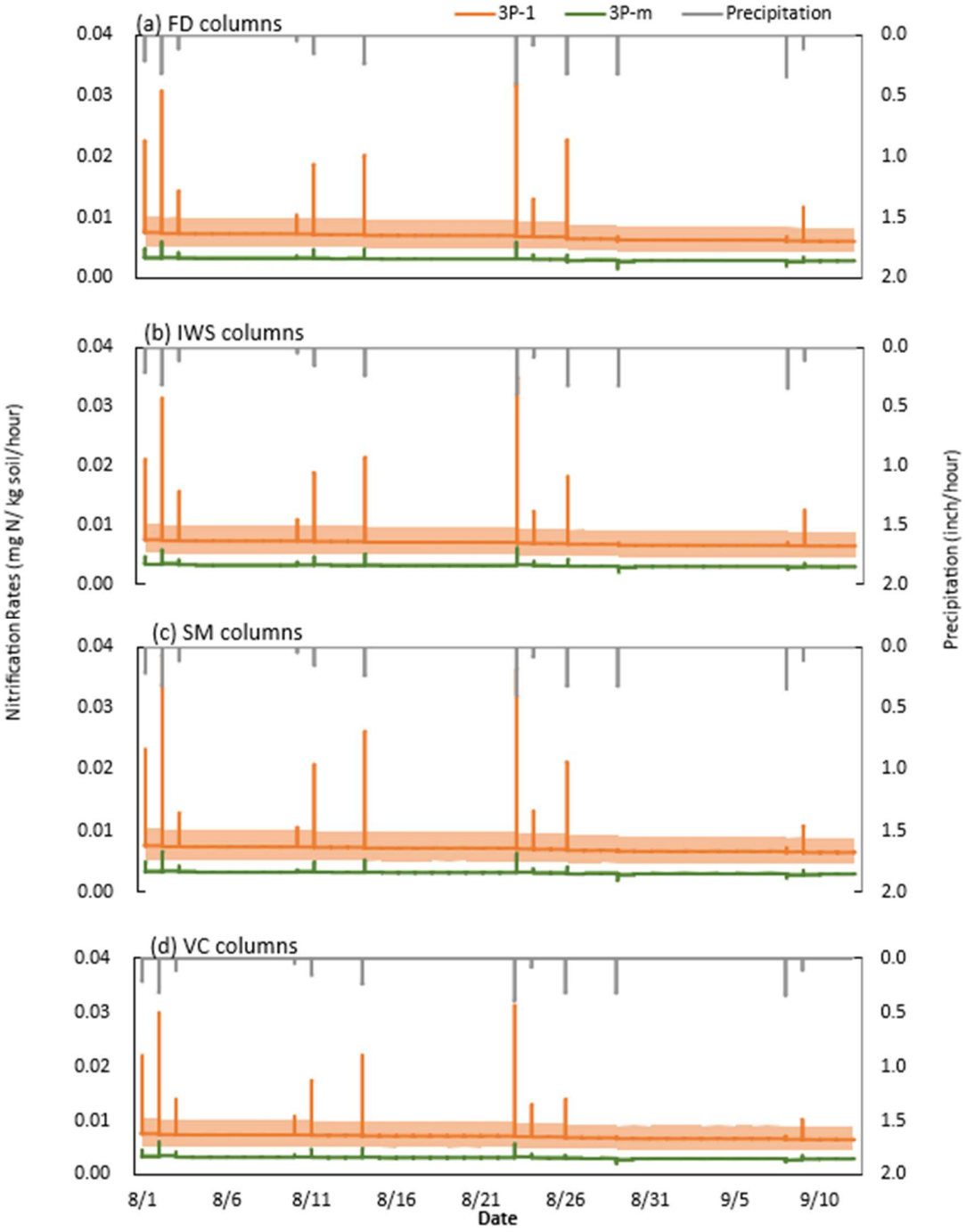

Figure S 4 Timeseries of nitrification rates predicted by 3P models for (a) FD columns, (b) IWS columns, (c) SM columns, and (d) VC columns together with records of precipitation.

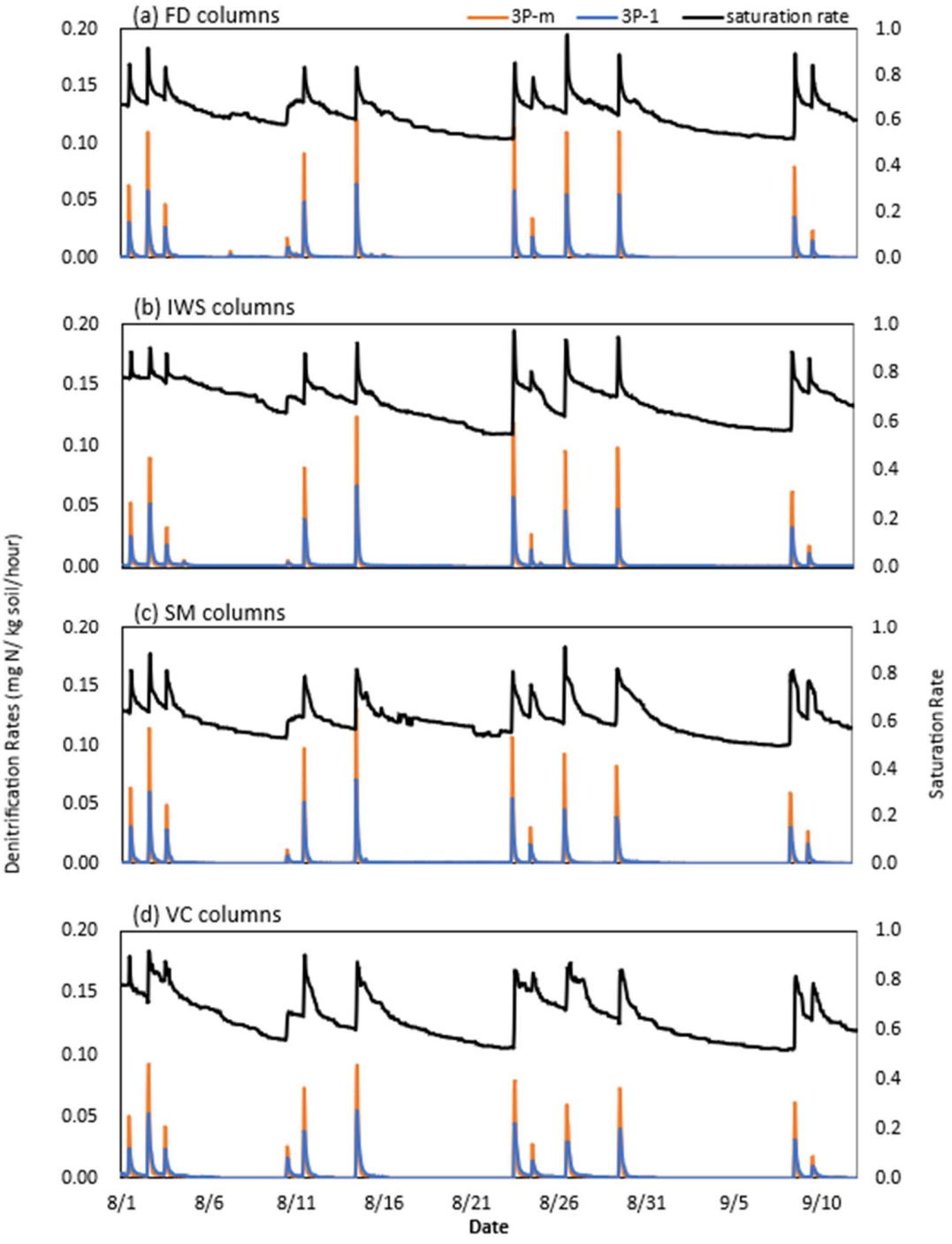

Figure S 5 Timeseries of denitrification rates predicted by 3P models for (a) FD columns, (b) IWS columns, (c) SM columns, and (d) VC columns together with soil saturation rates.

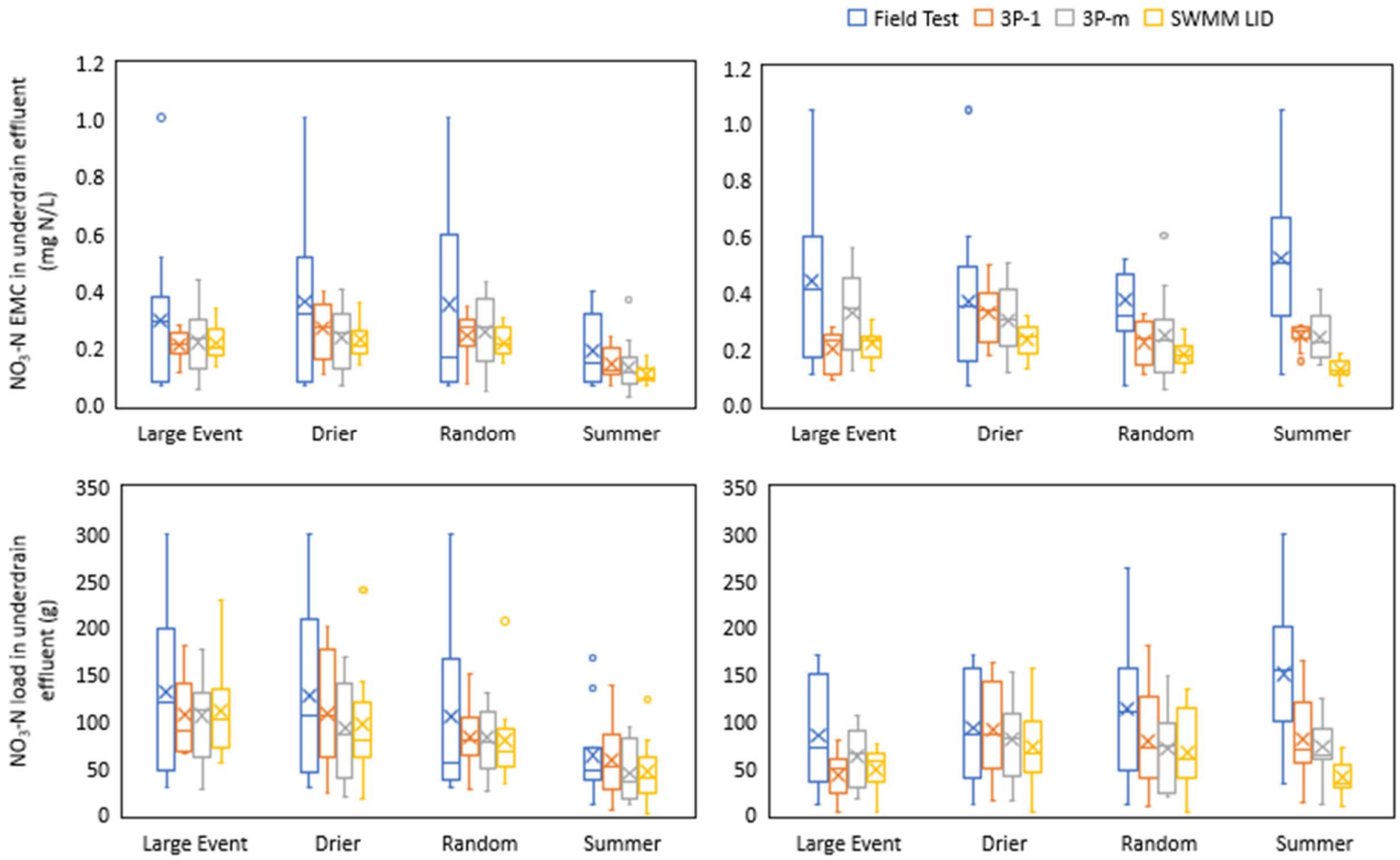

Figure S 6 Box plot of field and model simulated (a) NO_3-N EMC and (b) NO_3-N load in underdrain effluent. In each row, calibrated events are shown in the left panel, and validated events are shown in the right panel.

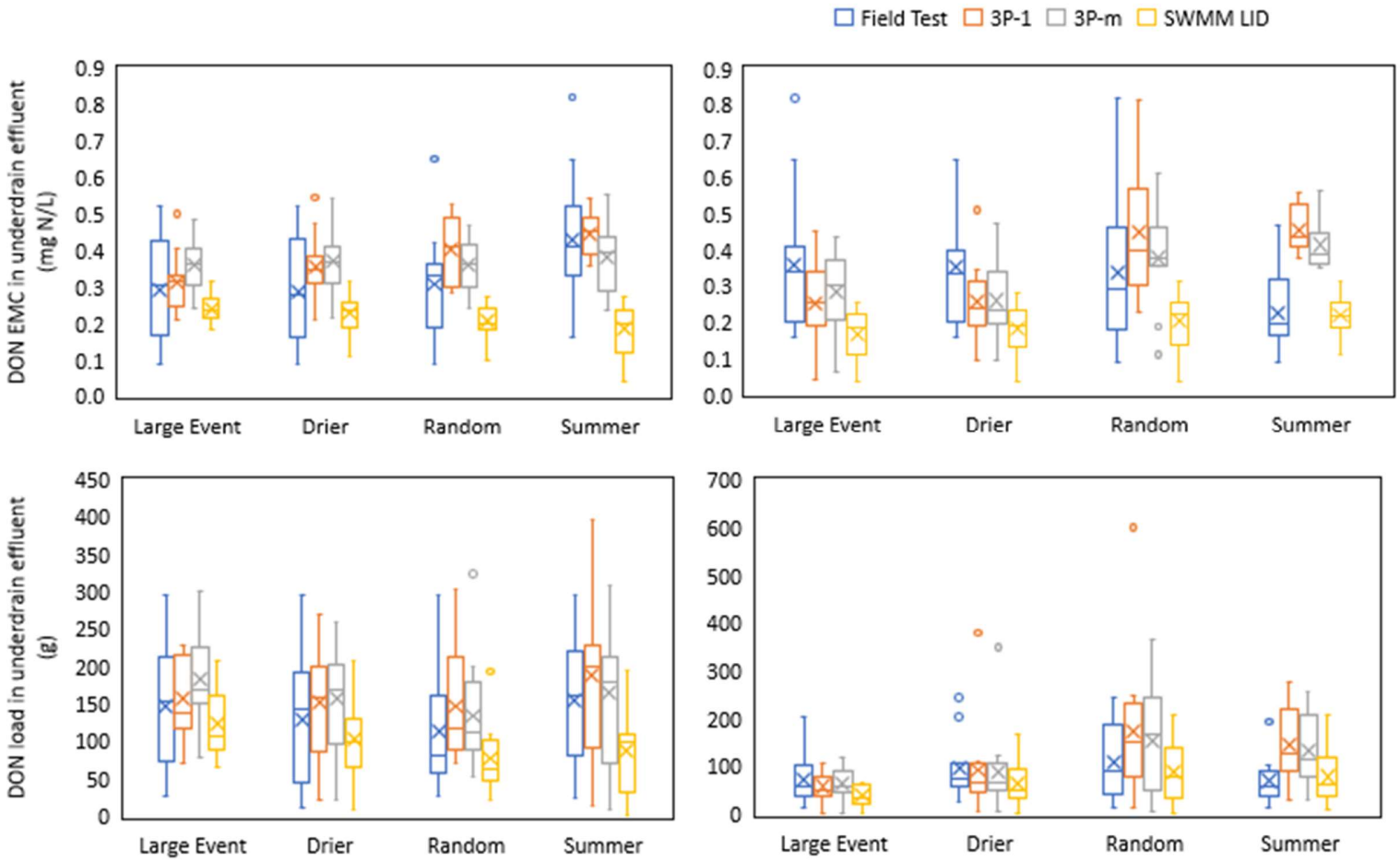

Figure S 7 Box plot of field and model simulated (a) DON EMC and (b) DON load in underdrain effluent. In each row, calibrated events are shown in the left panel, and validated events are shown in the right panel.

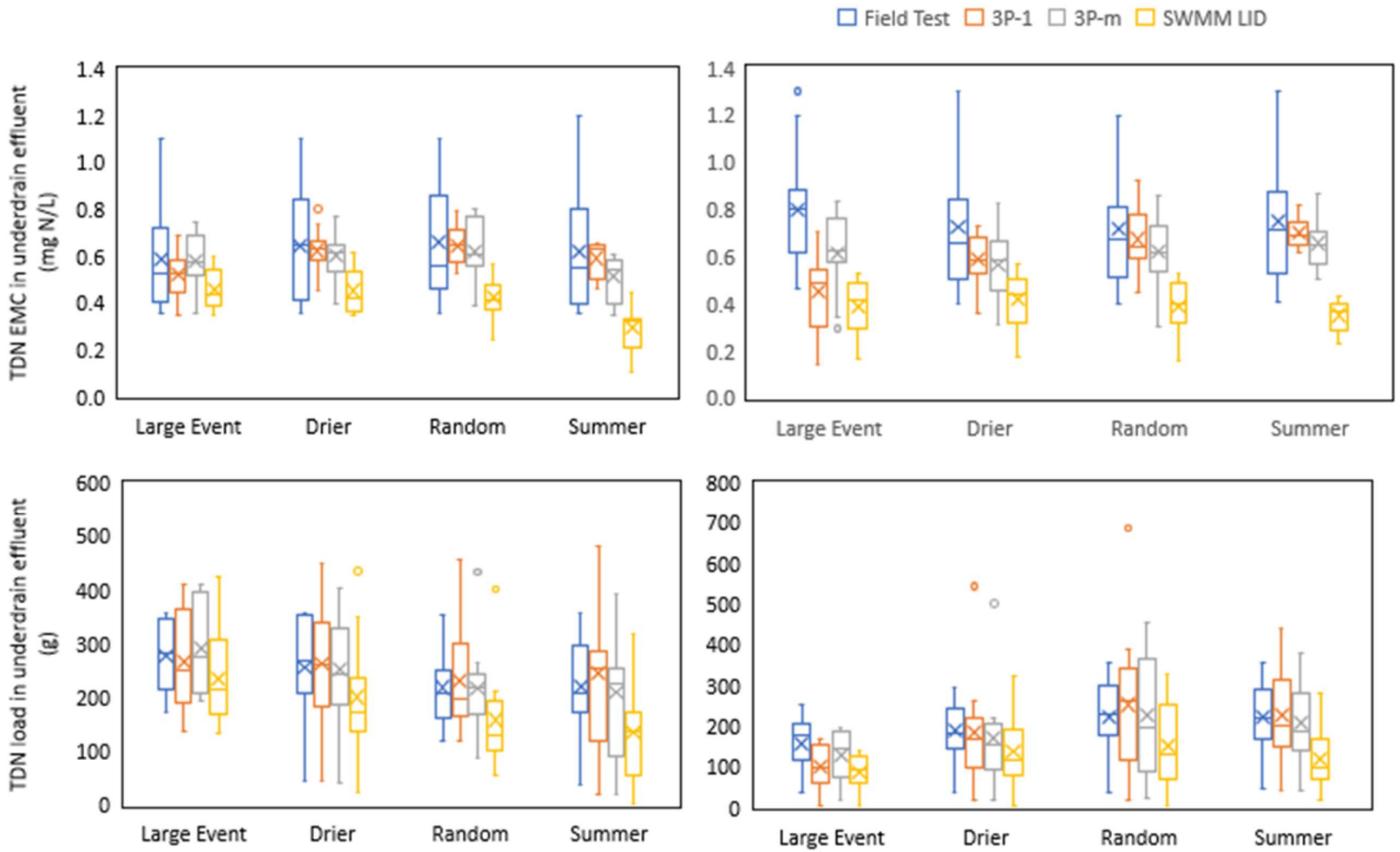

Figure S 8 Box plot of field tested, and model simulated (a) TDN EMC and (b) TDN load in underdrain effluent. In each row, calibrated events are shown in the left panel, and validated events are shown in the right panel.

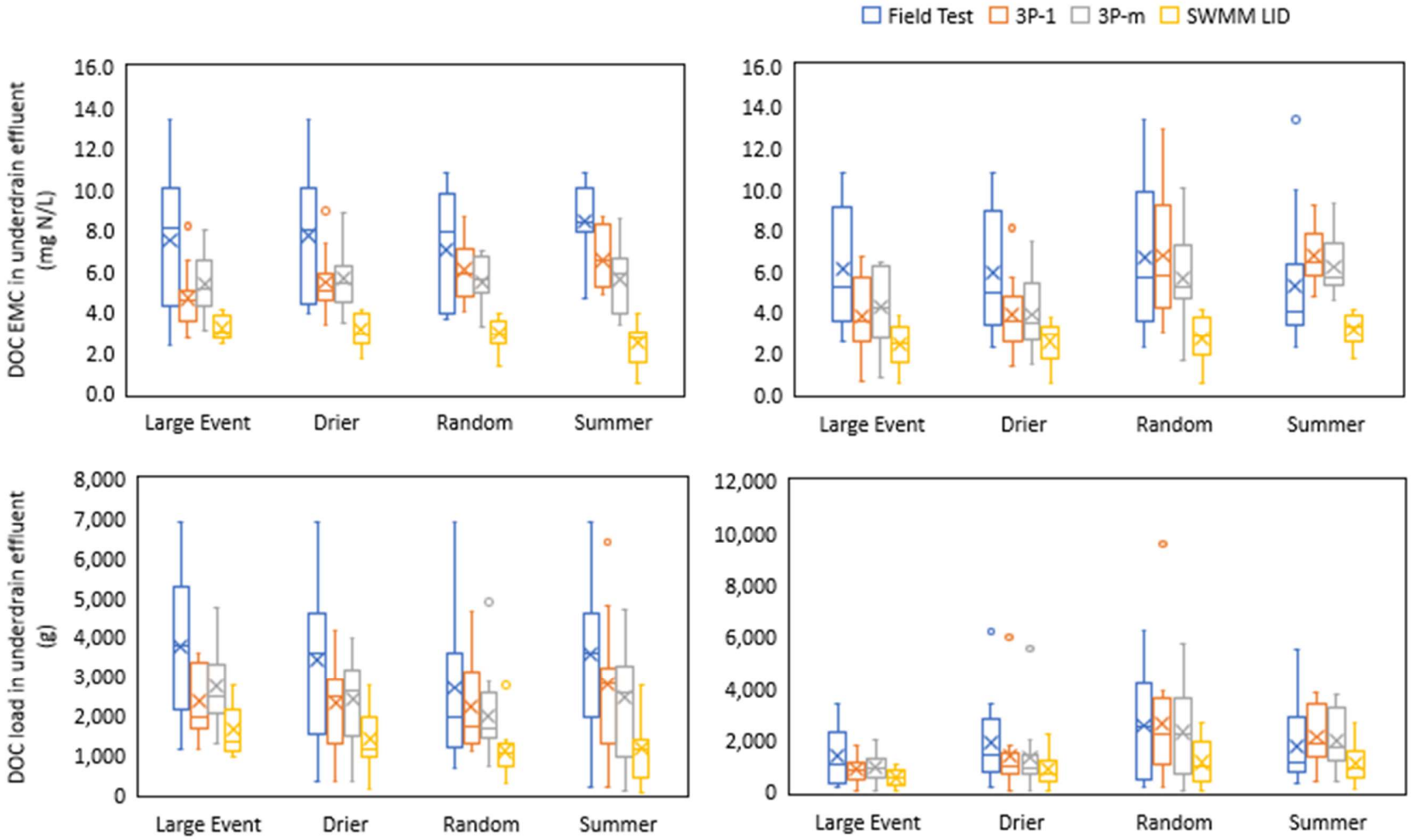

Figure S 9 Box plot of field tested, and model simulated (a) DOC EMC and (b) DOC load in underdrain effluent. In each row, calibrated events are shown in the left panel, and validated events are shown in the right panel.

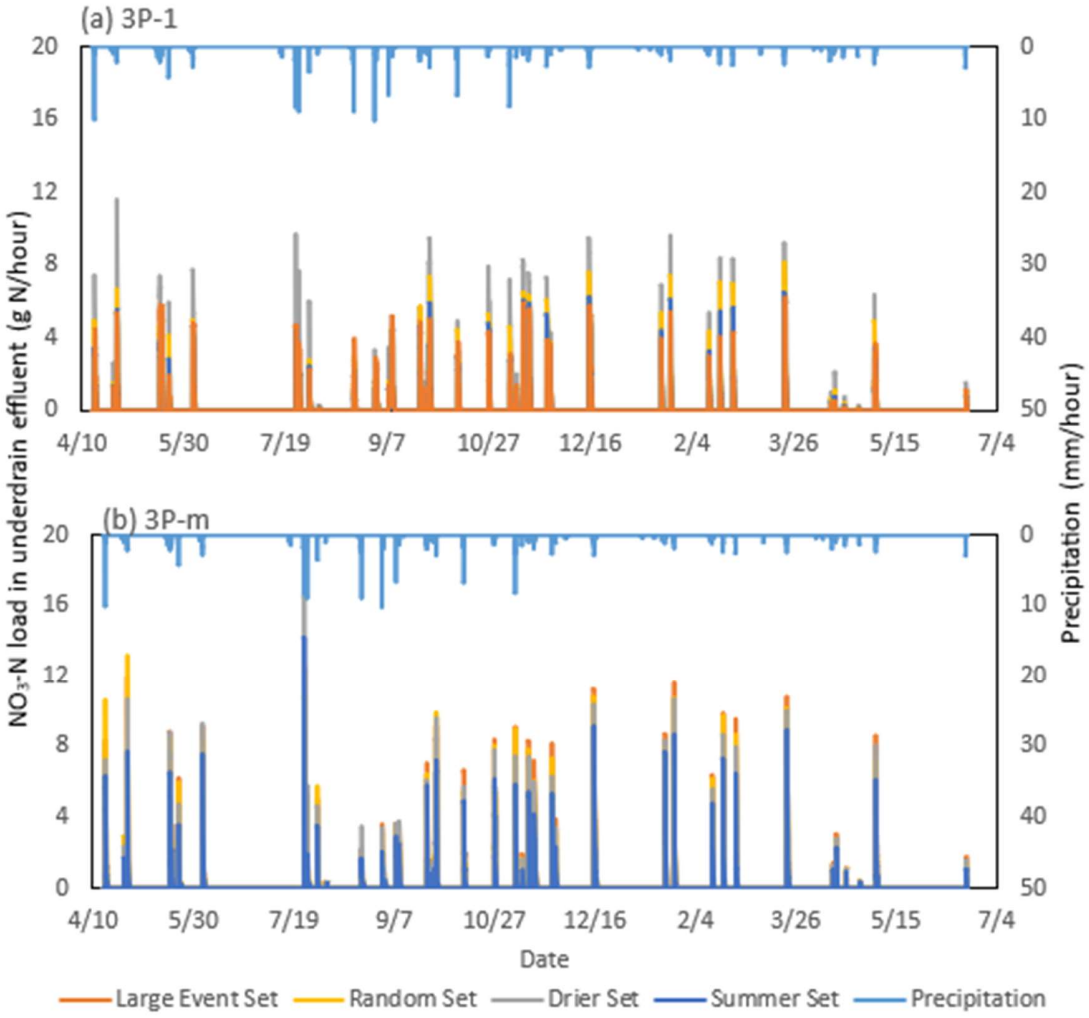

Figure S 10 Time series of d NO_3-N Load in underdrain effluent (g N/hour) predicted by (a) 3P-1 and (b) 3P-m models with best calibration run from four calibration sets.

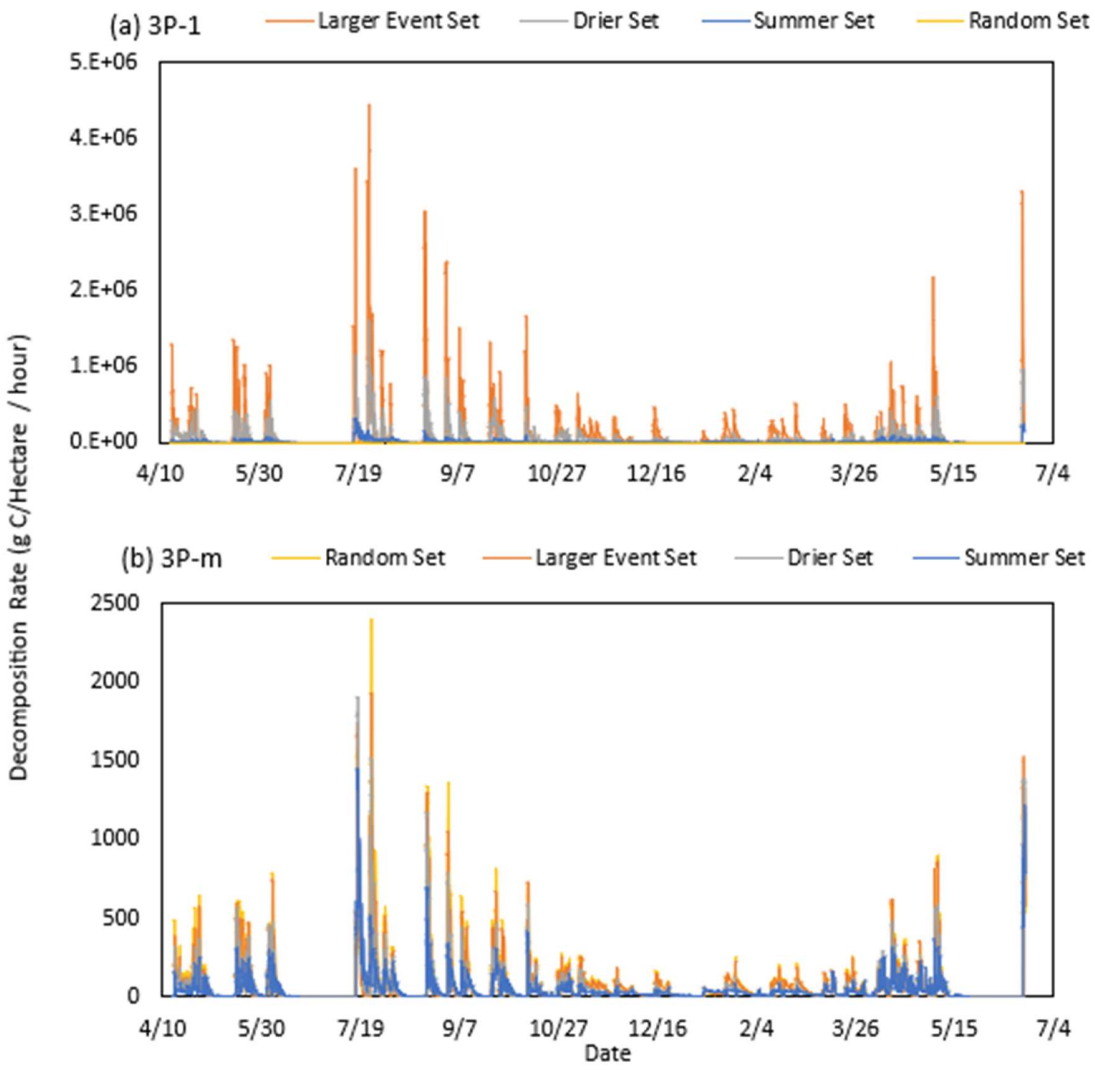

Figure S 11 Time series of decomposition rates predicted by (a) 3P-1 and (b) 3P-m models with best calibration run from four calibration sets.

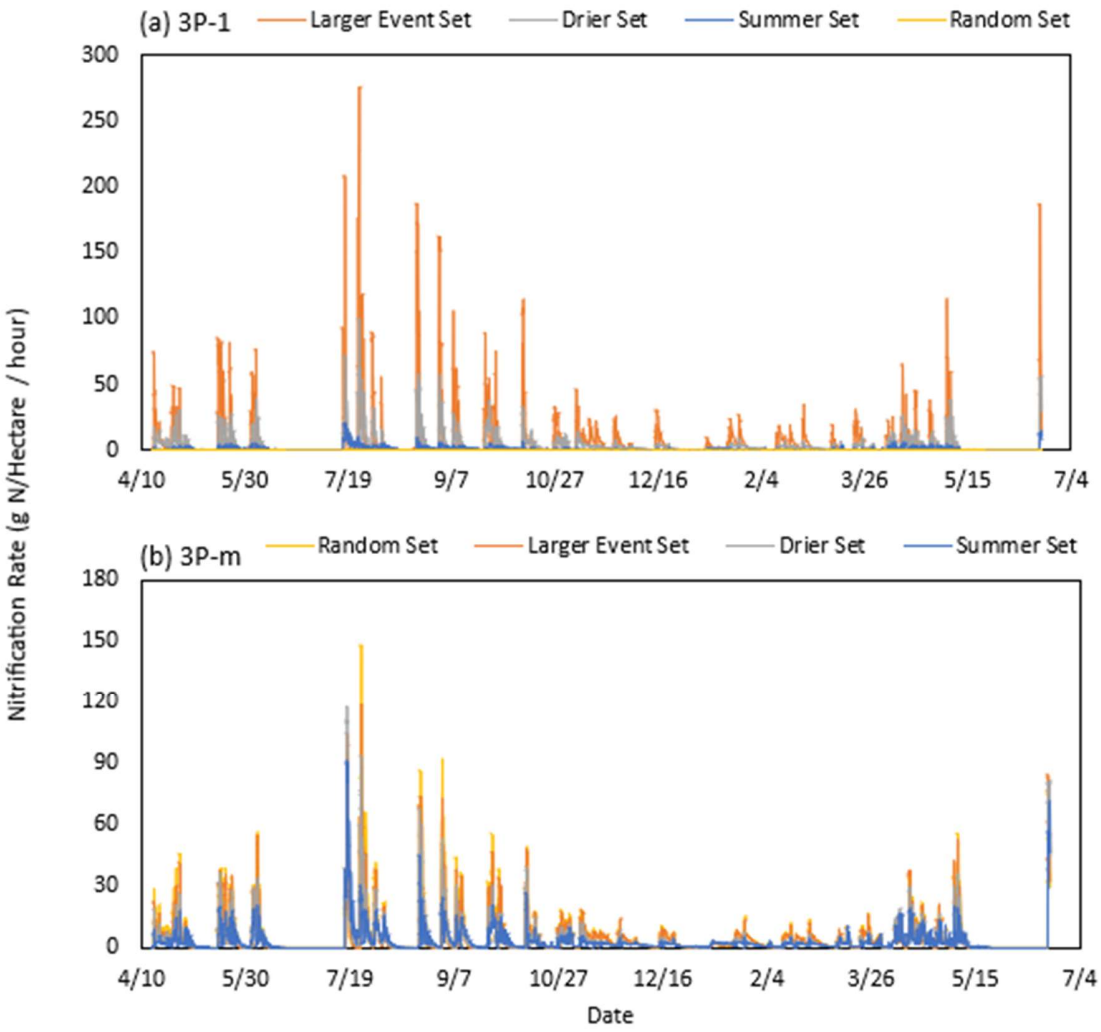

Figure S 12 Time series of nitrification rates predicted by (a) 3P-1 and (b) 3P-m models with best calibration run from four calibration sets.

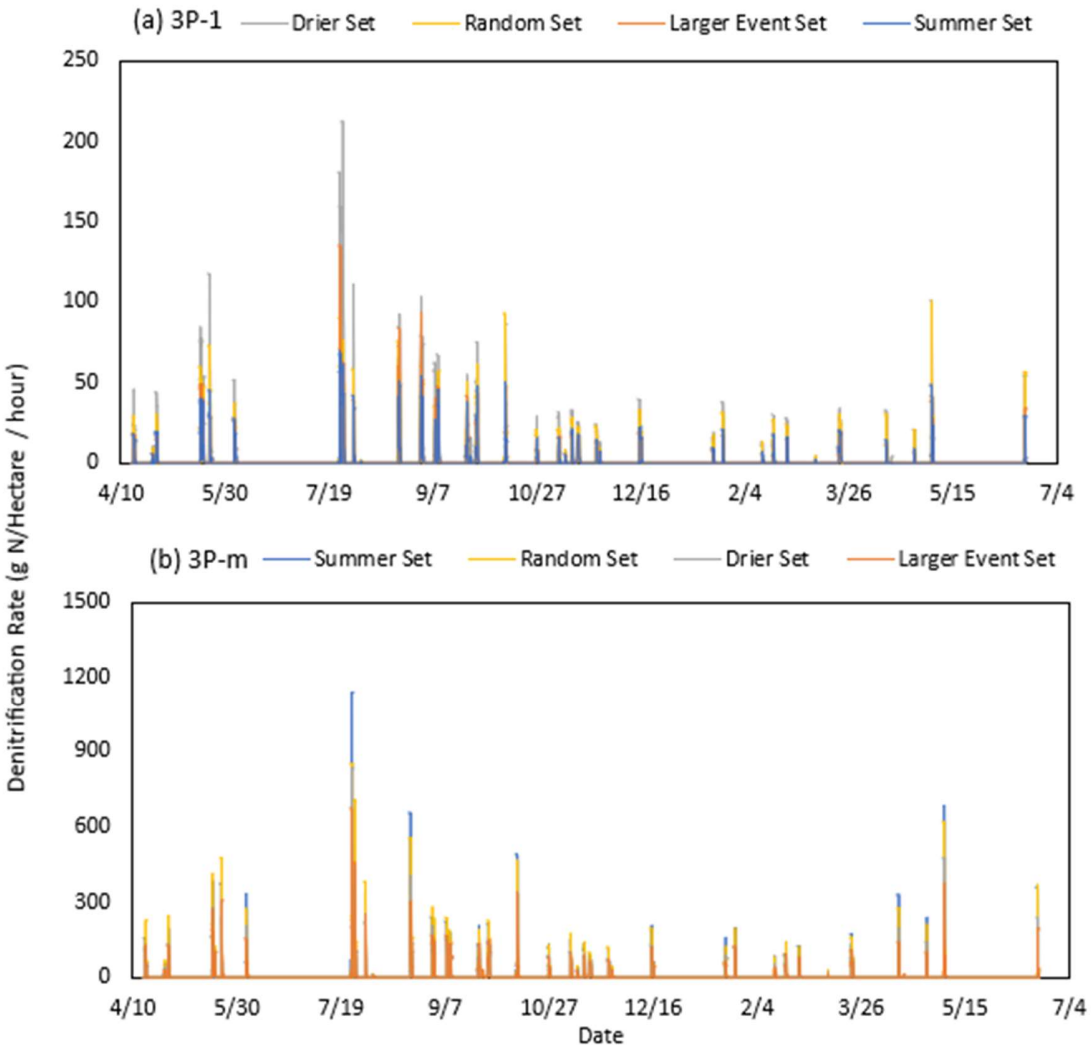

Figure S 13 Time series of denitrification rates predicted by (a) 3P-1 and (b) 3P-m models with best calibration run from four calibration sets.

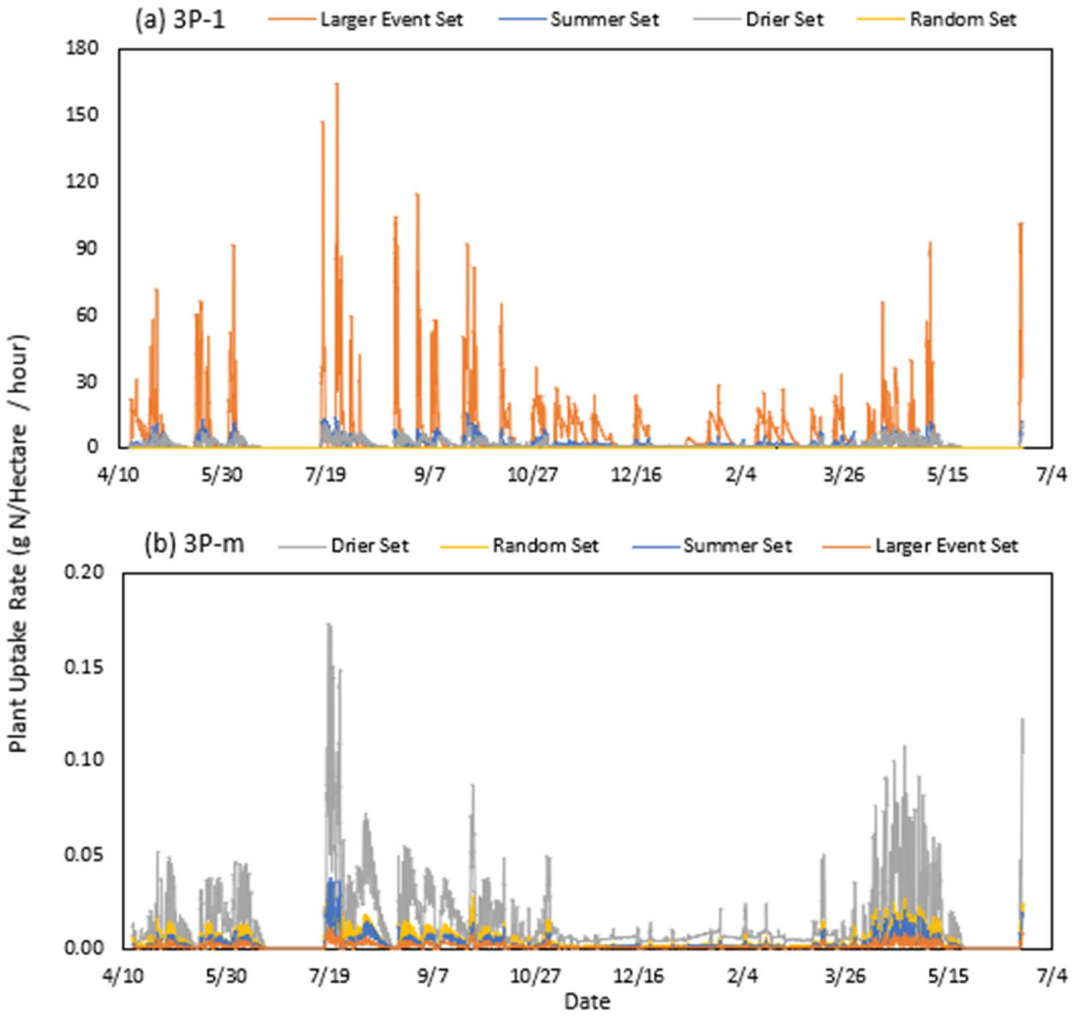

Figure S 14 Time series of plant uptake rates predicted by (a) 3P-1 and (b) 3P-m models with best calibration run from four calibration sets.

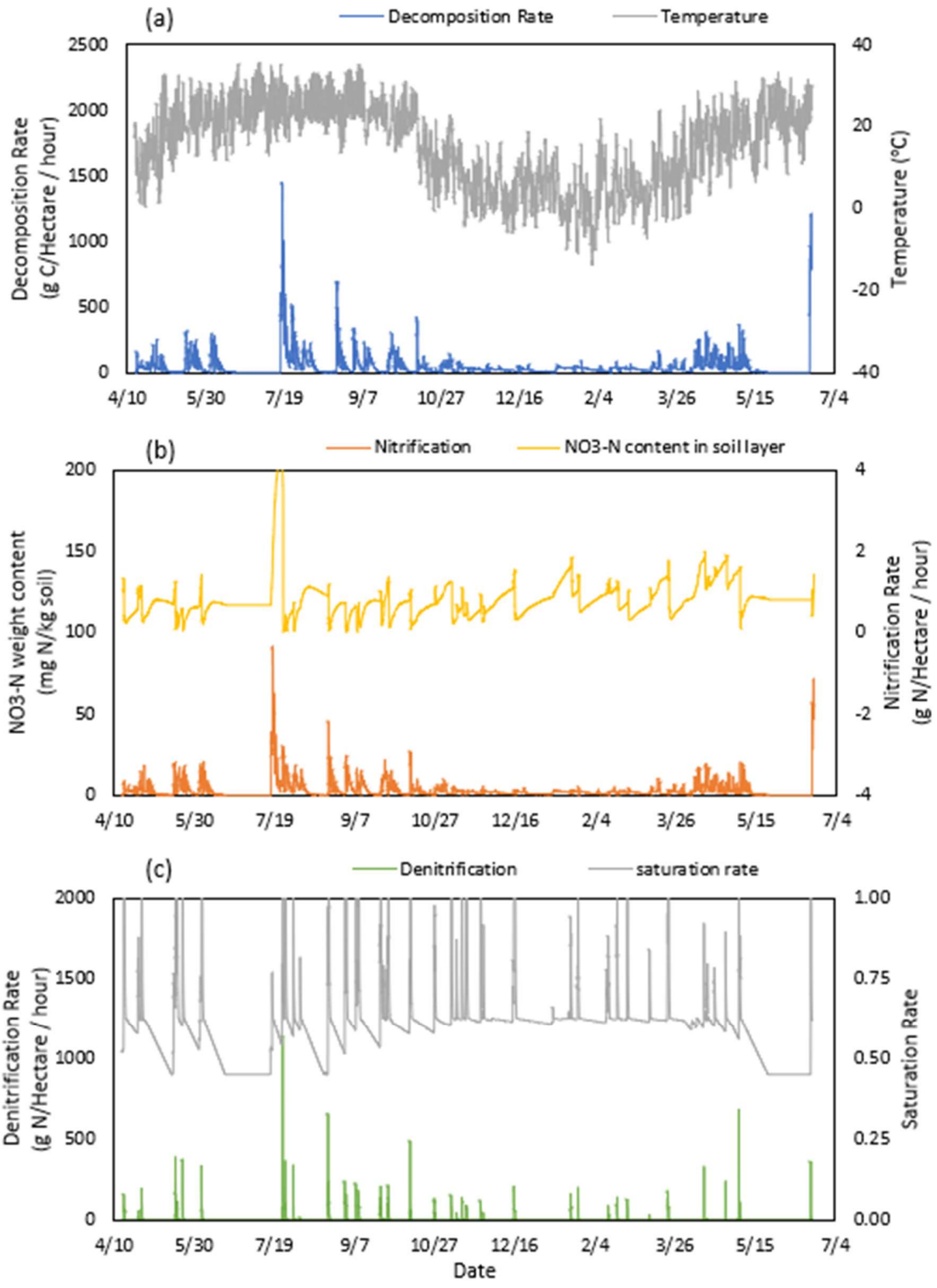

Figure S 15 Time series simulated by 3P-m model for the Summer Set (a) temperature and decomposition rates; (b) nitrification rates and mass of NO_3-N; (c) denitrification rates and saturation rates.

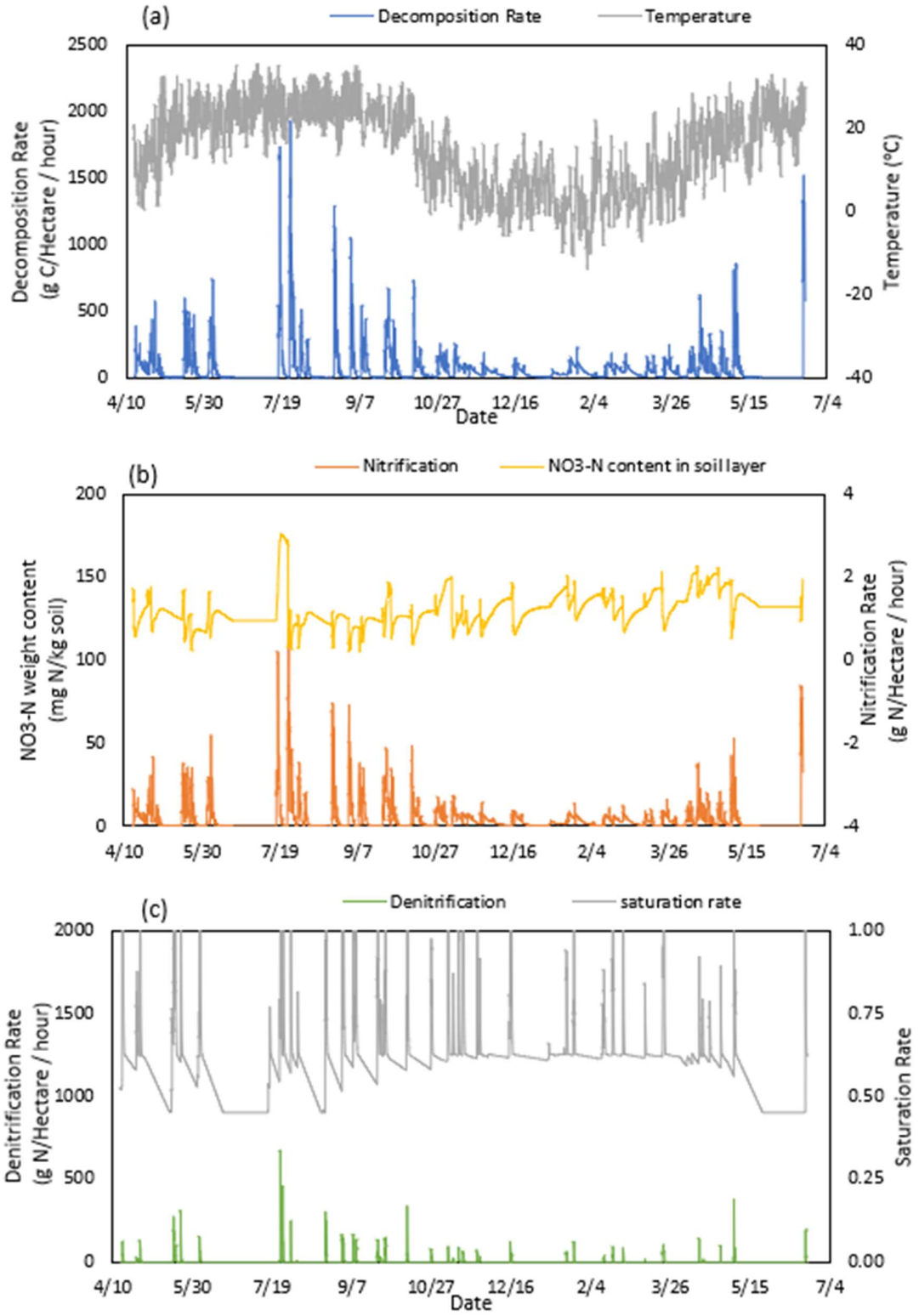

Figure S 16 Time series simulated by 3P-m model for the Larger Events Set (a) temperature and decomposition rates; (b) nitrification rates and mass of NO_3-N; (c) denitrification rates and saturation rates.

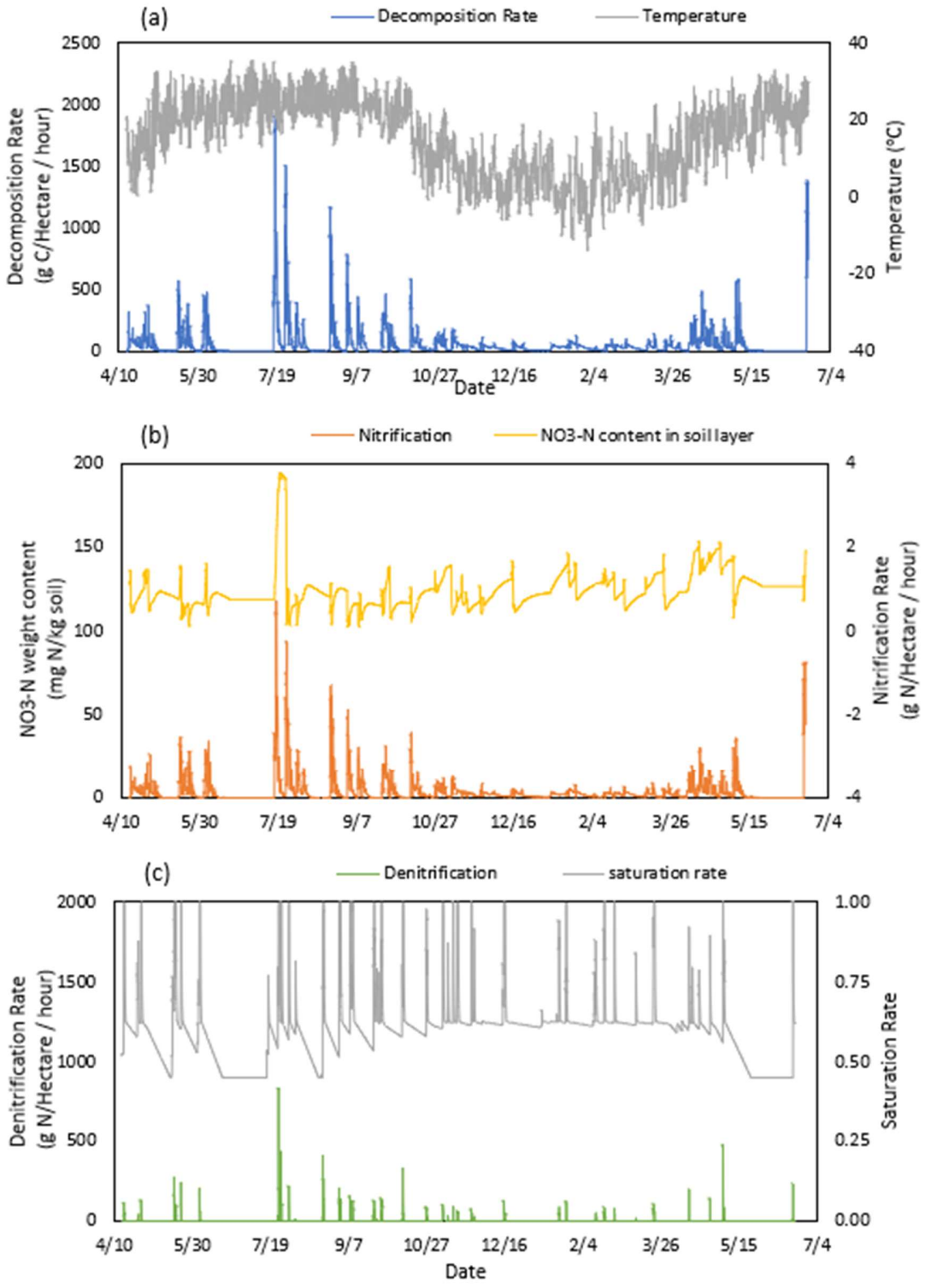

Figure S 17 Time series simulated by 3P-m model for the Drier Set (a) temperature and decomposition rates; (b) nitrification rates and mass of NO_3-N; (c) denitrification rates and saturation rates.

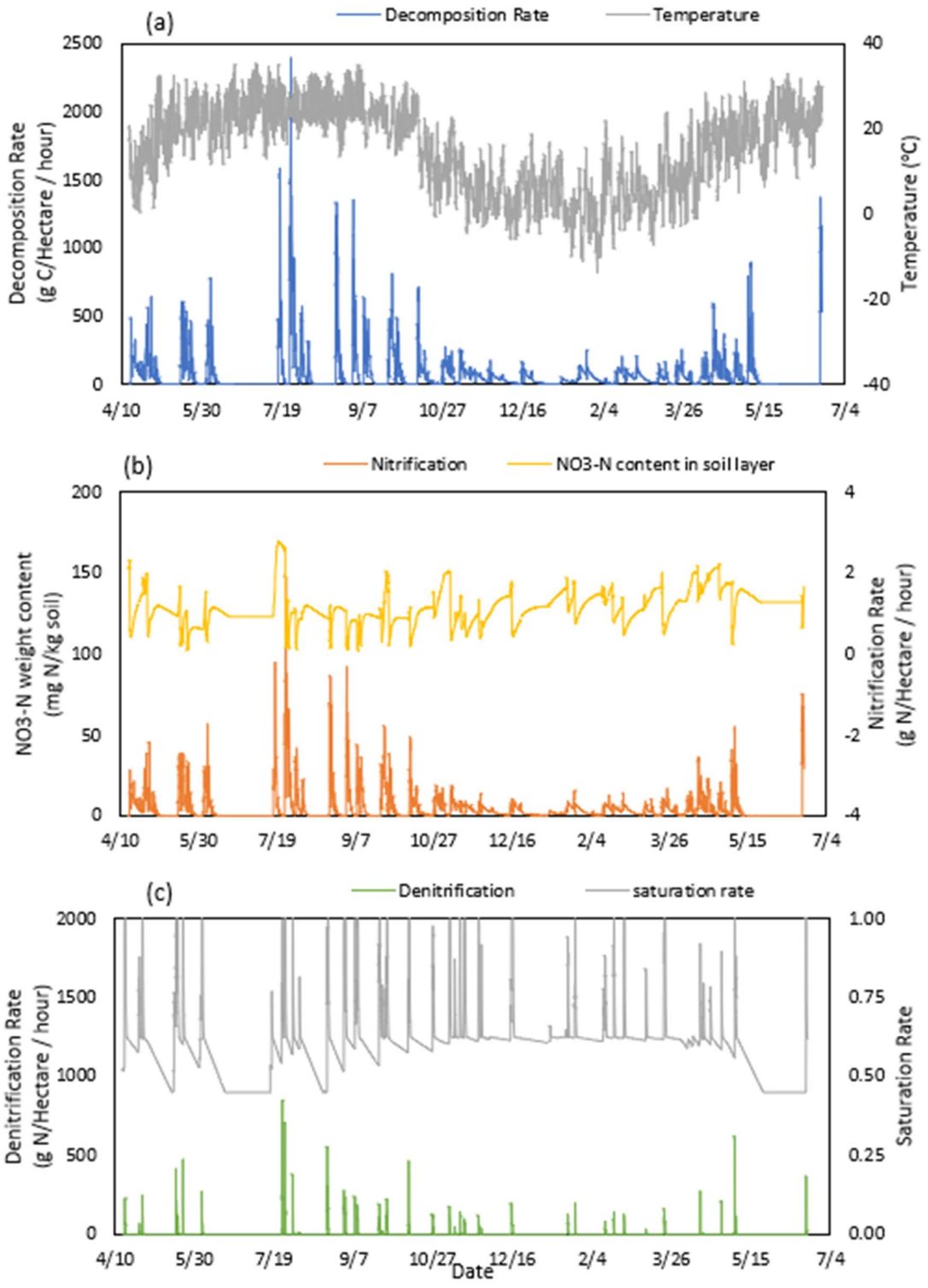

Figure S 18 Time series simulated by 3P-m model for the Random Set (a) temperature and decomposition rates; (b) nitrification rates and mass of NO_3-N; (c) denitrification rates and saturation rates.